UNIVERSITÀ DEGLI STUDI DI MILANO

PhD School of Pharmacologic Science

XXVIII CICLE

Impact of LRRK2 kinase activity at the pre-synaptic site: early and late effects on Parkinson's Disease

PhD course coordinator:

Prof. Alberto Corsini

Advisor:

PhD Fabrizio Gardoni

Co-Advisor:

PhD Giovanni Piccoli

PhD Thesis of:

Maria Daniela Cirnaru

Matr. Nr. R10231

Academic Year 2014/2015

Table of contents

SUMMARY **5**

1 INTRODUCTION **7**

1 PARKINSON'S DISEASE 7

1.1 Historical review *7*

1.2 Anatomy of PD *8*

1.3 Genetics of PD *9*

1.3.1 Autosomal dominant genes in PD 10

1.3.1.1 Alpha synuclein 10

1.3.1.2 LRRK2 11

1.3.1.3 VPS35 12

1.3.1.4 GBA 13

1.3.2 Autosomal recessive genes in PD 13

1.3.2.1 Parkin 13

1.3.2.2 PINK1 14

1.3.2.3 DJ-1 16

1.3.2.4 ATP13A 17

1.4 Take home messages *18*

1.4.1 PD related genes play a key role at the presynaptic site 18

1.4.2 PD related genes play a key role in protein clearance 19

2 LRRK2 20

2.1 Insight on LRRK2 ..... *20*

2.2 LRRK2 influences synaptic activity *21*

2.3 LRRK2 modulates protein clearance *22*

2 AIMS OF STUDY **24**

3 MATERIALS AND METHODS **25**

1 ANIMALS 25

2 PLASMIDS, LENTIVIRAL VECTOR CONSTRUCTS AND VIRUS PRODUCTION 25

3 CELL CULTURE, TRANSFECTION AND DRUG TREATMENTS 25

4 ANTIBODIES, SDS-PAGE AND WESTERN BLOT ANALYSIS 26

5 SYPHY ASSAY 27

6 EXO-ENDO 27

7 MORPHOLOGY ANALYSIS 28

8 IMMUNOCYTOCHEMISTRY 28

9 PROTEASOME ACTIVITY ASSAY 28

10 TUBE 29

11 IMMUNOPRECIPITATION 29

12 PROTEIN PURIFICATION 30

13 KINASE ASSAY 31

14 IN VITRO UBIQUITINATION 31

15 FILTER ASSAY 31

16 IMMUNOHISTOCHEMESTRY 32

17 TREHALOSE TREATMENT 32

18 BEHAVIOR 33

18.1 Spontaneous motor activity *33*

18.2 Balance Beam walking *33*

18.3 Pole test *34*

18.4 Hanging wire test *34*
18.5 Rotarod *34*
18.6 Novel Object recognition (NOR) *34*

4 RESULTS **36**
1 LRRK2 G2019S MUTATION INFLUENCES SV TRAFFICKING 36
2 LRRK2 PROTEIN LEVELS AND KINASE ACTIVITY INFLUENCE NEURONAL MORPHOLOGY 40
3 G2019S NEURONS SUFFER PROTEASOME INHIBITION 43
4 NSF ACCUMULATES IN PD PATIENT AND CO-AGGREGATES WITH ALPHA SYNUCLEIN IN LB. 45
5 LRRK2 G2019S MUTATION CORRELATES WITH DEPOSITION OF NSF AGGREGATES 46
6 LRRK2 G2019S KINASE ACTIVITY IMPAIRS NSF UBIQUITINATION 47
7 LRRK2 IMPAIRS NSF UBIQUITINATION IN VITRO 48
8 REDUCED NSF CLEARANCE IS TOXIC FOR G2019S NEURONS 52
9 TREHALOSE REDUCES NSF AGGREGATES AND AMELIORATES MOTOR PHENOTYPE IN BAC HG2019S MICE 54

5 DISCUSSION **59**
CONCLUSIONS **64**
REFERENCES **65**

Summary

Parkinson's disease (PD) is a common neurodegenerative disease clinically characterized by bradykinesia, rigidity and resting tremor. PD is characterized pathologically by the degeneration of nigrostriatal dopaminergic neurons and the presence of Lewy bodies containing a small protein, alpha-synuclein. Mutations in Leucine-rich repeat kinase 2 gene (*LRRK2*) are associated with familial and sporadic Parkinson's disease (PD). LRRK2 is a complex protein that consists of multiple domains executing several functions, including GTP hydrolysis, kinase activity, and protein binding. There are many single nucleotide alterations covering LRRK2's functional domains, but the main missense mutations that clearly segregate with PD in large family studies, cluster within the enzymatic domains. The G2019S mutation falls in the activation loop of the kinase domain generating a 2-fold increase in LRRK2 kinase activity. Although patients with LRRK2 mutations usually respond to levodopa therapy, this treatment is only symptomatic and it does not cure the cause of the disease. In particular, LRRK2 mutations lead to neuronal cell death and toxic protein aggregates and LRRK2 kinase activity seems to be responsible for the observed neurotoxicity. Our previous research pointed out that LRRK2 acts at the presynaptic site where interacts with synaptic vesicles (SV) and presynaptic proteins together with which it controls SV trafficking in a kinase depended manner. Our recent data indicate NSF not only as an interactor but also as a substrate for LRRK2 kinase activity in vitro. In the present work we analyze how LRRK2 increased kinase activity conferred by the PD related G2019S mutation influences the neuronal functions. We investigated whether G2019S mutation might affect presynaptic function in short term and substrate clearance in long term. Next, we evaluated the feasibility of two potential therapeutic strategies: the first implies the use of LRRK2 kinase inhibitors while the second focuses on treatment ameliorating protein degradation via induction of autophagy. By dynamic studies of SV release in cultured neurons of human LRRK2 G2019S (GS) overexpressing mice and in breed wild-type mice, we found that the increase of LRRK2 kinase activity positively correlates with an increase in the endocytosis rate of the SV. Moreover, we report also an impairment in the complexity of the neuronal tree of the GS neurons that depends on both increased protein level and kinase activity. We recently reported that LRRK2 phosphorylates NSF at threonine 645 inducing an increase in NSF's ATP hydroxylation rate that determine an increase in the SNARE

disassembly. Moreover, we found that aged GS mice show aberrant NSF protein accumulation and motor as well as cognitive impairment. We report also that the chronic treatment with trehalose, an autophagy inducing molecule, partially recovered the motor phenotype and NSF aggregation proposing it as an interesting therapeutic strategy.

1 Introduction

1 Parkinson's Disease

1.1 Historical review

In 1817, James Parkinson, an English surgeon, and political activist, described for the first time the symptoms of the disease that today bears his name. In his work, "An Essay on the "Shaking Palsy" he reports his observation on six individuals three of which were his patients. He referred to the disease as paralysis agitans or shaking palsy, identifying episodes of resting tremors and of tremors with motion. He originally charged these episodes to possible lesions in the cervical spinal cord and encouraged others to study this condition (McCall 2003). It was not until 1872 that the "shaking palsy" was named Parkinson disease by the French doctor Jean-Martin Charcot, who also made the distinction between rigidity, weakness and bradykinesia (Lees 2007). In 1912, Fritz Heinrich Lewy identified the protein aggregates that define Parkinson disease (PD) (Goedert et al. 2012). Lewy described the characteristic inclusions in the dorsal motor nucleus of the vagus nerve, the basal nucleus of Meynert, the globus pallidus, the lateral nucleus of the thalamus, and the periventricular nucleus of the thalamus. The inclusions described by Lewy were eosinophilic and were insoluble in alcohol, chloroform, and benzene, consistent with the presence of a major protein component.

In 1919, Tretiakoff reported the presence of Lewy bodies in the substantia nigra in PD (Kapp 1992). He also showed degeneration of the substantia nigra and postulated a connection between nerve cell loss, rigidity, and tremor. In 1938, Rolf Hassler (1914–1984) confirmed Tretiakoff's observation that degeneration of the substantia nigra was the cause of Parkinsonism. He also demonstrated the focal distribution of pathology, with the most pronounced nerve cell loss being found in the caudal and ventrolateral parts of the substantia nigra (Hassler 1938). The fact that nerve cells in the ventrolateral part of the pars compacta of the substantia nigra are severely affected in PD is now well established. These cells project mainly to the dorsal putamen, the most dopamine depleted region of the striatum in PD (Goedert et al. 2012).

Nowadays PD represents the second most common neurodegenerative disorder of aging. It affects 2% of the population over 60 years of age and occurs at an incidence of 16-19 in

100 000 individuals per year (Rudzińska et al. 2013)

1.2 Anatomy of PD

The basal ganglia are one of the areas in the encephalon involved in movement's control influencing the activity of the superior motorneurons. They are a subgroup of nuclei that include the caudate, putamen and globus pallidus. Their activity is associated with the one of other two structures: substantia nigra in the mesencephalon and the ventral subthalamic nucleus of the thalamus. All of these structures create a subcortical circuit that connects the inputs from cortical area to the superior motor neurons from the primary motor cortex, premotor cortex and brain stem. The canonical view of this circuit proposes the model of a direct and an indirect pathway (Fig. 1). In the first, the cortical activation produces a release of glutamate that activates caudate/putamen's MSNs (medium spiny neurons). These are GABAergic cells projecting and inhibiting the substantia nigra pars reticulate (SNpr) and the globus pallidus Pars Interna (GPi). The inhibition of the GABAergic cells of SNpr leads to a disinhibition of the thalamic glutamatergic neurons, which receive SNpr input and project to the cortex. The behavioral result of this chain of events is locomotor activation/movements. The indirect pathway activates the striatopallidal MSNs, which projecting to the SNpr via the globus pallidus pars externa (GPe) and the subthalamic nucleus (STN), inhibits the GABAergic neurons of the GPe. This leads to a disinhibition of the glutamatergic neurons of the STN that activates the SNpr GABAergic neurons projecting to the thalamus. Ultimately, this effect results in the reduction of locomotor activity and movement. These pathways interact in parallel and have two opposite actions: the activation of the direct way allows to basal ganglia to start the voluntary movement while the activation of the indirect way limits it, inhibiting abnormal movements.

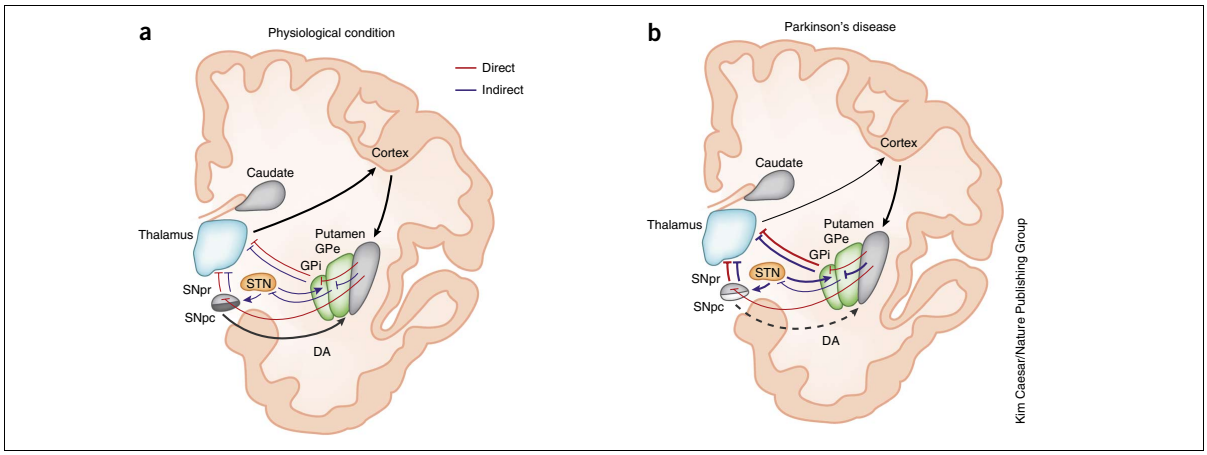

Figure 1. Schematic representation of the direct and indirect pathways in physiological conditions (a) and Parkinson's disease (b) Adapted from (Calabresi et al. 2014)

The overall activity of the direct/indirect way is finely controlled by another circuit belonging to the basal ganglia system that includes the dopaminergic cells from the substantia nigra pars compacta (SNc). The MSNs project directly to SNc and receive SNc wide dopaminergic afferents. The dopamine effect on the MSNs is rather complex as it has a dual action according to the receptor that it binds. The D1 and D2 dopaminergic receptors belong to the family of seven trans-membrane domain G proteins bound receptors, and the substantial difference between them is that D1 activation mediates the activation of the G proteins that stimulates the production of cAMP, while the D2 receptors inhibits it. Apparently the MSNs involved in the direct way express D1 receptors while the ones involved in the indirect way express D2 receptors. Therefore, dopamine release from SNc stimulates the direct way through the D1 receptors and inhibits the indirect way through the D2 receptors.

In pathological situations as PD (Fig 1b), the loss of dopaminergic neurons allows the reduction of the direct pathway and the increase of the indirect one. The result is an addition of inhibition on the basal ganglia that reduce that probability that the superior cortical motor neurons are correctly activated by the thalamic ones. This explains why the majority of PD patients have a reduced ability in movement initiation and once started also in its ending.

1.3 Genetics of PD

Despite the fact that for many years Parkinson's disease was considered a sporadic disease caused by synergistic environmental factors, alterations in various genes are now associated with the development of this disease. These were identified through unbiased research strategies that rely on the systematic scanning of the entire human genome without *a priori* hypotheses on the nature of the causal gene or the pathogenetic mechanisms (Vincenzo Bonifati 2014). Although most of the PD-related genes do not have a complete penetrance and a clear Mendelian inheritance is rarely seen, GWAS studies identified five causal PD genes: SNCA, leucine-rich repeat kinase 2 (LRRK2), parkin RBR E3 ubiquitin protein ligase (PARK2), PTEN-induced putative kinase 1 (PINK1), and Parkinson protein 7 (PARK7). Comparable family-based studies have also successfully identified genes for juvenile Parkinson syndromes, including ATPase type 13A2 (ATP13A2), phospholipase A2 group 6 (PLA2G6), and F-box protein 7 (FBXO7)(Verstraeten, Theuns, and Van Broeckhoven 2015; Vincenzo Bonifati 2014). Mutations in eukaryotic translation initiation factor 4 gamma 1 (EIF4G1) were also identified, but its role in PD etiology is heavily debated as a remarkably high number of non penetrant EIF4G1 mutation carriers have been reported (Schulte et al.

2012; Nuytemans et al. 2013). The genetics of PD was revolutionized by recent innovation of the sequencing strategy that lead to the identification of six more genes for PD and Parkinson-plus syndromes: [vacuolar protein sorting 35 homolog (VPS35), dnaJ homolog subfamily C member 13 (DNAJC13), dnaJ homolog subfamily C member 6 (DNAJC6), ATPase H^+ transporting lysosomal accessory protein 2 (ATP6AP2), synaptojanin 1 (SYNJ1), and coenzyme Q2 4-hydroxybenzoate polyprenyltransferase (COQ2)(Verstraeten, Theuns, and Van Broeckhoven 2015).

The discovery of genes mutated in PD and functional studies on their protein products have provided new insights into the pathologic events leading to neurodegeneration, proposing interconnected molecular pathways that may be deranged in all forms of PD. The better understanding of these events can pave the way to elaborate targeted therapies aimed at disease prevention and cure.

1.3.1 Autosomal dominant genes in PD

Nineteen loci that segregate with familial forms of the disease have been reported, collectively suggesting that monogenic PD accounts for 5–10% of all PD cases (Cookson 2015). Mutations in three genes (SNCA, LRRK2, VPS35) are conclusively established as a cause of autosomal dominant forms of PD while evidence for a fourth gene, EIF4G1, remains inconclusive. Last, heterozygous mutations in the GBA gene are important and strong risk factors for PD and diffuse Lewy-body disease (DLB).

In the following sections the identified genes in autosomal dominant PD will be briefly reviewed.

1.3.1.1 Alpha synuclein

In 1996, the first locus for autosomal dominant PD was mapped to chromosome 4q21-q23. Years later missense point mutation in SNCA gene, that encodes alpha-synuclein protein, were reported. The amino acidic substitution Ala53Thr (A53 T) was the first to be documented, present in a series of families from Greek and Italian descent (Polymeropoulos et al. 1997) followed by A30P present in a German family (Kruger et al. 1998) and E46K in several Basques families (Zarranz et al. 2004). Other PD-associated mutations involve SNCA gene multiplication (triplication or multiplication) indicating that higher levels of the normal protein can cause damage to the brain through a gain of toxic function (Cookson 2012; Sundal et al. 2012). Moreover, common variants at the SNCA locus are risk factors for PD, which are not strong enough to cause a Mendelian inheritance but increase the risk in developing PD by about 20-40% over the live time of an individual (Cookson 2012).

Alpha-synuclein is a 140 amino acid presynaptic enriched protein that acts in conjunction with the soluble N-ethylmaleimide-sensitive factor attachment protein receptor (SNARE) proteins to regulate neurotransmitter release (Hunn et al. 2015). It belongs to the family of synucleins formed by alpha, beta, and gamma-synuclein. These are highly homologous proteins that bind to phospholipids via alpha helices and play a role in dopamine release (Senior et al. 2008; Janezic et al. 2013).

Alpha-synuclein does not assume a predictable structure in aqueous solution, thus is has been commonly described as an intrinsically disordered monomer of approximately 14 kDa, conformation that has been recently confirmed by the studies of Burrè et al that reported the occurrence of acetylated alpha-synuclein monomer with an apparent molecular weight of around 16 kDa (Burré et al. 2013). Nonetheless, other studies focused on the definition of the physiological form of this protein reported a predominant endogenous species of 55-60kDa that can be an alpha-synuclein tetramer (Bartels, Choi, and Selkoe 2011). Even though the true physiological conformation of alpha-synuclein remains enigmatic there is an overwhelming amount of studies that indicates that accumulation of alpha-synuclein in insoluble aggregates such as fibrils is neurotoxic and give rise to deleterious effects in DA neurons (Tokuda et al. 2010; Winner et al. 2011; Rockenstein et al. 2014; Janezic et al. 2013). The more recent discovery that a-synuclein aggregates develop in dopaminergic neurons transplanted in the brain of PD patients, and further data from in vitro and in vivo animal studies, suggest that misfolded a-synuclein conformers have prion-like properties, can induce a cascade of protein misfolding, and spread from cell to cell in the brain (reviewed in (Olanow and Brundin 2013). These recent, important evidence needs to be taken in consideration and to be incorporated into all theories of pathogenesis in a way that also fits with the results of the genetic studies (Bonifati et al. 2013).

1.3.1.2 LRRK2

In 2002, the PARK8 locus on chromosome 12q12 was linked with PD in a large Japanese family (Funayama et al. 2002). This linkage was later confirmed in PD families of European descent and the first mutations identified were R1441G, R1441C, Y1699C and I2020T (Paisán-Ruíz et al. 2004; Zimprich et al. 2004). Shortly after that, the LRRK2 G2019S mutation was identified in the kinase domain (Nichols et al. 2007). However, Gly2019Ser has strongly incomplete penetrance, which explains why this founder mutation is detectable in patients with familial but also in some with sporadic PD (Bonifati 2014). The frequency of this mutation is different across the populations and is most prevalent in the Middle East and North Africa. The frequency decreases with distance from the

Mediterranean (Bardien et al. 2011).

PD patients who are carriers of LRRK2 mutations mainly suffer from Parkinsonism with clinical features indistinguishable from sporadic idiopathic late-onset PD. They present dopaminergic neuronal loss and gliosis in the substantia nigra, and classical LBs are found in the majority of them. However, in some cases only tau-positive or ubiquitin- positive inclusions are seen (Sundal et al. 2012; Bonifati 2014).

LRRK2 is a large protein with seven different domains harboring over 100 various provisional mutations (Sundal et al. 2012). The physiological function of LRRK2 is still unknown, but it was linked to vesicular trafficking (Piccoli et al. 2011; Parisiadou et al. 2014; Piccoli et al. 2014), degradation of proteins and organelles by the autophagy-lysosome pathways (MacLeod et al. 2013; Alvarez-Erviti et al. 2010), and to neuroinflammation and innate immunology (Gardet et al. 2010). The possible mechanisms through which mutated LRRK2 leads to cellular dysfunction might be related to an exaggeration of its normal function or gain of abnormal function (Dachsel et al. 2011).

Due to the overlap between LRRK2 parkinsonism and idiopathic PD, understanding the effect of the mutated LRRK2 gene on disease pathogenesis has enormous potential to generate insights into the mechanisms of PD and the development of new therapeutic agents (Sundal et al. 2012).

1.3.1.3 VPS35

In 2011 Vilarino-Guell et al. and Zimprich et al., using next-generation sequencing technology identified a missense mutation (p.Asp620Asn) in the vacuolar protein sorting 35 (VPS35) located on chromosome 16p12.1-q12.1. (Vilariño-Güell et al. 2011; Zimprich et al. 2011). This mutation was described as a novel autosomal dominant cause of PD after exome sequencing in affected relatives pairs from large families of Austrian and Swiss origins, respectively. The disease onset for these families was 52 years (range 37–72 years), and the phenotype associated with the Asp620Asn mutation is that of typical PD: asymmetric onset, good L-dopa response, and motor complications. The penetrance was incomplete and age dependent (Bonifati 2014).

VPS35 encodes a subunit of the retromer complex, which is involved in membrane trafficking between endosomes and the trans-Golgi network (Hunn et al. 2015; Bonifati 2014). More recently VPS35 mutations have been shown to impair autophagy and cause SNc neurodegeneration when expressed in rats (Zavodszky, Seaman, and Rubinsztein 2014).

Thus, the discovery of VPS35 mutations implicates the dysfunction of retromer in neurodegenerative processes opening yet another novel pathway of exploration for

therapeutic interventions.

1.3.1.4 GBA

The most recently identified dominant inherited mutation linked to the development of PD is in the glucocerebrosidase gene (GBA), initially described in patients who suffer from Gaucher's disease, a lysosomal storage disease. Patients affected by this disease are homozygous for mutations in GBA while the ones who carry heterozygous GBA mutation have an increased risk in developing PD. For this reason that some authors consider GBA a dominant causal PD gene with reduced penetrance (Anheim et al. 2012; Sidransky, Samaddar, and Tayebi 2009)..

Some mutations are prevalent in specific ethnic groups, such as the Asn370Ser mutation among Ashkenazi Jews. The patients with GBA pathogenic mutations have typical PD with possibly a slightly earlier onset age (Bonifati 2014).

GBA encodes glucocerebrosidase, a lysosomal hydrolase that cleaves the b-glucosyl linkage of glucosylsphingosine and glucosylceramide. Reduced glucocerebrosidase activity is correlated with alpha-synuclein accumulation in sporadic PD (Murphy et al. 2014).

1.3.2 Autosomal recessive genes in PD

Patients bearing homozygous mutations in parkin (PRKN, PARK2), PTEN induced putative kinase 1 (PINK1, PARK6), and Parkinson protein 7 (DJ-1, PARK7) genes, develop early onset PD, usually without atypical signs (Kitada et al. 1998; Enza Maria Valente et al. 2004; V. Bonifati et al. 2003). Also recessive mutations in ATPase type 13A2 (ATP13A2) have been associated with the development of juvenile-onset, levodopa-responsive parkinsonism (Ramirez et al. 2006). Recently other recessive mutations were reported in patients with juvenile levodopa-responsive dystonia-parkinsonism. Among them, phospholipase A2, group VI (PLA2G6), F-box only protein 7 (FBXO7), DNAJC6 and SYNJ1 (Paisán-Ruiz et al. 2012; Zhao et al. 2013; Krebs et al. 2013). The last two encode for auxilin respectively synaptojanin that are two proteins with close roles in the post-endocytic recycling of synaptic vesicles (Bonifati 2014).

In the following sections, the role of the first four genes related with recessive PD development will be briefly presented.

1.3.2.1 Parkin

PARK2 contains 12 exons that encode the 465 amino acid protein, Parkin (Kitada et al. 1998). Mutations in this protein are quite common and explain up to half of the cases with a

clinical diagnosis of familial PD compatible with recessive inheritance and disease onset before the age of 45 years, and also ~15% of the sporadic cases with onset before 45 (Vincenzo Bonifati 2014). The first mutation identified was a homozygous deletion of exon 3-7 (Kitada et al. 1998) followed by other deletions or point mutations that cause PARK2 protein loss of function (Hattori et al. 1998; Hattori et al. 1998; Leroy et al. 1998).

The parkin protein is a cytosolic protein belonging to the family of the RING–between-RING (RBR) E3 ubiquitin ligases (Seirafi, Kozlov, and Gehring 2015). It consists of an amino-terminal ubiquitin-like (Ubl) domain and four zinc-coordinating RING-like domains: RING0, RING 1, IBR, RING2. The Ubl domain is responsible for substrate recognition, proteasome association and regulation of parkin levels and activity while the RING domains are responsible for the ubiquitin ligase-transferase activity (Hristova et al. 2009; Shimura et al. 2000). The E3 ligase proteins are responsible of covalent attachment of ubiquitin and ubiquitin chains to lysine residues or the N-terminal amino group of a substrate protein targeting it for proteasomal degradation. Furthermore, mono-ubiquitination is involved in other cell processes, such as regulation of gene expression and protein sorting, autophagy signaling and lysosomal degradation.

Parkin activity is tightly controlled by multiple mechanisms of auto inhibition centered on the Ubl domain and on binding partners that bind the Ubl domain. However, parkin can be activated under different conditions such as depolarization of mitochondria or epidermal growth factor signaling. Once activated, it ubiquitinates a variety of cytosolic and outer mitochondrial membrane proteins (Sarraf et al. 2013). The ubiquitination of mitochondrial membranes signals the recruitment of the autophagosome and proteasome machinery to initiate the selective autophagic removal of the damaged organelle (mitophagy) (Narendra et al. 2008).

The disease-causing mutations, in line with a loss-of-function pathological mechanism associated with the autosomal recessive inheritance, abolishes the ubiquitin ligase activity. The loss of the Parkin function might lead to loss of quality control pathway and accumulation of impaired mitochondria, which are thought to be a source of toxic reactive oxygen species (ROS) and contribute to neuronal cell death and PD (Seirafi, Kozlov, and Gehring 2015).

1.3.2.2 PINK1

In 2001 the analysis of a large Italian pedigree revealed mutations on chromosome 1 at the PARK6 locus (E. M. Valente et al. 2001; E. M. Valente et al. 2002) leading to the discovery of the second gene involved in early-onset PD. These PARK6 mutation patients

had symptoms clinically identical to those of patients with sporadic forms of PD (Bentivoglio et al. 2001; E. M. Valente et al. 2002). The PARK6 gene encodes a 581 amino called protein acid phosphatase and tensin homolog (PTEN)-induced kinase 1 (PINK1) (Enza Maria Valente et al. 2004). The protein sequence reveals a C-terminal kinase domain and a mitochondrial targeting sequence at the N-terminus, suggesting that it is imported into the mitochondria. In fact, as shown by Valente et al., PINK1 has mitochondrial localization in cells (Enza Maria Valente et al. 2004), which supports the involvement of mitochondrial dysfunction in the pathophysiology of PD.

There is a consistent amount of cell biology studies that report that PINK1 acts upstream of Parkin and is required for Parkin activation and recruitment to depolarized mitochondria, to mediate the selective autophagic removal of the damaged organelle (mitophagy)(Narendra et al. 2008). The precise mechanism is not yet clear, but it is thought that PINK1 accumulates specifically on damaged mitochondria flagging them for elimination. What seems to difference a healthy mitochondrion from a damaged one is PINK1 degradation. In steady state conditions, PINK1 is imported into the inner mitochondrial membrane (IMM) through Transport of the Outer Mitochondrial Membrane (OMM) TOM and TIM complex of the inner mitochondrial membrane (IMM), where it is cleaved by the mitochondrial processing peptidase (MPP) (Greene et al. 2012). Subsequently. PINK1 is cleaved in its hydrophobic domain spanning the inner mitochondrial membrane by presenilin-associated rhomboid-like protein (PARL) (Meissner et al. 2011). This cleavage generates a 52 kDa, an N-terminal-deleted form of PINK1 (Meissner et al. 2011) that is released in the cytosol where it is recognized by its E3 ubiquitin ligase and send to the proteasome for degradation (Yamano and Youle 2013). In the presence of mitochondrial depolarizing agents, OXPHOS inhibitors, genetic or environmental stresses, and even unfolded proteins the mitochondrial import through the TIM complex is disrupted. This prevents PINK1 import in the IMM and its cleavage by MPP and PARL leading to accumulation of uncleaved PINK1 on the OMM (Lazarou et al. 2012; Okatsu et al. 2013). Therefore, upon mitochondrial damage, PINK1 becomes stabilized on the OMM, and from there it recruits Parkin to mitochondria and activates Parkin's E3 ubiquitin ligase activity.

But how a mitochondrial protein can recruit and activate a cytosolic protein?

In the first step, the selective accumulation of PINK1 on the damaged mitochondrion leads to the phosphorylation of low, basal levels of ubiquitin or Parkin present on it (Ordureau et al. 2014; Koyano et al. 2014; Kane et al. 2014). This acts as positive effector as both ubiquitin and Parkin phosphorylation increase Parkin ubiquitin ligase activity (Ordureau et al. 2014; Koyano et al. 2014; Kane et al. 2014).

In fact, the studies of Kane et al., Kazlauskaite et al., Koyano et al., indicate that PINK 1 not only phosphorylates Parkin in its Ubl domain at Ser65 leading to its activation but also ubiquitin at Ser65. Moreover, Ser65 phospho-ubiquitin derepresses Parkin E3 ligase activity (Kane et al. 2014; Kazlauskaite et al. 2014; Koyano et al. 2014). Also, they report that phosphomimetic mutants of ubiquitin Ser65Asp are sufficient for Parkin activation while Parkin Ser65Asp are not (Kane et al. 2014; Kazlauskaite et al. 2014), indicating that ubiquitin phosphorylation is a condition *sine qua non*, in Parkin activation. The study of Ordureau et al., support the hypothesis of a positive loop of activation generated by the phosphorylation, centered in changes of binding affinity. In fact they report that phospho-ubiquitin binds to Ser65 phosphorylated Parkin with 21 times higher affinity that to Parkin (Ordureau et al. 2014).

There are records of other substrates of PINK1 involved in mitophagy such as Miro1, mitofusin2 (Mfn2) that upon phosphorylation at Ser195 and, Thr111 and Ser 442, respectively follows the Parkin-mediated proteasomal degradation pathway (Wang et al. 2011; Chen and Dorn 2013).

The central role of PINK1 kinase activity in mitophagy makes it a target for therapeutic approaches. In a recent study, it was reported that kinetin triphosphate, an ATP analog, rescues kinase activity of a patient mutant form of PINK1 and increases wild-type PINK1 activity, revealing a new way to drug the PINK1/Parkin pathway (Hertz et al. 2013).

1.3.2.3 DJ-1

In 2003, the DJ-1 gene was identified as PARK7. Mutations in PARK7 are associated with autosomal recessive early-onset PD. Several mutations of DJ-1 were found in familial forms of PD. The point mutations L166P and M26I of DJ-1 have been reported to cause DJ-1 destabilization and loss of function (V. Bonifati et al. 2003). DJ-1 is a multifunctional protein that is involved in various physiological processes such as transcriptional regulation, antioxidative defense, and mitochondrial function and signal transduction and dopamine homeostasis (Waak et al. 2009; Zhou and Freed 2005). In fact, it was first identified as an oncogene that cooperated with Ras in regulating cellular transformation (Nagakubo et al. 1997; Cully et al. 2006).

DJ-1 protein is formed of two monomers of 189 amino acids, (Nagakubo et al. 1997) and is ubiquitously expressed throughout the body. Alterations in DJ-1 levels or isoforms have been documented in brains (Bandopadhyay et al. 2004), cerebrospinal fluid (Herbert et al. 2014) and plasma (Waragai et al. 2007) of sporadic PD patients, implying a role also in the common sporadic disease.

A lot of research effort was invested in the characterization of the DJ-1 neuronal putative role in cell protection against oxidative stress (Taira et al. 2004). Many studies focused on deciphering the role of Cys-106, a highly conserved residue (Girotto et al. 2014) as the activity of DJ-1 protein is mainly regulated by oxidation in this residue and in a lesser extent by the oxidation of C46 and C56 (Canet-Avilés et al. 2004; Kinumi et al. 2004; Meulener et al. 2005). This may be due to the reduced pKa value of Cys-106 (5.4) that confers a high reactive cysteine thiolate anion at physiological pH (Witt et al. 2008). Cys-106 also has a marked susceptibility to dopaquinone reactivity It has also been proved that oxidation of Cys-106 has a different but most likely complementary role, which is its ability to drive and control DJ-1 mitochondrial localization.

DJ-1 may regulate different cellular functions depending on its subcellular localization. It has been found to be present in the cytosol, nucleus and to a lesser degree the mitochondria. Upon exposure to growth factors and oxidation of the C106 residue, DJ-1 is translocated to the nucleus where it plays a pivotal role in the regulation of transcription, and specifically antioxidant gene regulation (Ariga et al. 2013).

The role of DJ-1 in autophagy/mitophagy is poorly understood, although it is suggested that a decrease in mitochondrial membrane potential will result in the translocation of DJ-1 to the mitochondria, where mitophagy would be initiated through mechanisms that are still unknown (Krebiehl et al. 2010).

DJ-1 has various other diverse biological implications such as its role in oncogenesis and male infertility (Kahle et al. 2009). Furthermore, it has been found to have chaperone and protease activity, enabling it to inhibit a-synuclein aggregation death (Shendelman et al. 2004; Zhou and Freed 2005). It was recently discovered that DJ-1 is implicated in the protection of neurons from dopamine toxicity. By activating VMAT2 (which transfers dopamine as well as toxic dopamine by products into synaptic vesicles for its exocytotic release), DJ-1 can increase the resistance to dopamine toxicity and to decrease ROS levels in the cell (Lev et al. 2013). Furthermore, DJ-1 regulates the transcription of the tyrosine hydroxylase gene, key enzyme in dopamine synthesis pathway (Ishikawa et al. 2010). It is clear that this protein is critical for maintaining a healthy mitochondrial environment and reducing oxidative stress levels in the cell through major roles in transcriptional regulation and the elimination of ROS (van der Merwe et al. 2015).

1.3.2.4 ATP13A

In 2006, the group of Kubisch described for the first time the role of ATP13A2 in the Kufor-Rakeb syndrome (KRS), a hereditary rare form of early onset PD named after the

Jordanian district where the families involved in the first genetic linkage study lived. The KRS affected patients show juvenile onset PD, the youngest patient was reported as 12 years-old Lithuanian boy (Park, Blair, and Sue 2015), with most of PD clinical symptoms including rigidity, bradykinesia, postural instability, and in some cases cognitive impairment and hallucinations (Park, Blair, and Sue 2015).

ATP13A2 gene encodes a vacuolar/lysosomal P5B-ATPase of around 129 kDa with ten trans-membrane domains, predominantly expressed in the brain with high expression level reached in cortex, thalamus and SNc (Ramirez et al. 2006; Rinaldi et al. 2015). Moreover, ATP13A2 expression was found in dopaminergic neurons from both ventral tegmental area and SNc (Ramirez et al. 2006). The KRS associated mutations are caused by missense or deletion/insertion of few nucleotides that generate a frameshift that alters the transmembrane topology leading to a loss of function of the protein. Exception is made with mutation identified in a Chilean family that falls in an intronic region creating an alternative splicing site that excludes ATP13A2 exon 13 (Park, Blair, and Sue 2015; Ramirez et al. 2006)

ATP13A2 protein is involved in different biological mechanisms ranging from Zn2+ homeostasis that insures correct mitochondrial function to alpha-synuclein lysosomal degradation and internalization in multivesicular bodies (Park, Blair, and Sue 2015; Usenovic et al. 2012; Kong et al. 2014).

1.4 Take home messages

1.4.1 PD related genes play a key role at the presynaptic site

Accumulating pieces of evidence are pointing out how the genes involved in PD have a role in the regulation of the presynaptic activity. Increasing amount of studies associate α-synuclein function to the regulation of exocytosis of neurotransmitter vesicle pools, depicting it as a chaperone for SNARE complexes protecting them from misfolding or non specific associations upon disassembly (reviewed in(Hunn et al. 2015)

Combinatory knock out mice studies indicate that it acts on the same pathway as cysteine string protein-alpha (CSPa), a known SNARE chaperone. Moreover, the study of Garcia-Reibock that used a transgenic mouse that expresses truncated human alpha synuclein (1-120) developing alpha synuclein aggregates, reports that it presents also, age dependent redistribution of SNARE proteins and striatal DA release reduction that translates in reduced locomotion (Garcia-Reitböck et al. 2010). Reduced DA transmission and alteration in the distribution of synaptic vesicles was reported also in a study of the BAC transgenic mouse

that incorporates the human SNCA genomic locus with flanking regulatory elements (Janezic et al. 2013). Furthermore, alpha-synuclein knockout mouse showed an increased evoked DA release, suggesting alpha-synuclein as an activity-dependent negative regulator of dopamine (DA) neurotransmission (Abeliovich et al. 2000). Interestingly, also DJ-1 and PINK1 knockout mice exhibit reduced DA overflow and impaired striatal synaptic plasticity (Kitada et al. 1998). Finally, severe neurotransmission defects have been repeatedly observed in different LRRK2 rodent models [reviewed in (Belluzzi, Greggio, and Piccoli 2012)]. Thus, presynaptic neurotransmitter release could arise as the first pathway compromised in PD and contribute to early stage symptoms of the disease.

1.4.2 PD related genes play a key role in protein clearance

Protein misfolding and aggregation have been instead suggested as the final trigger of the neurodegeneration occurring in the late phase of PD. The first indications are suggesting degradation impairment in neurons were the detection of protein inclusions in post-mortem specimen from PD patients [reviewed in (Cookson 2005)]. The protein inclusions in PD patients may be due to failure of the three major intracellular protein breakdown pathways, the i.e. ubiquitin-proteasome system (UPS), and autophagy and endosome-lysosome system. Protein clearance plays pivotal roles in maintaining the homeostasis of the nervous system: in fact, neurons are particularly prone to accumulate abnormal proteins as they do not regenerate, and proteasomal activity pronouncedly declines with aging. Basal autophagy is especially high in neuronal cells, and neurons undergo degeneration when basal autophagic degradation is disrupted (Cherra and Chu 2008). Autophagy failure seems to underlie a variety of neurodegenerative diseases (Chu 2006) and deregulation of autophagy is evident in the brains of PD patients (Janda et al. 2012). Among brain areas, the SN is particularly vulnerable because the oxidative metabolism of dopamine promotes free radical formation and protein misfolding. Furthermore, dopamine can interact with alpha-synuclein to promote the formation of toxic protofibrils and protein aggregation (Olanow and McNaught 2006). Further confirmation for the linkage between protein clearance and PD came from the observation that the systemic administration of proteasomal inhibitors causes Parkinson-like neuropathological changes, including the formation of Lewy-like inclusions in rodents (McNaught et al. 2002). The investigation of the familial form of PD brought the final confirmation to the connection between impaired protein clearance and PD. In fact, Parkin is an ubiquitin protein ligase (Goldberg et al. 2003) and alpha-synuclein protofilaments, but not oligomers, inhibit the catalytic activity of the 26S proteasome in vitro (Zhang, Tang, and Liu 2008). Finally, mitochondrial autophagy was proved to be regulated by the PD genes Parkin,

PINK1 and DJ-1 (de Vries and Przedborski 2013). Mouse brains or primary neurons with deficiencies in Parkin, PINK1 and DJ-1, exhibit mitochondrial abnormalities that may be due to insufficient mitophagy [reviewed in (Giordano, Darley-Usmar, and Zhang 2014)].

2 LRRK2

2.1 Insight on LRRK2

Mutations in LRRK2 gene (PARK8; OMIM 609007) are linked to late-onset autosomal dominant Parkinson's disease, accounting for up to 13% of familial PD cases compatible with dominant inheritance and 1 to 2% of sporadic PD patients, thus suggesting this protein as the most significant player in PD pathogenesis identified to date. Several single nucleotide alterations have been identified in LRRK2 covering all functional domains, but only five missense mutations clearly segregate with PD in large family studies (Tong et al. 2012). Disease segregating mutations in LRRK2 have been reported in the kinase domain (G2019S, I2020T), the Roc domain (R1441C/G) and in the COR domain (Y1699C) [reviewed in (Mata et al. 2006)]

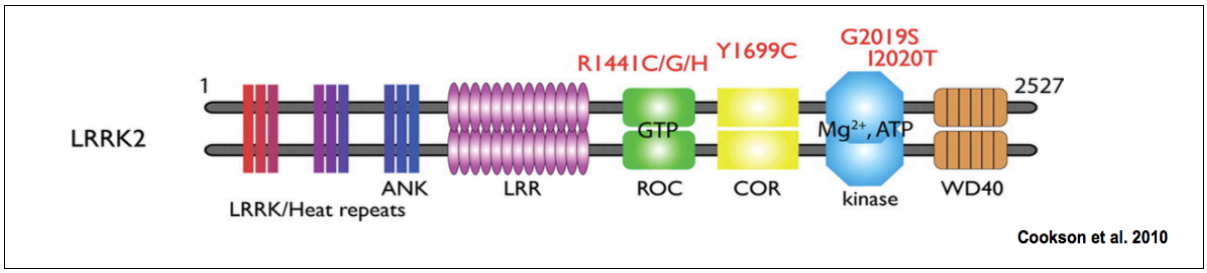

Figure 2. Schematic structure of LRRK2 protein highlighting the most common PD related mutations sites.

The literature suggests that the G2019S mutation in the kinase domain increases LRRK2 kinase activity, whereas mutations in the Roc domain appear to decrease the GTPase activity of LRRK2, to affect protein dimerization and may increase kinase activity [reviewed in (Moore 2008)]. The G2019S mutation has also been identified in Parkinsonism patients with no family history of the disease (Gilks et al. 2005) and accounts for up to 40% of sporadic parkinsonism in certain populations [reviewed in (Benamer and de Silva 2010)]. Clinically and pathologically, the features of LRRK2-associated parkinsonism are often indistinguishable from idiopathic PD [reviewed in (Whaley et al. 2006)]. Thus, this molecule has become one of the most attractive therapeutic targets for scientific investigation, intervention, and neuroprotection in parkinsonism. Although studies show little concordance regarding the level of LRRK2 mRNA/protein expression in the SN, LRRK2 protein

expression has been demonstrated in tyrosine-hydroxylase positive neurons of the SN pars compacta and in medium-sized spiny neurons of the striatum (Mandemakers et al. 2012). At the sub-cellular level, precedent studies showed that LRRK2 is mainly associated with mitochondria but also with multiple vesicles structure, including multivesicular bodies (Alegre-Abarrategui et al. 2009) and synaptic vesicles (Piccoli et al 2014). The LRRK2 protein has a molecular weight of approximately 280 kDa and contains several domains including a Ras/GTPase-like (Roc), a C-terminal of Roc (COR), a kinase (similar to Mitogen-activated protein kinase kinase kinases) and a WD40 domain (Anand and Braithwaite 2009). LRRK2 is a serine/threonine kinase with low endogenous tyrosine kinase activity(West et al. 2005). In particular, LRRK2 preferentially phosphorylates threonine residues with the F/Y-x-T-x-R/K sequence as the main phosphorylation consensus (Pungaliya et al. 2010). In vitro assays have suggested the nature of some LRRK2 substrates, including auto-phosphorylation, moesin, 4E-BP, MKKs, tubulin beta, alpha-synuclein and S15 ribosomal protein (Lobbestael, Baekelandt, and Taymans 2012). However despite its predominance in PD, the physiological function of LRRK2 and the meaning of such phosphorylations are not known and, therefore, the implication of LRRK2 and its kinase activity in the etiology of PD are far from being understood.

2.2 LRRK2 influences synaptic activity

Recent studies have provided strong evidence that LRRK2 impacts directly secretory and endocytic molecular machinery. Shin and colleagues (Shin et al. 2008) demonstrated that LRRK2 interacts with Rab5b, a regulator of endocytic vesicle trafficking. Xiong and colleagues showed that LRRK2 overexpression reduces the rates of synaptic vesicle endocytosis and exocytosis in hippocampal neurons (Xiong et al. 2010). Matta and colleagues proposed that LRRK2 regulates vesicle cycling via phosphorylation of Endophilin A (Mata et al. 2012). The molecular mechanisms underlying these synaptic transmission defects, however, remain largely elusive. Synaptic vesicles undergo in the nerve terminal to high-frequency trafficking cycles thanks to the presence of extremely specialized machinery, allowing very rapid triggering and switching off of synaptic vesicle exocytosis in response to depolarization-evoked calcium influx. The process is finely tuned and depends on the interaction between protein expressed on SV membranes and protein expressed on the presynaptic membranes (Rizo and Südhof 2012). This complex network of interaction is plastically shaped by post-translational modifications: the presynaptic modulation of neurotransmitter release is in fact altered by protein kinases and protein phosphatases

(Turner, Burgoyne, and Morgan 1999) by protein degradation (Ehlers 2003). As wild-type LRRK2 is characterized by a low kinase activity in absolute term, it might be argued that physiologically LRRK2 acts as a scaffold protein and its residual kinase activity is important to regulate monomer-dimer ratio (Sen, Webber, and West 2009). Instead, given the pre and postsynaptic alteration seen in the LRRK2 disease model, an attractive hypothesis is that mutant LRRK2 influences synaptic structure and function through gain-of-function effects on synaptic proteins. One possibility worth to be explored is that LRRK2 pathological kinase activity alters SV trafficking and thus synaptic function via modification of presynaptic proteins. Our hypothesis is that targets of pathological LRRK2 kinase activity might be hidden among LRRK2 interactors.

It will be of critical interest to determine which regulatory proteins in the secretory, endocytic or autophagic pathways, if any, are LRRK2 kinase substrates to gain insight into the pathology. Strikingly, an increased dopamine turnover has been noticed in pre-symptomatic LRRK2 mutation carriers (Sossi et al. 2010). Increased turnover might arise as a compensatory mechanism to counteract DA-neurons loss (Adams et al. 2005), but it has also been suggested that increased DA turnover might by itself contribute to the progression of disease secondary to DA associated toxicity (Zigmond, Hastings, and Perez 2002). The dysregulation of DA cycle might arise as one the first biological pathway compromised during PD onset and account for premotor symptoms happening in the preclinical stage of the disease.

2.3 LRRK2 modulates protein clearance

While a presynaptic impairment might indeed explain early stage or preclinical manifestation of PD, it is difficult to envisage how aberrant vesicle release could cause the neuronal loss in the substantia nigra reported in the late phase of the disease. Post-mortem brain investigation demonstrated that LRRK2G2019S kindred most often show synucleinopathy, occasionally tauopathy, suggesting a role for LRRK2 in protein inclusion pathology (Taymans and Cookson 2010). Recent studies showed that LRRK2 overexpression led to proteins accumulation without affecting the catalytic activity of the proteasome or expression levels of proteasomal core sub complexes (Lichtenberg et al. 2011; Skibinski et al. 2014). Interestingly, a recent paper by Tong and collaborators shows that loss of LRRK2 causes accumulation alpha-synuclein, increased autophagy and cell death in kidneys of aged mice (Tong et al. 2012). An impaired autophagic balance has been observed upon overexpression of LRRK2 in neuronal, non-neuronal and yeast cells (Gómez-Suaga et al.

2014). This comes in agreement with findings showing that a significant portion of endogenous LRRK2 is localized to membranous structures including endosomes, lysosomes, and phagosomes (Schapansky et al. 2014). Finally, experimental evidence suggests that LRRK2 kinase activity controls autophagy via the modulation of Ca2+ release from lysosomes in an mTOR-independent manner (Gómez-Suaga et al. 2014). All together, these data clearly suggest a tight implication of LRRK2 in the regulation of protein clearance via autophagy. Although alpha-synuclein is a major component of LB, immunohistochemical studies have shown that LB contains more than 90 molecules. Intriguingly, several proteins we have described as LRRK2 interactors (Piccoli et al. 2014, Piccoli et al. 2011) have been found in LB [i.e. AP-2, HSP-90, spectrin, clathrin heavy chain, CADPS, VPS-35 (Xia et al 2008)] or in the related intranuclear inclusion body [i.e. NSF, dynamin, MUNC-18-1, Rab3A and HSP-90 (Pountney et al. 2008)]. There is a consensus that LRRK2 phosphorylates threonine residues flanked by positively charged residues such as lysines (Pungaliya et al. 2010). Interestingly, lysine residues are the acceptor site for ubiquitination reaction. Ubiquitin chains tags on lysine residues are the major signal directing proteins towards degradation. Ubiquitinated proteins are cleared via either proteasome or autophagy. Also, the endosome-lysosome system is likewise regulated by ubiquitin [reviewed in (Luzio et al. 2009).

2 Aims of study

Mutations in the LRRK2 gene account for 1-2% of all PD cases and are associated with a form of dominantly inherited PD with clinical and pathological presentation similar to the sporadic syndrome. We have provided robust demonstration that LRRK2 acts at the presynaptic site. Moreover, our previous data suggest that LRRK2 binds and phosphorylates presynaptic targets and that G2019S mutation in LRRK2 associated with altered neurotransmitter release. Here we investigated whether G2019S mutation might affect presynaptic function in short term and substrate clearance in long term. Next, we evaluated the feasibility of two potential therapeutic strategies: the first implies the use of LRRK2 kinase inhibitors while the second focuses on treatment ameliorating protein degradation via induction of autophagy. In order to address the goals outlined above, we achieved these objectives:

1. **LRRK2 G2019S pathological function at the synaptic site.**
   We have identified the substrates of LRRK2 kinase activity and evaluated the functional outcome of these modifications, by studying the SV dynamics and neuronal morphology of cortical neuronal cultures derived from BAC human LRRK2 G2019S mouse.
2. **LRRK2 G2019S impact on substrate clearance**
   We evaluated whether LRRK2 phosphorylation influences the ubiquitination of the substrates for LRRK2 kinase activity and we investigated the mechanism underlying such effect
3. **Pharmacological treatment to counteract LRRK2 G2019S dysfunctions**
   We characterized a murine model of G2019S LRRK2 mutation in terms of protein clearance focusing on the characterization of a biochemical and motor phenotype of BAC human LRRK2 G2019S mouse model. Next we evaluated the feasibility of a treatment stimulating protein clearance in this animal model.

3 Materials and methods

1 Animals

Non-transgenic wild-type (WT) and BAC LRRK2 G2019S (GS) mice, back-crossed on a C57BL/6J strain, were a kind gift from Prof. M. Morari after agreement with Dr. Heather Melrose at MayoClinic (Jacksonville, FL, USA) (Melrose et al. 2010). Animals were kept following guidelines of Ministry of Education, Universities and Research (MIUR) in a normal light/dark cycle (12 hours light/ 12 hours dark) and had free access to food and water.

2 Plasmids, lentiviral vector constructs and virus production

pCHMWS 3xFlag-tagged LRRK2 wild-type, K1906M and G2019S, 2x-Myc LRRK2 LRRK2 –GFP constructs have been previously described (Civiero et al. 2012)(Civiero et al 2012)], NSF constructs (full-length and domains) were cloned into p3XFLAG-CMV-7.1 vector (Sigma-Aldrich).

NSF mutants were generated using the QuickChange mutagenesis kit (Agilent Technologies, CA, USA) according to the manufacturer's instructions. All plasmids were validated by restriction analysis and DNA sequencing.

Myc ubiquitin and HA ubiquitin constructs were bought from Addgene.

Lrrk2 silencing sequences were identified as presented in (Piccoli et al. 2011). The silencing sequence (5'-3') for both human and murine Lrrk2 is mib3, AAGTTGATAGTCAGGCTGAAT while AGTGCTCCCGGTATCAGATG olig 6 sequence was used for the silencing of murine Lrrk2. The sequences were synthesized and cloned into green fluorescent protein (GFP)-expressing pLVTH as described in Bauer et al. 2008.

The lentiviral viruses were produced by transient transfection of HEK293T cells according to standard protocols (Wiznerowicz and Trono 2003).

3 Cell culture, transfection and drug treatments

Neuron cultures were prepared from the mouse cortexes obtained from embryonic day 15.5–16.5 Wild-type or GS mice (C57BL/6J). Briefly, after brain dissection the cortexes were mechanically dissociated after 15 min incubation with 2,5% Trypsin (Euroclone) at 37

°C in agitation. The resulting cells were counted and plated on previously poly-D-lysine (Sigma) treated wells or cover slips, according to the desired density. High density (750–1000 cells/mm2) and medium-density (150–200 cells/mm2) neuron cultures were plated and grown on 12-well plastic tissue culture plates (Iwaki; Bibby Sterilin Staffordshire, UK) or 12mm diameter cover slips put into 24-well plastic tissue culture plates (Iwaki) at 37°C and 5% CO2 (Piccoli et al., 2007). Neuronal transfection was carried out using Lipofectamine 2000 (Life Technologies) following the manufacture's instruction. The cells were treated with LRRK2 kinase inhibitor, GSK-2578215A (Tocris Bioscience, Bristol, UK), MG132 (Tocris Bioscience, Bristol, UK) and Trehalose (Sigma) by addition to culture media at the concentrations indicated through the text.

Human embryonic kidney cells (HEK293T) were cultured in DMEM complete: Dulbecco's modified Eagle's medium (DMEM, Euroclone) supplemented with 10% fetal bovine serum (FBS, Euroclone) at 37°C and 5% CO2. HEK293T were transiently transfected using linear polyethylenimine (PEI, Polysciences) with ratio DNA: PEI 0.8:100. 4 µg of DNA were dissolved in 0.5 ml of PEI solution and vortexed for 20 sec. Then, the DNA-PEI mix was incubated for 10 minutes at room temperature (RT). Finally, the solution was added directly to the cells in Petri dishes of 10 cm2 and used after 48-72 hours.

4 Antibodies, SDS-PAGE and western blot analysis

Antibodies used for Western blotting were as follows: anti-Flag M2 (Sigma-Aldrich), anti-NSF (Cell Signaling), anti-LRRK2 (MJFF2, Abcam), anti-actin (Sigma), anti-Myc (Millipore), anti-HA (Millipore). Between 10 and 20 µg of protein samples were resolved on to 10-15% Tris-glycine polyacrylamide gels in SDS/Tris-glycine running buffer. Precision plus molecular weight marker (Biorad) were used for size estimation. Solubilized proteins were then transferred to nitrocellulose or polyvinylidenedifluoride (PVDF) membranes in blotting buffer containing 10% methanol. The membranes were blocked in 5% nonfat dry milk in Tris-buffered saline and 0.1% Triton (TBS-T) for 1 hour at RT and then incubated overnight at 4°C with primary antibody in blocking solution. The sheets were washed in TBS-T (3x10 min) at RT followed by incubation for 1 h at RT with horseradish peroxidase-conjugated anti-mouse/rat/rabbit IgGs. Blots were then washed in TBS-T (3x10 min) at RT, and immunoreactive proteins were visualized using enhanced chemiluminescence plus (ECL+, GE Healthcare, Little Chalfont, England). Densitometric analysis was carried out using Image J software.

5 SypHy assay

Cortical cultures were generated from E16.5 embryos from Wild-type and GS mice as previously described. At DIV3 primary neurons were infected with viruses expressing sypHy, a fusion construct of synaptophysin and super ecliptic pHluorin (Granseth et al. 2009). Neurons were chronically treated with 0.2um GSK or DMSO every two days starting at DIV 0. SypHy positive boutons were assayed in a stimulation chamber on the stage of an Applied Precision Delta Vision RT microscope. The assay was carried out as described previously (Sankaranarayanan & Ryan 2000). Briefly, cells were submerged in 200µl of KRH Buffer (25mM HEPES, 130mM NaCl, 5mM KCl, 6mM D-glucose, 1.3mM MgSO4, 1.2mM KH2PO4, 2mM CaCl2, pH 7.4) plus 25µM CNQX and 50µM APV inhibitors of AMPA and NMDA receptors. SypHy was excited at 475 nm and its fluorescence emission collected at 525 nm using a 60X, oil immersion objective. Images were acquired every second for 200 seconds using TillVision software (TILL Photonics). At frame 30, cells were stimulated with 40 action potential (AP) (20Hz) then at frame 70 with 300 AP (20 Hz). Total fluorescence was measured upon incubation with 50mM NH4Cl. Quantitative measurements of the fluorescence intensity at individual boutons were obtained by averaging a selected area of pixel intensities using ImageJ. Net fluorescence changes (ΔF) were obtained by subtracting the average intensity of the first 15 frames (F0) from the intensity of each frame (Ft) for individual boutons and normalized F0 (ΔF/F0). The fluorescence increase and decay, reflect exo- and endocytosis, respectively [28]. Both the fluorescence upstroke and decay were fitted with a single exponential τ (τupstroke and τdecay respectively). Data are expressed as mean ± SEM and statistical significance were assessed by unpaired two-tailed Student's t-test (GraphPad Prism).

6 Exo-endo

At DIV 14 Wild-type or GS cortical neuronal cultures were incubated for 5 min at 37°C with rabbit anti-synaptotagmin 1 (SynapticSystem) 1:400 in DMEM (Euroclone). The cells were then washed for 3x with PBS 1X and fixed with 4% paraformaldehyde, 4% sucrose in PBS. The antibody used in this initial phase, recognizes the intravesicular domain of synaptotagmin 1 that is exposed to the neuronal membrane after the vesicles exocytosis, marking the recycling synaptic vesicles (SV). After fixation and permeabilization, a synaptophysin counterstaining with mouse anti-synaptophysin, 1:400 (Sigma-Aldrich) visualized the totality of SV. Acquired images were processed and quantitatively analyzed

with ImageJ software using the analyse particles function to automatically count synaptophysin positive clusters and synaptophysin positive clusters present in the region of interest.

7 Morphology analysis

Wild-type and GS cortical neurons plated on 12mm diameter cover spills treated with poly-D-lysine at a medium-low density (111-150 cells/mm2) were transduced at DIV 3 with mib3 (human and murine LRRK2 shRNA), olig 6 murine LRRK2 shRNA and c1 scramble shRNA for control using a viral MOI (Multiplicity of Infection) of 3. The cells were chronically treated with LRRK2 inhibitor GSK as previously described, and fixed at DIV 14 with 4% paraformaldehyde, 4% sucrose in PBS. Images were acquired using an Axioplan Zeis Epifluorescence microscope and the neurites were tracked using NeuronJ.

8 Immunocytochemistry

DIV 14 GS and Wild-type neurons previously treated or transfected were fixed for 10 min at RT with 4% para-formaldehyde, 4% sucrose pH 7.4. Fixed cells were washed three times with PBS 1X for 10 min, and then incubated over night at 4oC with primary antibody diluted in GDB 1X (0.1% gelatin, 0.1% Triton X 100, 450mM NaCl). We used as primary antibodies: mouse anti-NSF (SySy 1:500) and rabbit anti-caspase 3 clivated (Life Technologies 1: 200). After 3 washes with High Salt solution (NaCl 500mM, NaPO4 20mM) 10 min each, the coverslips were incubated for 1 hour at RT with the secondary antibodies anti-rabbit Alexa 630 (1:500), anti-mouse Alexa 555 (1:500) and Dapi 1:2000 in GDB 1X. Then they were washed three times in High Salt solution, 10 min each and once in PBS. After washing thoroughly with PBS, coverslips were rinsed in distilled water and mounted on glass slides with MOVIOL. The mounted coverslips were kept at 4°C until observation under with laser scanning confocal microscope Zeiss LSM 510.

9 Proteasome activity assay

Proteasome activity of GS and Wild-type brain tissue was analysed following the 20S Proteasome activity assay kit protocol Millipore (APT280). The assay is based on the detection of the fluorophore 7-Amino-4-methylcoumarin (AMC) after cleavage from the labeled substrate LLVY-AMC. The free AMC fluorescence is quantified using a 380/460 nm

filter set in a fluorometer. Briefly, 3µg of protein from each sample was incubated for 1 h at 37°C with proteasome labeled substrate in 96 dark multiwells. In parallel we test the sensibility of the assay performing a dilution series of proteasome positive control (1:4 to 1:256) by diluting the stock solution in 1X Assay buffer. Fluorescence data was collected using a PE Biosystems CytoFluor 400 plate reader using a 380 nm excitation and 460nm emission filters.

10 Tube

12 or 6 months old GS and Wild-type mice whole brains were lysed my mechanical homogenization in 5ml glass potters followed by 1 h incubation at 4°C in rotation in 5 ml of lysis buffer (50mM HEPES pH 7.4, 150mM NaCl, 1% Triton X-100, 0.5mM EDTA, protease inhibitors (Calbiochem) and phosphatase inhibitor cocktails II and IV (Calbiochem). The samples were centrifuged for 15 min at 15000xg at 4°C and the surnatant was recovered. The amount of protein was determined by interpolation to a Bradford-BSA standard curve. 1 mg of protein from each sample was incubated for 2h at 4°C in rotation with the previously equilibrated Agarose TUBE resin in 50mM HEPES pH 7.4, 150mM NaCl. Then the agarose beads were washed in 50mM HEPES pH 7.4, 150mM NaCl, 1% Triton X-100, 0,2% Triton X-100, and the ubiquitinated proteins bound to the resin were eluted in 60µl of Laemil buffer 1X after 10 min incubation at 52°C. The immunoprecipitated proteins were analysed through SDS-PAGE and western blot as previously described.

11 Immunoprecipitation

HEK293T cells were transiently transfected for 48 hours with LRRK2 G2019S–GFP, NSF WT–N-terminal Strep-Flag and Myc-ubiquitin and treated for 24 hours with 10 µM MG132 with or without 2 µM LRRK2 kinase inhibitor IN-1. The cells were resuspended in 5ml ice cold PBS 1X, centrifuged at 150xg for 5 min and lysed in 1 ml of 50mM HEPES pH 7.4, 150mM NaCl, 0.5mM EDTA, 0.5% Triton X-100, protease inhibitors (Calbiochem) and phosphatase inhibitor cocktails II and IV (Calbiochem), after incubation for 1 h at 4°C in rotation. The cell lysate was recovered after 10 min centrifugation at 15000xg at 4°C and 10% of supernatant was kept as input. The remaining supernatant was incubated with 50 µl of strep resin (50% ethanol) for 1 hour at 4°C in rotation. The beads were then washed 3X with 0.5 ml of 50mM HEPES pH 7.4, 150mM NaCl, 0,2% Triton X-100 and NSF bound was eluted in three elution steps in Biotin elution buffer.

The eluted NSF was next incubated with 30 µl of FLAG M2 resin (Sigma) for 1 hour at 4°C in rotation.

The resin was then washed 3X with 0.5 ml of 50mM HEPES pH 7.4, 150mM NaCl, 0,2% Triton X-100, and the protein eluted in 60µl of Laemil buffer 1X after 10 min incubation at 52°C. The immunoprecipitated proteins were analysed through SDS-PAGE and western blot as previously described.

12 Protein purification

Human NSF with a N-terminal Strep-Flag tag and human LRRK2 G2019S with a 3X Flag tag were purified from HEK293T cells after transient transfection as following. Cells were resuspended in 1 ml of a Lysis buffer (20mM Tris-HCl pH 7.5, 150mM NaCl, 1mM EDTA, 2.5mM Na4P2O7, 1mM beta-glycerophosphate, 1mM Na3VO4, Protease Inhibitor Mixture (Sigma-Aldrich)) and then lysed with 5 cycles of freezing and thawing in liquid nitrogen. The cell lysate was collected after centrifugation at 15000xg for 40 minutes at 4°C. The supernatant was incubated overnight with 40µl of Anti-Flag M2 Affinity gel (Sigma-Aldrich) at 4°C in rotation. After 1 min centrifugation at 2000xg, the supernatant was discarded and the beads with human NSF or LRRK2 G2019S were washed with 1 ml of different buffers. For NSF the washing buffers is Tris-HCl pH 7.5, 150mM NaCl used for four times while for LRRK2 G2019S the washing buffers are: WB1 (20mM Tris-HCl pH 7.5, 500mM NaCl, 1% Triton X-100) twice, WB2 (20mM Tris-HCl pH 7.5, 300mM NaCl, 1% Triton X-100) twice, WB3 (20mM Tris-HCl pH 7.5, 150mM NaCl, 1% Triton X-100) twice, WB4 (20mM Tris-HCl pH 7.5, 150mM NaCl, 0.1% Triton X-100) twice, WB5 (20mM Tris-HCl pH 7.5, 150mM NaCl, 0.02% Triton X-100). The proteins were eluted by incubating the beads with 100 µl of 20mM Tris- HCl pH 7.5, 150mM NaCl with 150 ng/µl Flag peptide for NSF and 3xFlag peptide for LRRK2G2019S at 4°C in agitation for 30 min. The sample was centrifuged to pellet the resin, and the supernatant was collected. The elution step was repeated and the resulting elutions combined at a final volume of 200 µl. Purified proteins were separated on SDS-PAGE and quantified by comparison with different concentrations of BSA (Bovine Serum Albumin). Proteins were electrophoretically resolved on 10% Tris-glycine polyacrylamide gels (Biorad) using SDS/Tris-glycine running buffer. To estimate the molecular weight of proteins Precision Plus molecular weight marker (Biorad) was used. After the run, proteins were stained with Coomassie Brillant Blue to enable the quantification with ImageJ software.

13 Kinase assay

NFS and LRRK2 G2019S purified human proteins at a ratio of 2:1, were incubated in 25mM 25mM Tris-HCl pH 7.5, 5mM beta-glycerophosphate, 2mM DTT, 0,1mM Na3VO4, 10mM MgCl2, 5mM ATP for 3 hours at 30°C in agitation. The reaction was stopped by adding 600µl of ubiquitination buffer (40mM HEPES, pH 74, 40mM NaCl, 5mM $MgCl_2$ plus protease and phosphatase inhibitor cocktails Calbiochem).

14 In vitro ubiquitination

In order to eliminate LRRK2 G2019S protein from the kinase assay reaction product dissolved in 600 µl of ubiquitination buffer (40mM HEPES, pH 74, 40mM NaCl, 5mM MgCl2 plus protease and phosphatase inhibitor cocktails Calbiochem), the phosphorylated NSF protein was bound to Strep resin beads after 2 hours incubation with 50µl of Strep resin previously equilibrated in 500µl of ubiquitination buffer. The beads were washed 3 times with 500 µl ubiquitination washing buffer (40mM HEPES, pH 74, 40mM NaCl, 5mM MgCl2 , 0,2% Triton X-100) and divided for the incubation with the in vitro ubiquitination reaction mix (1 µg of Myc-Ubiquitin transfected or control not transfected HEK cells lysate diluted in 40mM HEPES, pH 74, 40mM NaCl, 5mM MgCl2 , plus 5mM ATP, 0.1mM MG132, 0.2mM PR-619) for 30 min at 37°C at 700 rpm. The reaction was stopped by a short centrifugation at 2000xg and removal of the supernatant. The beads were washed once with 1 ml of UB 1x, and the ubiquitinated NSF bound was eluted in 60µl of Laemil buffer 1X after 10 min incubation at 52°C.

15 Filter assay

DIV 14 high-density GS and Wild-type cortical neurons treated for 24 h with 100mM Trehalose (Sigma) and controls, were rinsed once in cold PBS 1X and mechanically detached in PBS 1 X plus protease and phosphatase inhibitor cocktails Calbiochem (40 µl/well 12 wells plate). Every two wells were pulled together and sonicated 3x with 1s pulse and 1s stop sequence at 10% pulse amplitude. The protein quantity was determined by interpolation at a BSA standard curve, and 10 µg of each sample were diluted to 120 µl pre-loading volume in PBS 1X. Through a dot blot void system, the samples were exposed to a previously methanol equilibrated cellulose acetate membrane that keeps on its surface the protein aggregates. The membrane was saturated for 1 h at RT in 5% nonfat dry milk in Tris-buffered saline and

0.1% Triton (TBS-T) and then incubated with the primary antibody mouse anti-NSF (SySY) (1:1000) or mouse anti Rab3A (SySY) 1:1000 in saturating solution for 90 min at RT. The unbound primary antibody was sheets was washed out in TBS-T (3x10 min) at RT and the membrane was incubated for 1 h at RT with horseradish peroxidase-conjugated anti-mouse IgGs. After 3 washes in TBS-T 10 min/each at RT, the immunoreactive proteins were visualized using enhanced chemiluminescence plus (ECL+, GE Healthcare, Little Chalfont, England). Densitometric analysis was carried out using Image J software.

16 Immunohistochemestry

6 and 12 months old Wild-type and GS mice were anesthetized with avertine and transcardially perfused with PBS followed by 4% paraformaldehyde in PBS. Brains were dissected, postfixed for 2 h in 4% paraformaldehyde at 4°C, and then placed into a 30% sucrose solution in PBS for 24 h. Brains were sectioned coronally on a Leica microtome with cut thickness of 30 µm. Free floating brain sections were quenched for 15 min in TBS 1X plus 3% H_2O_2, 10% methanol at RT, then washed three times with TBS 1X. Sequently the slices were saturated in TBS 1X plus 3% BSA, 10% NGS, 0,1% Triton X-100 for 90 min in agitation at RT and incubated with the primary antibody (mouse anti-NSF 1:1000) O/N at 4°C in agitation. Next, the sections were washed 2 times /10 min each, in TBS 1X – 0.1% Triton X-100 and incubated for 30 min with the blocking solution TBS 1X plus 3% BSA, 10% NGS, 0,1% Triton X-100 and for 2 hours with the secondary antibody anti-mouse HRP 1:200 at RT in agitation. The slices were incubated for 1 h with Vectastain ABC kit 1:1 mix (Vectorlab), washed 3 times in TBS 1X – 0.1% Triton X-100 and developed with DAB quanto mix (Thermo Scientific) for 30 sec. The stained sections were rinsed in TBS 1X, dehydrated and mounted using DPC mounting reagent (Sigma) and kept at RT until acquisition with a Zeiss Axio Imager m2m.

For immunofluorescence, the blocked sections were incubated with the primary antibody as previously described, followed by incubation with Cy3-conjugated goat anti-mouse (1:500 Life Technologies), and mounted on poly-lys coversplips using the Calbiochem mounting reagent. The stained sections were kept at 4°C until acquisition with Zeiss Axio Imager m2m.

17 Trehalose treatment

At 4 or 10 months, Wild-type and GS male littermates were divided into Trehalose and control groups. In the Trehalose group, mice were treated daily for 2 months with 1%

Trehalose drinking water solution. The treatment solution was changed every week. In the control group, mice were given untreated drinking water. Mice body weight was measured every week since the start of treatment.

18 Behavior

18.1 Spontaneous motor activity

Motor function was evaluated in an activity cage (43 × 43 × 32 cm) (Ugo Basile, Varese, Italy), placed in a sound attenuating room, as previously described (Sala et al. 2011). The cage was fitted with two parallel horizontal and vertical infrared beams located 2 cm and 4 from the floor, respectively. Before the start of the test each mouse was habituated to the testing room for 1 h. Cumulative horizontal and vertical movement counts were recorded every 10 min for 180 min.

18.2 Balance Beam walking

The beam apparatus consists of 1-meter beams with a flat surface of 12mm or 6mm width resting 50 cm above the tabletop on two poles. A black box is placed at the end of the beam as the finish point. Nesting material from home cages is placed in the black box to attract the mouse to the finish point. A lamp (with 60 watt light bulb) is used to shine light above the start point and serves as an aversive stimulus. A video camera is set on a tripod to record the performance. On training days, each mouse crosses the 12mm beam 3 times and then the 6mm beam 3 times. The time required to cross to the escape box at the other end (80 cm away) is measured a stopwatch. The stopwatch is started by the nose of the mouse entering the center 80 cm, and stopped when the animal reaches the end of the 80 cm. Once the mice are in the safe box, they are allowed some time (~15 secs) to rest there before the next trial The mice rest for 10 min in their home cages between training sessions on the two beams. On the test day, times to cross each beam are recorded. Two successful trials in which the mouse did not stall on the beam are averaged. The beams and box are cleaned of mouse droppings and wiped with towels soaked with 70% ethanol and then water before the next beam is placed on the apparatus.

18.3 Pole test

In the vertical pole task, the mouse was placed on a vertical wire-mesh pole with its head facing upwards. Mice were habituated to the task in 2 trials per day for 2 days. On test day (third day) mice were subjected to 5 trials: the total time taken to turn the body and to descend was recorded according to Hickey et al. (2008). A cut-off of 60sec was given. Data were shown as mean of 5 trials evaluated during the test day.

18.4 Hanging wire test

Each mouse was placed on a wire cage lid and the lid was gently moved back and forth so as to enable the mouse to grip the wire according to Glynn et al. (2005). The lid was then turned upside down about 15 cm above the surface of the bedding material. Latency to fall onto the bedding was recorded with a cut-off of 180 sec.

18.5 Rotarod

The rotarod apparatus (Ugo Basile, Biological Research Apparatus, Varese, Italy) was used to measure fore and hindlimb motor coordination and balance. During the training period, each mouse was placed on the rotarod at a constant speed (12 or 32 rpm) for a maximum of 120sec, and the latency to fall off the rotarod within this time period was recorded. Mice received four trials per day for 4 consecutive days. The fourth trial of each day was evaluated for statistical analysis.

18.6 Novel Object recognition (NOR)

Object recognition was conducted over a two-day period in an open plastic arena (38cm × 30cm × 18cm) (Fig. 1). The apparatus was illuminated by a fluorescent lamp placed centrally above it (75W). The animals were first habituated to the test apparatus for 10 min on day 1 and then subjected to a familiarization trial (T1) and a novel object recognition trial (T2) on day 2. In NOR, real objects were used. They consisted of white plastic cylinders and coloured plastic Lego stacks of different shapes. Each mouse was placed in the centre of the arena between the two objects for a maximum of 20 min or until it had completed 30 s of cumulative object exploration. Object recognition was scored when the animal was within 0.5 cm of a object with its nose towards the object. Exploration was defined as follows: directing the nose to the object and/or touching the object with the nose. Sitting on, or leaning to, an

object was not considered to be an exploratory behavior. Care was taken to minimize the difference between the to-be discriminated objects in order to prevent a greater preference for one of the two objects. An experimenter blind to the treatment group manually recorded the exploration times to the objects in each animal. Mice that did not explore any of the two objects for at least 30 s during T1 were excluded from the data analysis. During T2 each mouse was placed again in the same arena (retention session) in which one of the two identical familiar object was replaced with a novel one.

4 Results

1 LRRK2 G2019S mutation influences SV trafficking

Previous work of our group demonstrated that LRRK2 controls synaptic transmission acting as a presynaptic scaffold (Piccoli et al. 2011; Piccoli et al. 2014) and that inhibition of LRRK2 kinase activity impairs SVs trafficking, indicating a role for LRRK2 catalytic activity in SV fusion cycle (Cirnaru et al. 2014). Our recent data further depicts the role of LRRK2 kinase activity at the presynapse. We have recently identified the presynaptic ATPase NSF as a substrate of LRRK2 kinase activity, which once phosphorylated displays enhanced ATP hydrolysis and SNARE complex dissociation activity in vitro (Belluzzi et al. 2015; appendix). These effects disappeared when we mutated the threonine 645 in the ATP binding pocket of D2 domain of NSF with an alanine, indicating this residue as *bona fide* LRRK2 phosphorylation site on NSF. Moreover, we confirmed the role of LRRK2 kinase activity in SV recycling. All together, these data arose the need to analyze the impact of LRRK2 G2019S, pathologic hyperactive kinase mutation, at the presynaptic site. For this purpose, we analyzed the dynamics of SV fusion through sypHy assay in the primary cortical culture obtained from BAC hLRRK2 G2019S (GS), and wild-type E18 mice chronically treated with 0.2µM GSK or DMSO as control. SypHy is a pH-sensitive fluorescent reporter that, by analogy with the original synaptopHluorin (synaptobrevin-pHluorin, (Sankaranarayanan et al. 2000; Miesenböck, De Angelis, and Rothman 1998) is quenched in the acidic intracellular space of the SV and will only become fluorescent upon SV fusion, when the contents of the SV is exposed to the more basic pH of the extracellular space. As shown in figure 3 B, at the onset of the stimulus, exocytosis caused a rapid increase in sypHy fluorescence, which after cessation of the stimulus, through endocytosis, slowly returned to baseline (Fig.3 A-B). The first stimulus, 40 AP, is predicted to mobilize SV belonging to the ready releasable pool while 300 AP are sufficient to trigger the fusion of SV belonging to the total recycling pool. We measured a significant increase of fluorescence in GS neurons impaired to the wild-type upon either 40 or 300 AP stimuli (Figure 3 C), that is cancelled upon GSK treatment (Fig 4). These results confirmed our expectation that hyperactive LRRK2 kinase activity influence SV fusion. Nonetheless, we wanted to exclude a dysregulation in the functioning of vacuolar H+ATPase responsible for the acidification of the endocytic vesicles (Inoue et al. 2005; Morel and Poëa-Guyon 2015). For this, we analyzed the effect of LRRK2 G2019S mutation

on the presynaptic SV recycling by exposing living GS and wild-type DIV 14 neuronal cultures to rabbit polyclonal antibody directed against the intraluminal vesicular NH2 terminus domain of synaptotagmin 1 (Matteoli et al. 1992). Upon endocytosis, the antibody is trapped inside the vesicle lumen, marking the recycling vesicle. To track the neuronal processes, the cells were infected at DIV 4 with control GFP-expressing virus. The cycling vesicles appear as clusters positive for synaptotagmin 1 and synaptophysin. In agreement with the results obtained with the sypHy assay, we observed a significant increase of synatptagmin positive clusters in GS neurons compared to the Wild-type (Fig.5) Interestingly the chronic treatment with GSK significantly reduced the amount of synaptotagmin positive clusters. Nonetheless, in this case, the treatment had no effect on the SV recycling in the Wild-type neurons. This might be due to the difference of the events detected by the two assays: synchronous neurotransmitter release trigger by action potential in the case of the sypHy assay and spontaneous exocytotic events in the last one characterized by different regulation in SNARE complex formation (Ramirez et al. 2006).

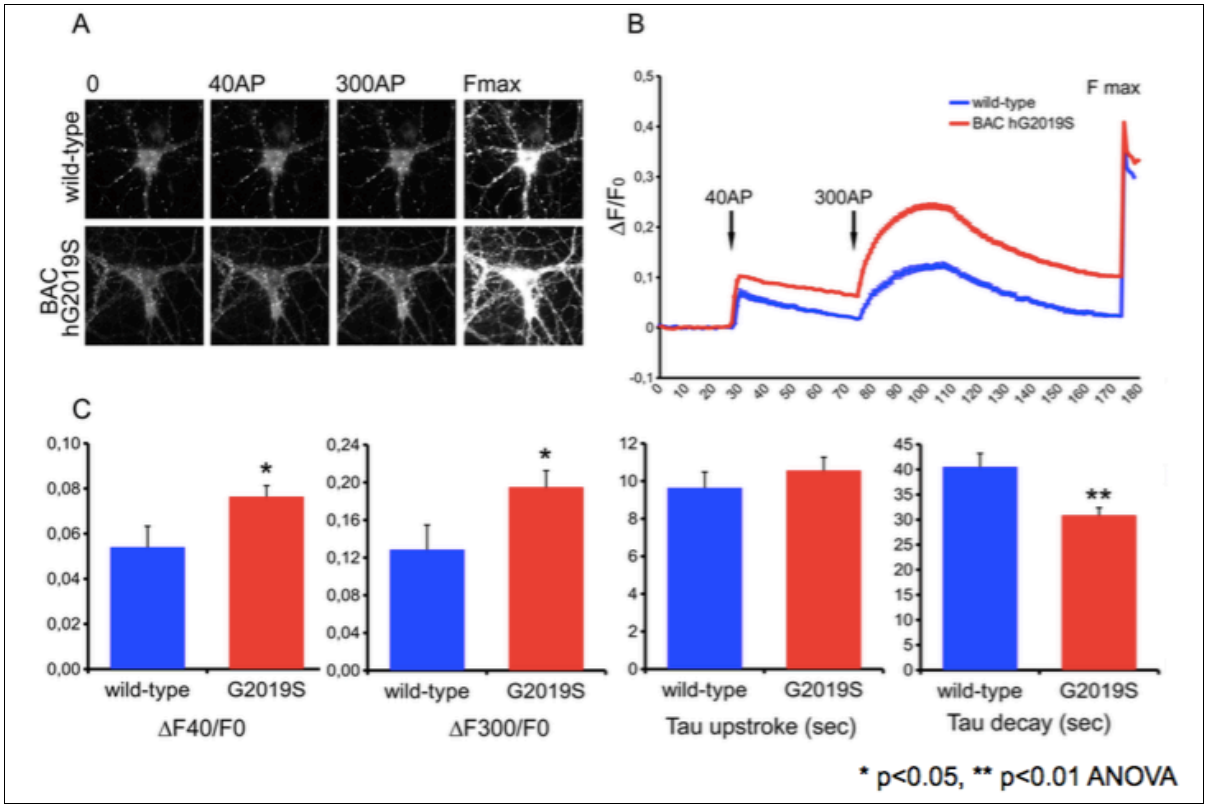

Figure 3. (A) Synaptophluorin fluorencesce was recordered from DIV 14 wild-type and BAC hLRRK2 G2019S (BAC hG2019S) cortical neurons. Representative snapshots were taken from 1Hz recordings at rest (0), after 40 action potential stimulation (40AP), after 300 action potential stimulation (300AP) and upon neutralization with 50mM NH_4Cl, F (max). (B) The graph shows rappresentative pattern of fluorescence. The Y-axis reports the ΔF/F0 at the given time point (second). (C) the graphs report the increase in the fluorescence after 40 AP (ΔF40/F0) and 300 AP (ΔF300/F0) and the kinetic signal after 300AP expressed as time constant describing the increase (tau uspstroke) and decay (tau decay) of fluorescence. Data are expressed as mean ± SEM, n=4, at least 50 boutons from minimum 6 neurons were analyzed per experiment.

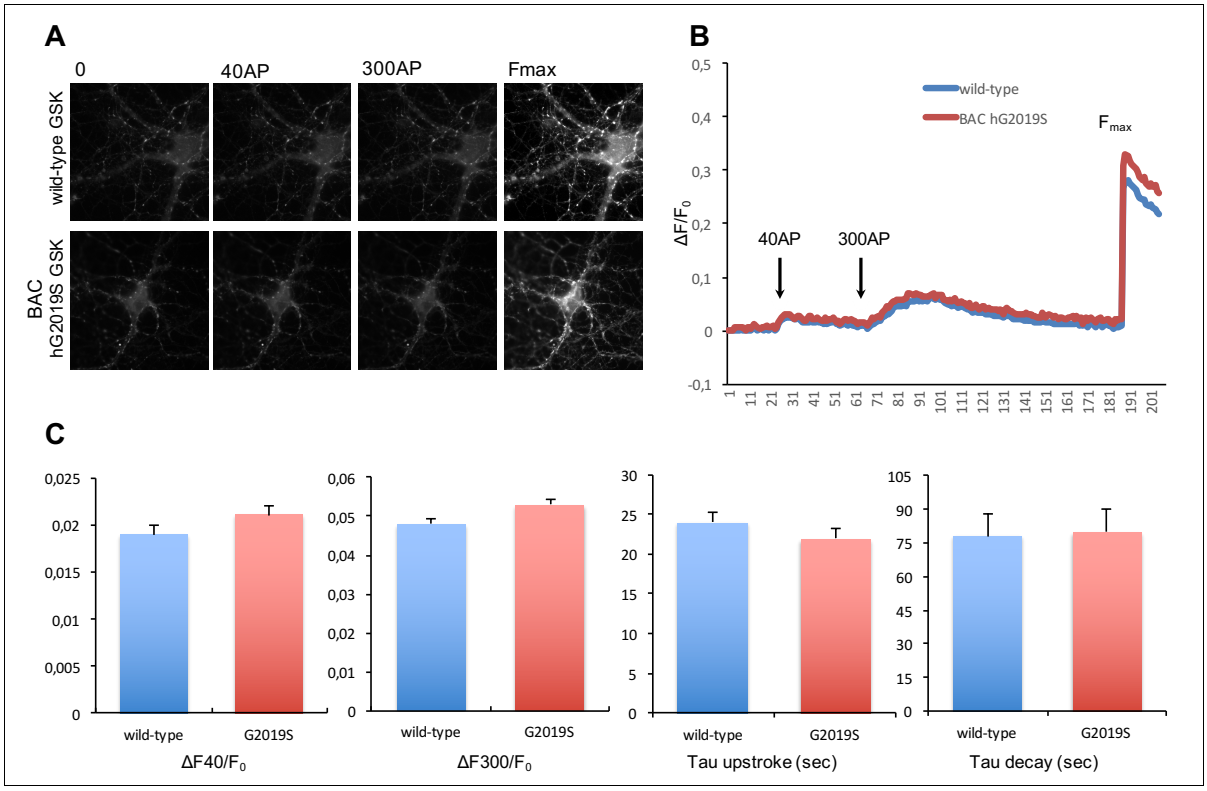

Figure 4. (A) Synaptophluorin fluorencesce was recordered from DIV 14 wild-type and BAC hLRRK2 G2019S (BAC hG2019S) cortical neurons chronically treated with LRRK2 kinase inhibitor GSK 0.2μM or DMSO as control. Representative snapshots were taken from 1Hz recordings at rest (0), after 40 action potential stimulation (40AP), after 300 action potential stimulation (300AP) and upon neutralization with 50mM NH_4Cl, F (max). (B) The graph shows rappresentative pattern of fluorescence. The Y-axis reports the ΔF/F0 at the given time point (second). (C) the graphs report the increase in the fluorescence after 40 AP (ΔF40/F0) and 300 AP (ΔF300/F0) and the kinetic signal after 300AP expressed as time constant describing the increase (tau uspstroke) and decay (tau decay) of fluorescence. Data are expressed as mean ± SEM, n=4, at least 50 boutons from minimum 6 neurons were analyzed per experiment.

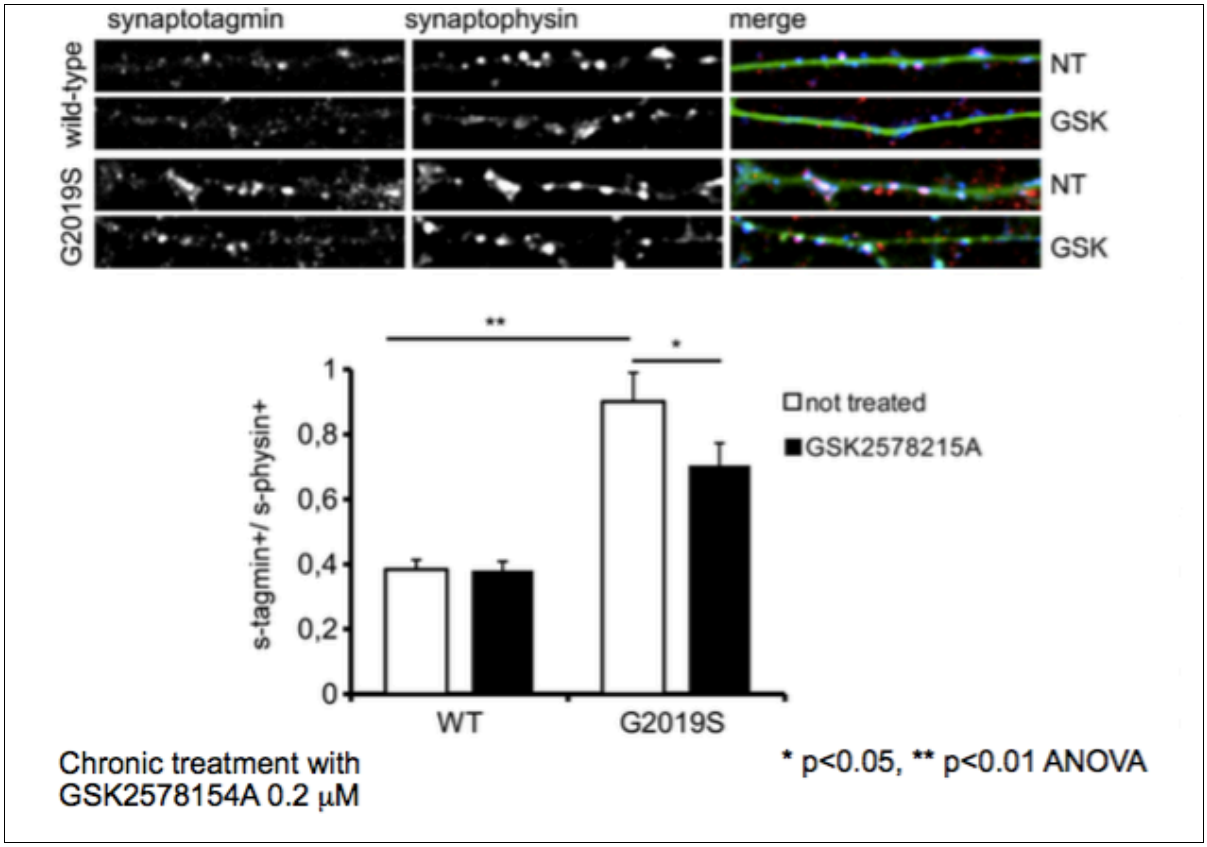

Figure 5. The exo/endocytotic assay was performed at DIV 14 on wild-type and BAC hLRRK2 G2019S cortical neurons, chronically treated with LRRK2 kinase inhibitor GSK 0.2 μM, trasduced at DIV 4 with control virus expressing GFP. Cycling SV appears as synaptotagmin (s-tagmin) positive cluster along neuron processes. The total vesicular pool was marked by incubation with anti-synaptophysin antibodies upon fixation and permeabilization. Images show signals for synaptotagmin and synaptophysin merged with the GFP channel. The graph indicated the ratio of synaptotagmin and synaptophysin positive clusters on the synaptophysin positive ones, that indicates SV recycling rate. Data are expressed as mean ± SEM, n=4, minimum 7 neurons were analyzed per experiment.

2 LRRK2 protein levels and kinase activity influence neuronal morphology

LRRK2 hG2019S BAC mouse overexpress the human mutated in G2019S LRRK2 protein together with the murine wild-type LRRK2 protein. The human transgenic protein expression resembles endogenous mLRRK2, being more expressed in the hippocampus (Melrose et al. 2010). Deficits in neurite outgrowth of LRRK2 hG2019S BAC mouse cultured neurons have been thoroughly described in a consistent amount of studies (Winner et al. 2011; Kawakami et al. 2012; Dachsel et al. 2011) but none dissects the specific contribution to the impaired phenotype of LRRK2 kinase activity versus the increase in protein level. Wanting to fill this gap, we analysed the morphology of BAC hLRRK2 G2019S and wild-type cortical neurons in different experimental conditions. We modulated the murine LRRK2 gene expression by using a virus which expresses a miRNA sequence that specifically silences murine LRRK2 (olig 6) and human and murine expression by is using a virus that express a miRNA sequence that silences both murine and human LRRK2 protein (mib3). Both of these viruses co-express GFP protein that allows the investigation of neuronal morphology. We verified the selective silencing of murine and human LRRK2 in primary mice neurons and in HEK293T cells overexpressing hLRRK2 by western blot (Fig 6).

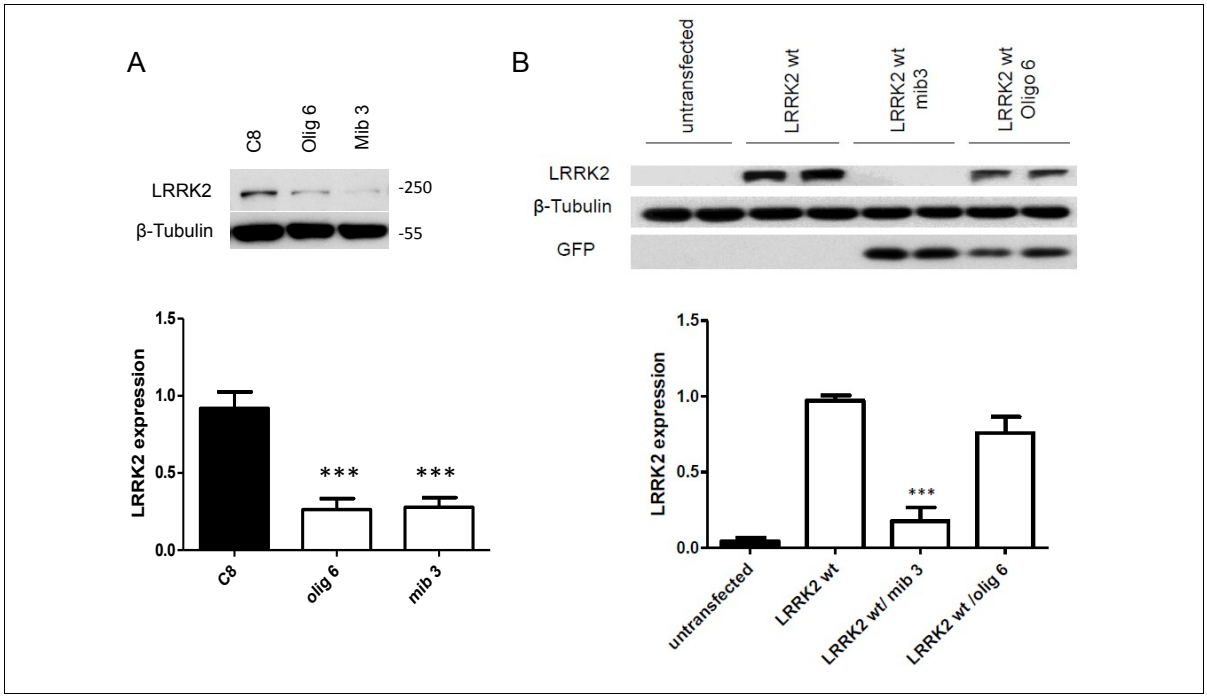

Figure 6. (A) mib3 and olig6 LRRK2 silencing efficiency was tested in wild-type cortical neurons infected at DIV 4 and lysed at DIV 14. 15 µg of protein from each sample were resolved in SDS-PAGE and the expression of LRRK2 investigated by incubation with LRRK2 specific antibody. The total amount of protein was normalized using β tubulin signal. The graph indicates the levels of expression of LRRK2 in control condition (C8), olig 6, mib3 ***p<0.001 T-test. (B) mib3 and olig6 LRRK2 silencing efficiency was tested HEK293T cells by co-trasfection with human LRRK2 wild type construct. The graph indicates the levels of LRRK2 expression in untrasfected, trasfected with LRRK2 wild type, LRRK2 wild and mib3, LRRK2 wild type and olig6 ***p<0.001 T-test.

In order to characterize the morphological phenotype of the GS neurons versus wild-type ones, cortical neuronal cultures were infected at DIV 4 with control viruses expressing GFP. Neurons were processed for imaging purposes at DIV14. Interestingly we noticed that GS neurons were characterized by a significant reduced complexity of the neurite tree, as judged by the measurement of total neurite length. To understand which is the impact of LRRK2 kinase activity on the morphological phenotype, the infected cultures were chronically treated with 0.2μM GSK or DMSO as control starting from DIV0 to DIV14. The analysis revealed a partial recovery of the neurite outgrowth (Fig 7 GS C1 Ct and GS C1 GSK lanes). Wanting to analyse the specific impact of LRRK2 G2019S mutation and protein levels on the morphology we infected the GS and wild-type neuronal cultures with viruses expressing murine LRRK2 silencing vector (olig 6) and performed the chronic treatment with GSK LRRK2 kinase inhibitor as previously described. Surprisingly we observed that murine LRRK2 silencing induced a partial recovery of the phenotype similar to the one induced by the inhibition of LRRK2 kinase activity. Moreover, murine LRRK2 silencing combined with the inhibition of LRRK2 kinase activity lead to a full recovery of the neurite tree in LRRK2 G2019S. We asked next which was the role of LRRK2 protein in the neurite outgrowth so we infected the GS and wild-type neuronal cultures at DIV4 with both human and murine LRRK2 silencing vector (mib3) and analysed their morphology upon chronic treatment with GSK. Strikingly we observed that the overall LRRK2 silencing induced an increase in the neurite tree of the GS neurons compared to the wild-type ones.

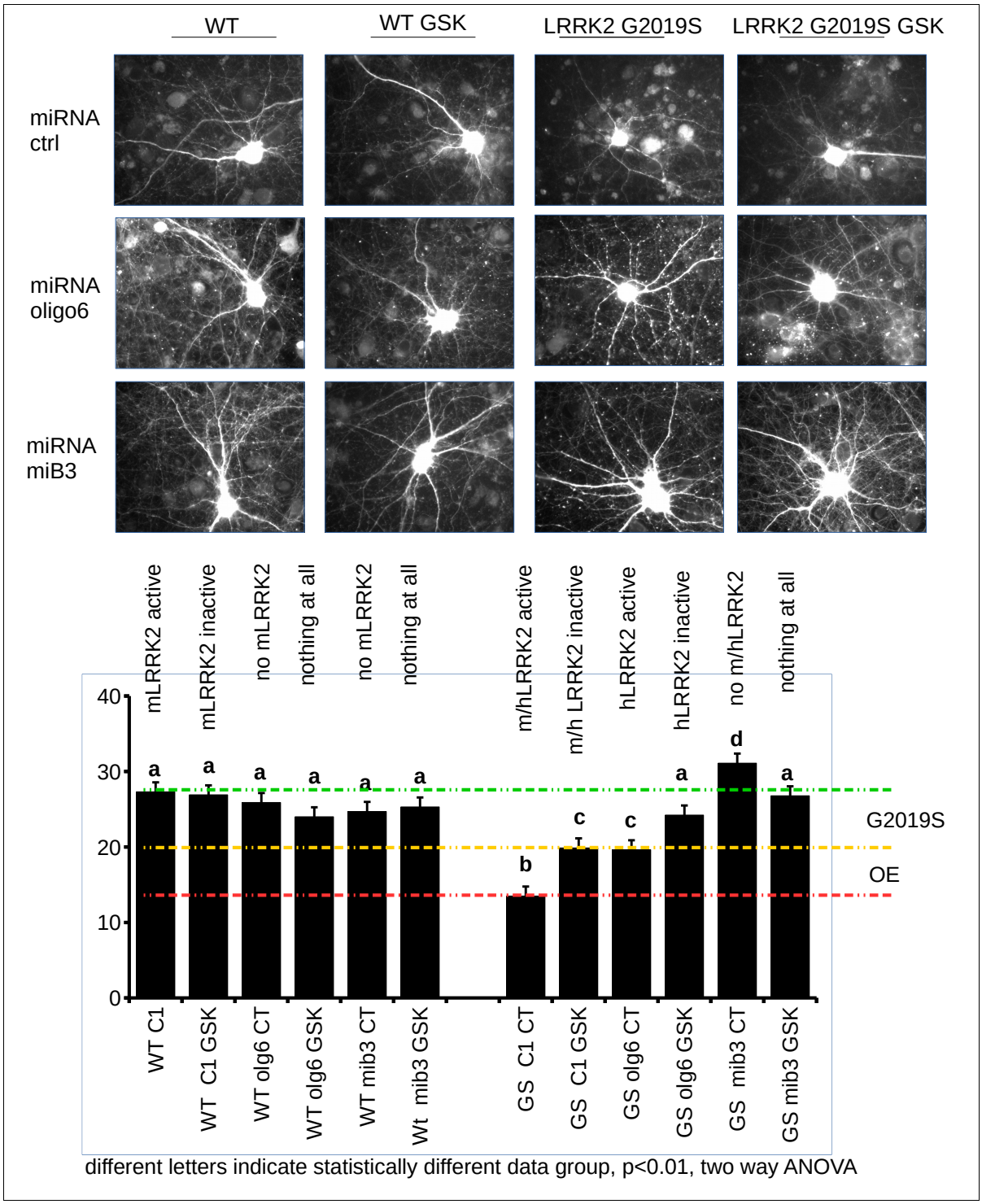

Figure 7. The total number of neurites was analyzed in DIV 14 wild-type and BAC hLRRK2 G2019S cortical neurons chronically treated with LRRK2 kinase inhibitor GSK 0.2μM or DMSO as control. The neurons were infected at DIV 4 with C1 control virus, olig 6 murine LRRK2 silencing virus or mib3 human and murine LRRK2 silencing virus. Neurites were tracked using Neuron J plugin. The graph indicates the number of neurites in each condition indicating the contribution of LRRK2 overexpression (OE) or kinase hyperactivity (G2019) to the phenotype. Data are expressed as mean ± SEM, n=4, a minimum 15 neurons were analyzed per experiment.

As previously reported, we observed a significant reduction in neurite number and length in the GS neurons compared to wild-type. This difference was reduced upon chronic LRRK2 kinase inhibition. Surprisingly, murine LRRK2 silencing produced the same effect suggesting that both kinase activity and LRRK2 protein levels mediate this effect (GS olg6 condition).

Nonetheless, the selective murine LRRK2 silencing via Olig 6 in GS was also associated to a reduction in neuronal complexity, indicating the contribution of LRRK2 G2019S mutation to the phenotype. Strikingly, inhibition of LRRK2 kinase activity in olig 6 infected neurons, by GSK treatment, reverts the morphologic phenotype to a Wild-type level, while the silencing of both murine and human LRRK2 via mib3 (comparable to a KO model) generates an increase in neuronal complexity. These results indicate the importance of both LRRK2 protein levels and kinase activity in the regulation of neuronal morphology outlining the importance of LRRK2 in a fine-tuning regulation mechanism that impacts the neuronal morphology.

All together these data demonstrate the usefulness of BAC hG2019S model: in fact, the over-expression of human LRRK2 protein and the increased kinase activity cause a similar phenotype in terms of neurite tree complexity reduction.

3 G2019S neurons suffer proteasome inhibition

The ubiquitin-proteasome system (UPS) is one of the pathways involved in the control of a correct protein turnover and clearance of misfolded proteins, regulating protein concentration accordingly to the cell cycle phases. The function of UPS is often linked to the development of neurodegenerative disease where damaged proteins tend to accumulate and generate toxic aggregates that alter the normal cellular function. Alteration of the UPS was observed in both sporadic and hereditary PD (Olanow and McNaught 2006; McNaught et al. 2002) and its different enzymatic activity deeply analyzed. In particular, LB were reported in the basal ganglia of LRRK2 G2019S patients Thus, we assessed UPS functionality in brain lysate obtained from GS and Wild-type 12-months old mice by using a fluorimetric assay that detects the fluorophore 7-Amino-4-methylcoumarin (AMC) after cleavage from the labeled substrate LLVY-AMC. Proteolytic activity resulted similar in GS, and Wild-type samples (Fig 8 A) and the relative activity values fell within the range expected for physiological proteasome activity (Fig 8 B).

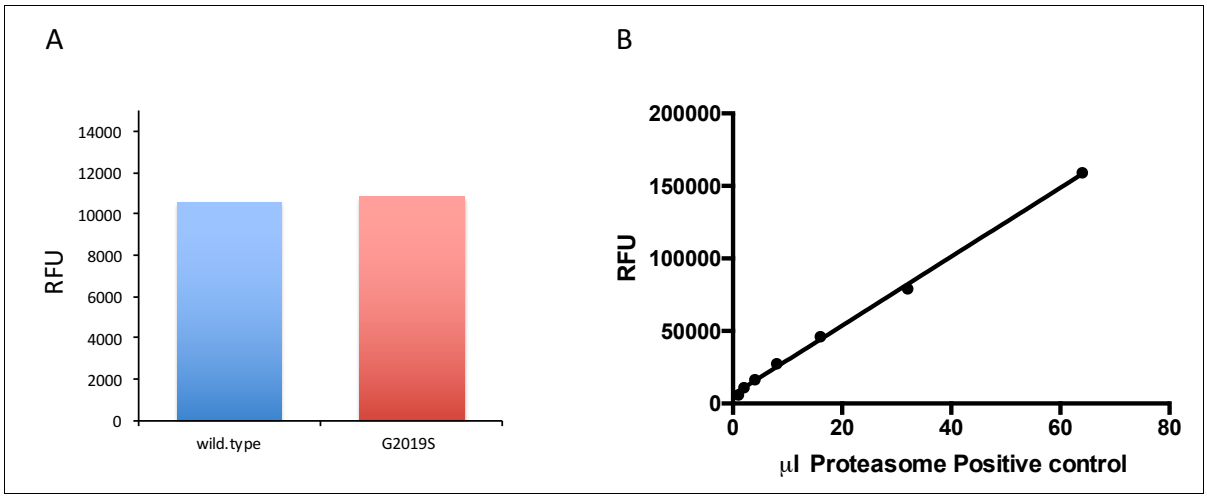

Figure 8. (A) 20 S proteasome activity was measured in brain lysate obtained from 12 months old BAC hLRRK2 G2019S and wild-type mice., by fluorimetric detection of the fluorophore 7-Amino-4-methylcoumarin (AMC) (B) Standard curve of proteasome positive control.

Next we asked whether GS neurons might have different susceptibility to blockage of UPS activity. Thus we exposed wild-type and GS neurons to sub-optimal acute proteasome inhibition.

To this aim, we treated cortical cultures with 75nM MG132 for 24 hours. Next, neurons were processed for immunofluorescence analysis and stained for cleaved caspase 3 (CC-3), a reporter of cell death. Interestingly we found that GS neuron suffer more for proteasome inhibition, respect to the wild-type ones (Fig 9).

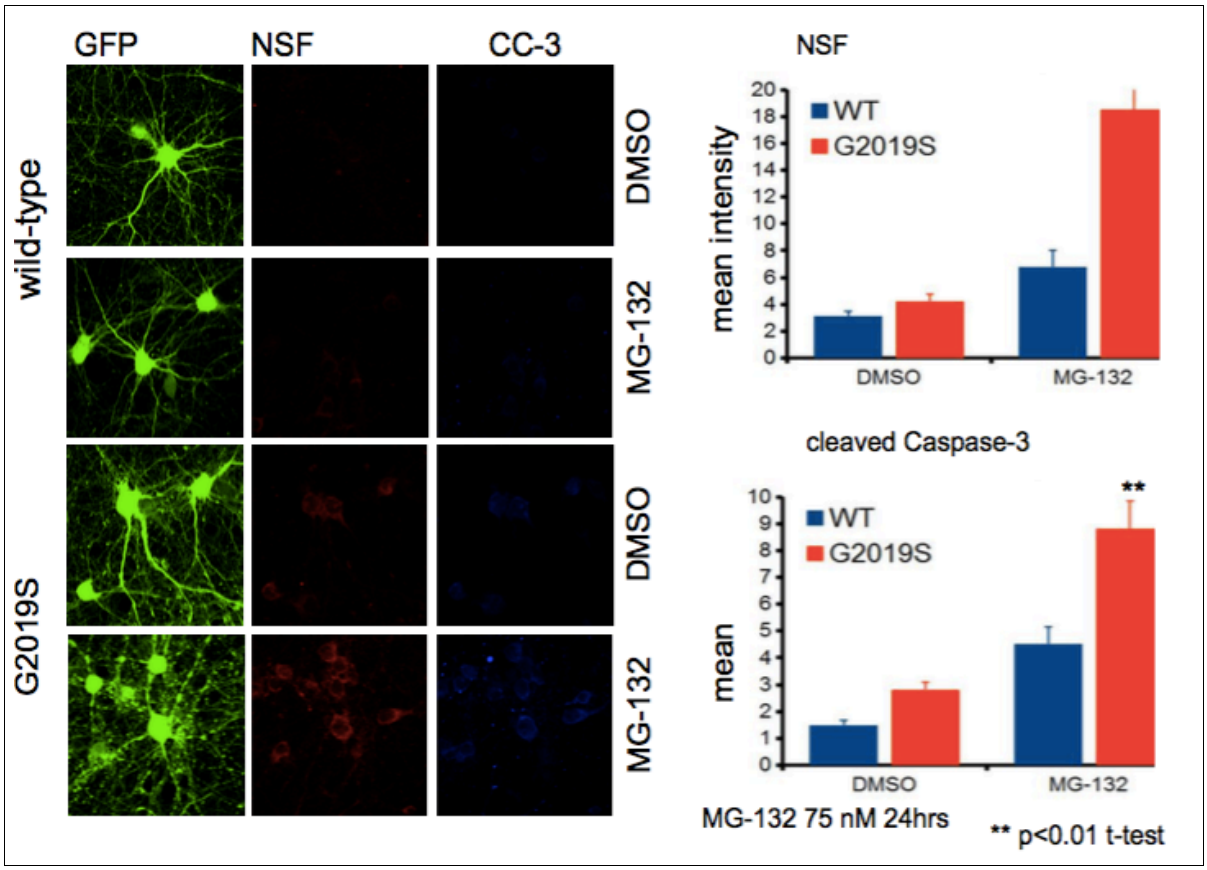

Figure 9. The susceptibility to proteasome inhibition was tested in DIV 14 wild-type and BAC hLRRK2 G2019S cortical neurons by treatment with 75nM MG-132 proteasome inhibitor for 24 hours. The neurons were infected at DIV 4 with control virus expressing GFP stained after fixation with 4% paraformaldehyde, for cleaved caspase 3, that marks the apoptotic cells and NSF. The image presents the neuronal morphology stained by the GFP, the signal of NSF in red channel and of CC-3 in blue. The graph indicates the mean intensity levels of total fluorescence for NSF (Upper panel) and CC-3 (lower panel). Data are expressed as mean ± SEM, n=4, a minimum 10 neurons were analyzed per experiment.

4 NSF accumulates in PD patient and co-aggregates with alpha synuclein in LB.

It is commonly accepted that alpha-synuclein is the main constituent of the LB, but recent studies reveals the presence of other proteins including LRRK2 (Alegre-Abarrategui et al. 2009). Moreover, the work of Pountney et al, reports the presence in the LB related intranuclear inclusion bodies of NSF, Munc18-1 and dynamin 1(Pountney et al. 2008), recently identified LRRK2 interactors (Piccoli et al 2014). Considering that NSF is not only an interactor but also of substrate of LRRK2 kinase activity that modifies its ATPase activity upon phosphorylation, leading to an alteration in the SV dynamics, we asked whether there is a pathologic connection among the presence of LRRK2 G2019S and the distribution of NSF in G2019S PD patients basal ganglia. For this, we performed immunofluorescence analysis on basal ganglia sections of G2019S LRRK2 patient (Fig 10) and we observed that NSF can be found in large aggregates. Moreover, NSF aggregates co-localize with alpha synuclein. This evidence suggests that NSF precipitates in structures resembling LB.

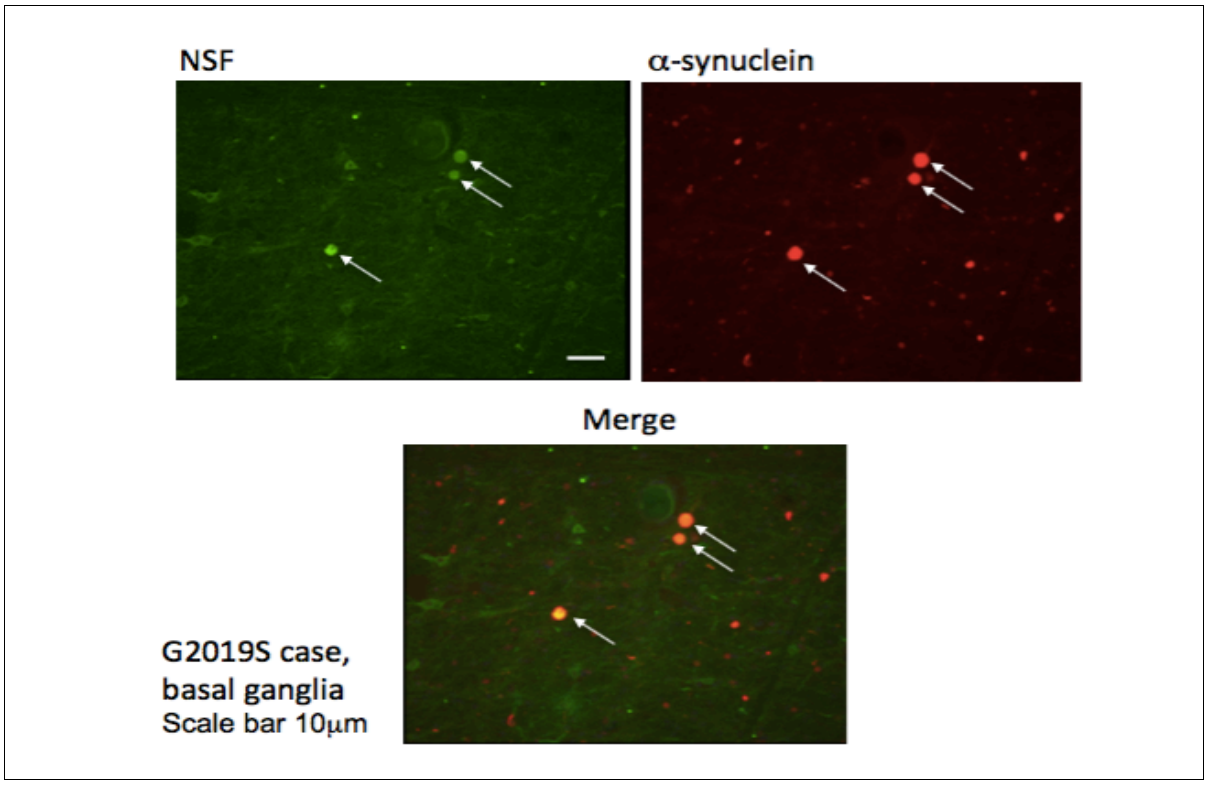

Figure 10. The presence of NSF aggregates and their co-localization with alpha synuclein was tested in basal ganglia of G2019S PD patient by staining with NSF antibody (Synaptic System) and alpha synuclein (Cell Signaling).

5 LRRK2 G2019S mutation correlates with deposition of NSF aggregates

Wanting to deepen the understanding of NSF accumulation in the PD G2019S patients we further investigate the levels and distribution of NSF taking advantage of the GS mice. We performed immunohistochemistry analysis of NSF distribution in coronary 30um free floating slices of 12 months old GS and wild-type mouse brain. As expected, we observed that NSF antibody decorates perinuclear aggregates in the striatum of 12 months old G2019S mice (Fig 11A).

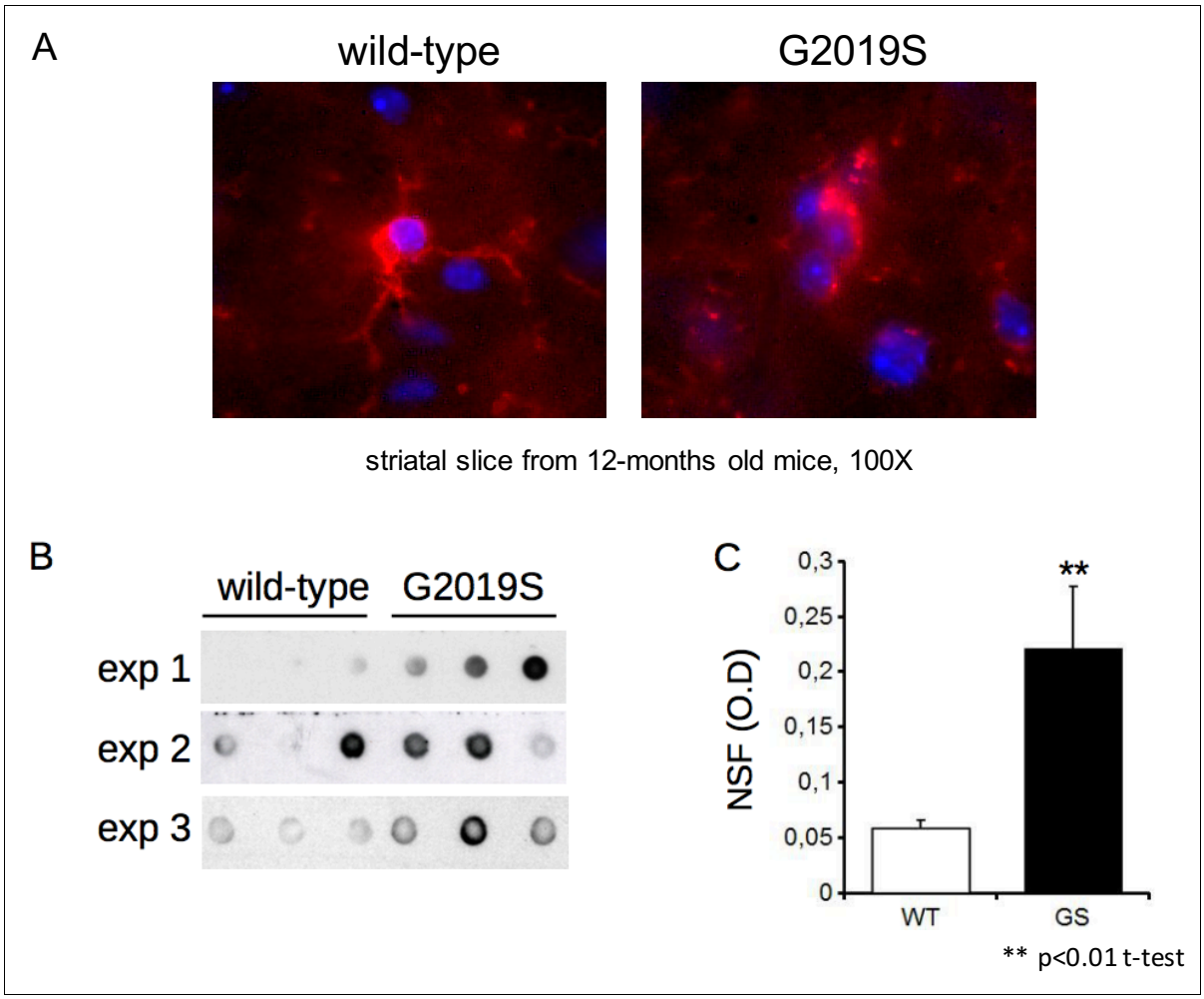

Figure 11. (A) The presence of NSF aggregates in the striatul of 12 months old wild-type and BAC hLRRK2 G2019S was evaluated by staining of 30 µm coronal free floating brain coronal slices with anti-NSF antibody. The image presents a normal cytosolic distributed signal in the wild-type sample and a perinuclear aggregated signal in the BAC hLRRK2 G2019S one. (B) Filter retention assay performed on sonicated wild-type and BAC hLRRK2 G2019S cortical neurons reveals aggregation of NSF in the G2019S sample. (C) Graph presents the quantification of filter assay optical density of NSF signal on the wild-type (WT) and BAC hLRRK2 G2019S (GS). Data are expressed as mean ± SEM, n=4.

In order to further characterize NSF aggregation we performed a filter assay on GS and wild-type cultured neurons at DIV 14. This assay is able to identify the soluble but aggregated protein species as well as insoluble ones by retaining them on a cellulose acetate membrane (Rusmini et al. 2013). We report a significant increase in NSF aggregation in GS sample compared to the wild-type (Fig 11B).

6 LRRK2 G2019S kinase activity impairs NSF ubiquitination

There is a general consensus that LRRK2 phosphorylates threonine residues flanked by positively charged residues such as lysines (36) acceptor site for the ubiquitination of target proteins, and that the G2019S mutation induces a 2 fold increase in LRRK2 kinase activity. Considering our recent data that report NSF as one of LRRK2 interactors and substrate (Belluzzi et al.2015 appendix), we hypothesized that NSF phosphorylation by LRRK2

G2019S mutation might induce an alteration of its clearance. Thus we asked whether NSF aggregation in both neuronal cultures and tissue obtained GS mice might arise from an altered ubiquitination. To this aim we used the TUBE resin that is able to bind any ubiquitinated protein, to isolate ubiquitinated proteins. To test the potentiality of our strategy we first assayed neuronal culture treated or not with MG132. Upon TUBE enrichment, proteins were eluted in Laemmli buffer and analysed by immunoblotting. Interestingly we noticed an increased yield of NSF purification upon MG-132 treatment. These data suggest that 1) NSF can be ubiquitinated, 2) TUBE assay enriches in ubiquitinated proteins. Next we assayed by TUBE protein samples extracted from midbrain of wild-type and G2091s animals sacrificed at 6 and 10 months. By western-blotting, we detected a reduced amount of ubiquitinated NSF in G2019S mice sacrificed at the age of 10 months.

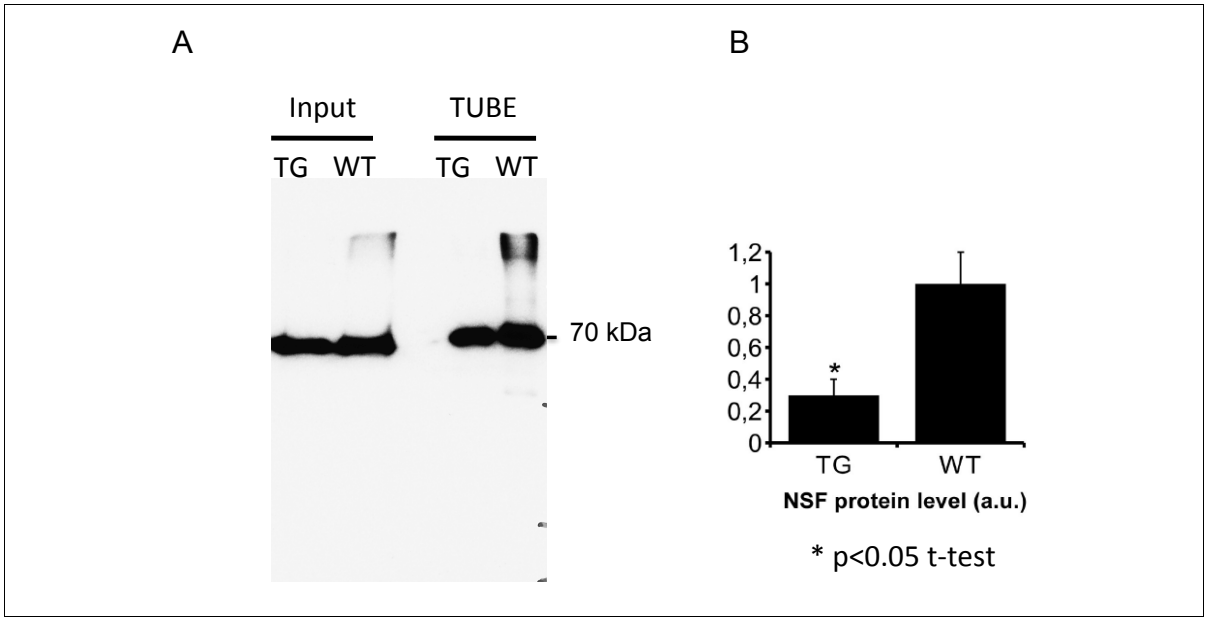

Figure 12. NSF ubiquitination levels were analysed by immunoprecipitatin of the ubiquitinated proteins using the Tandem Ubiquitin Binding Elements (TUBE) resin from 10 month old wild-type and BAC hLRRK2 G2019S (TG) midbrain lysate. Proteins were eluted and analysed by western-blotting with anti-NSF specific antibody. (B) Graph shows NSF yield upon TUBE purification in 10 months old mice. Data are expressed as mean ± SEM, n=4.

7 LRRK2 impairs NSF ubiquitination in vitro

Thus, we asked whether LRRK2 phosphorylation might alter NSF ubiquitination. To this aim, we investigated the pattern of ubiquitination of NSF upon LRRK2 phosphorylation. We tested three NSF construct; wt, phosphodeficient T645A and phospho competent T646A. Recombinant Strep-FLAG-NSF wild-type or FLAG-NSF T645A or FLAG-NSF T646A were co-trasfected with GFP-LRRK2 G2019S, and Myc-Ubiquitin in HEK293T cells. One day before cell lysis, cells were treated with the UPS inhibitor MG- 132 (10 μM) in combination or not with the LRRK2 kinase inhibitor IN-1 (2μM). After solubilisation, NSF proteins were

purified with a double immunoprecipitation protocol on Streptavidin resin followed by FLAG-M2 resin and eluted in Laemmli buffer. Eluates were separated on SDS- PAGE and the yield of NSF-ubiquitination was investigated by immunoblotting with anti-Myc antibodies. Interestingly, we noticed that the pattern of NSF ubiquitination was significantly increased in sample purified from cells expressing NSF and LRRK2 G2019S upon with IN-1(Fig 13). Moreover, in the sample expressing NSF T645A that cannot be phosphorylated by LRRK2, NSF ubiquitination pattern does not change after the treatment with IN-1, suggesting that the alteration in the ubiquitination level of NSF is dependent of NSF phosphorylation by LRRK2.

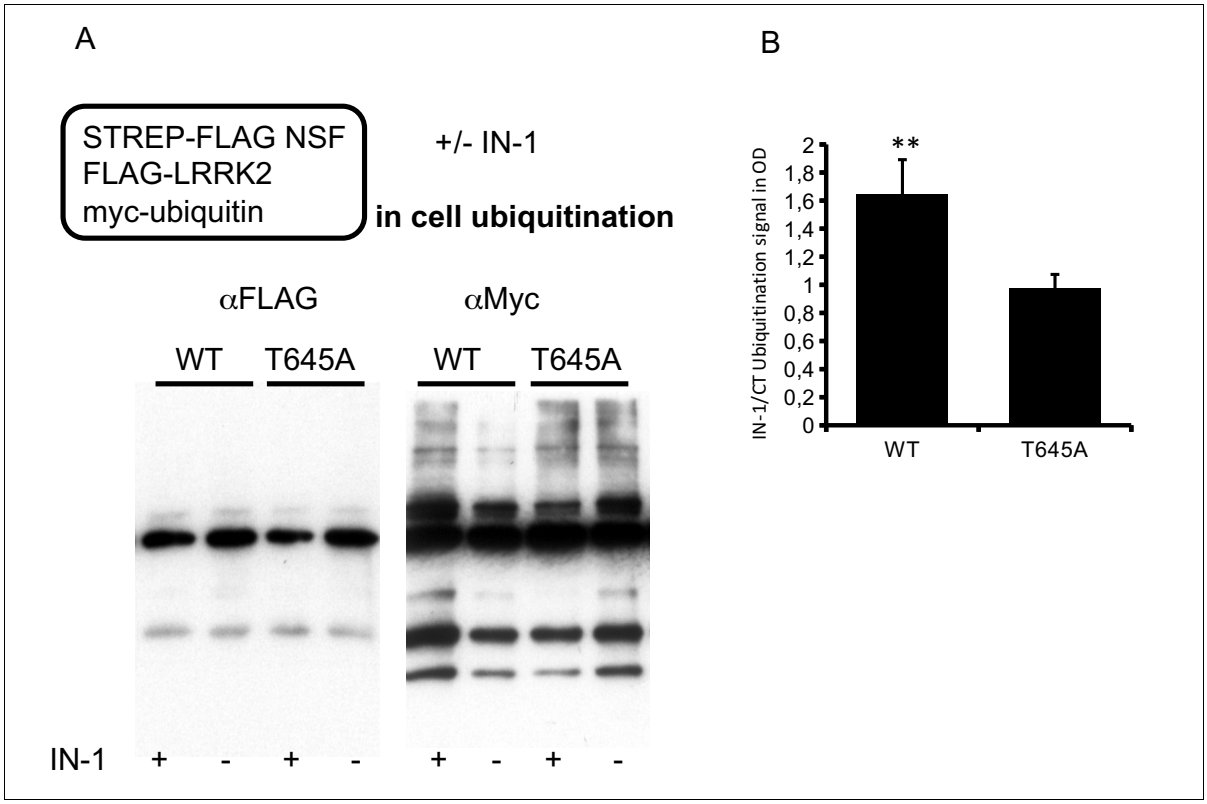

Figure 13. The impact of LRRK2 kinase activity on NSF ubiquitination was evaluated by double immunoprecipitation of NSF WT–Strep-Flag (WT) and phosphoresistant NSF T645A- Strep-Flag protein, overexpressed in HEK293T cells in presence of LRRK2 G2019S and Myc-ubiquitin. The cells were treated for 24 hours with 10μM MG132 and LRRK2 inhibitor 1 IN-1 or DMSO as control. The proteins were eluted in Laemmli buffer and analysed by western-blotting. The iimunoprecipitation of NSF was verified with anti-Flag antibody while the ubiquitination of the immunoprecipitates was verified by incubation with anti- Myc antibody. The graph indicated the variation of ubiquitination signal of NSF (WT) and NSF T645A in presence of LRRK2 IN-1 calculated the ratio of the ubiquitination signal from IN-1 treated samples (+) and control (-). Data are expressed as mean ± SEM, n=5 **p< 0.001, T-test.

To further explore the link between LRRK2 phosphorylation and NSF ubiquitination, we took advantage of a kinase-dead variant of LRRK2, LRRK2 K1906M. This artificial variant has undetectable kinase activity (Civiero et al. 2012) We purified NSF from culture expressing FLAG-NSF, myc-LRRK2 K1906M, and HA-Ubiquitin treated with MG-132 or MG- 132 + IN-1. Anti-HA immunoblotting revealed that in this experimental setting, IN-1

does not modify NSF ubiquitination level (Fig. 14). Finally, to exclude off-side effect due to unspecific binding of IN-1 to NSF, we studied the ubiquitination patter of NSF purified from cells expressing NSF or GFP, treated or not with IN-1. We noticed that in the absence of LRRK2 co-expression, IN-1 does not influence NSF ubiquitination (Fig 14). Altogether these data indicate that NSF ubiquitination is specifically impaired upon LRRK2 phosphorylation.

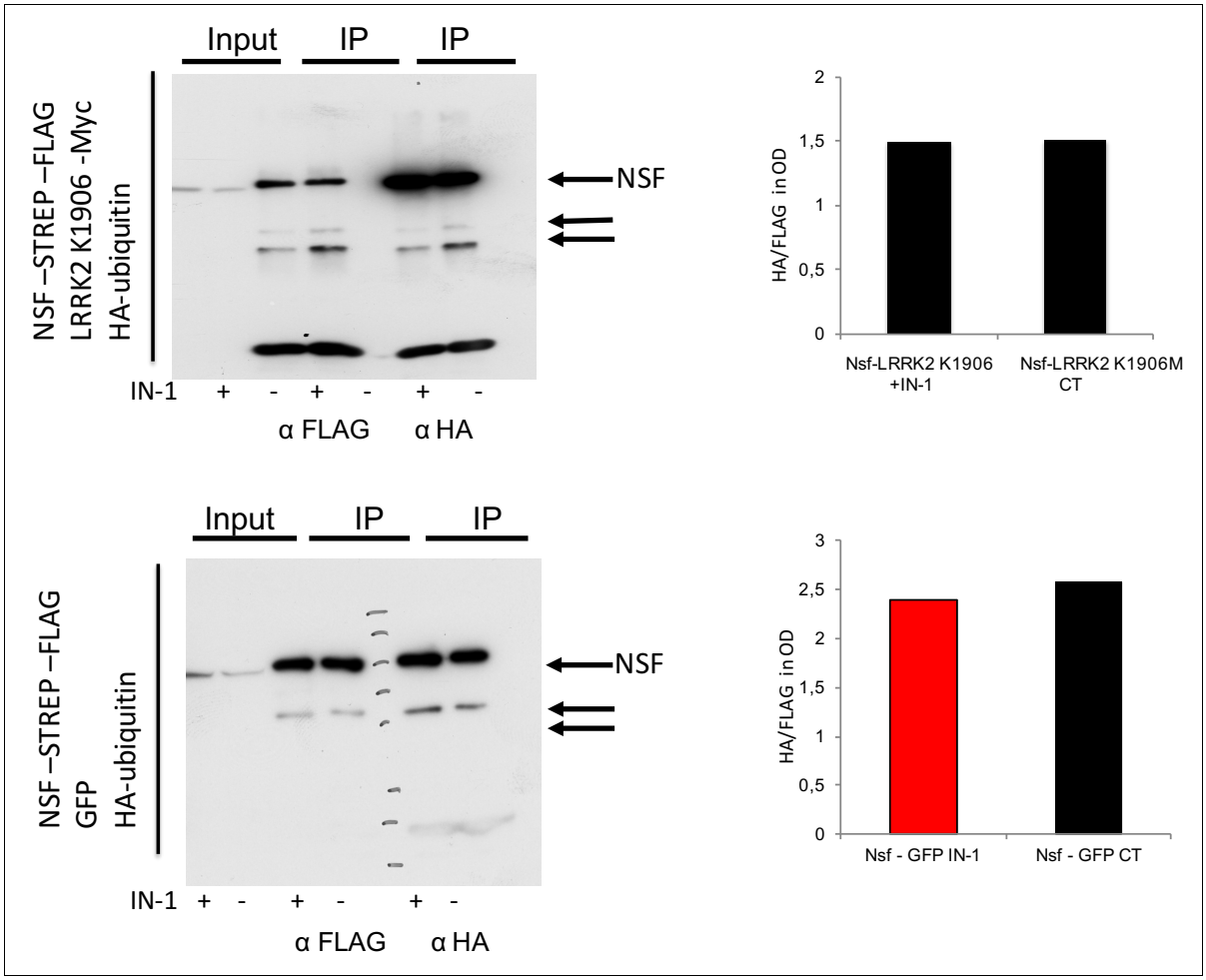

Figure 14. The specificity of LRRK2 kinase activity on NSF ubiquitination was analyzed by immunoprecipitation of NSF wild-type –Strep protein overexpressed in HEK 293T cells in presence of LRRK2 K1906M (kinase dead) and HA ubiquitin (upper panel) or GFP protein used as control (lower panel). The cells were treated for 24 hours with 10μM MG132 and LRRK2 inhibitor 1 IN-1 or DMSO as control. The proteins were eluted in Laemmli buffer and analysed by western-blotting. The immunoprecipitation of NSF was verified with anti- Flag antibody while the ubiquitination of the immunoprecipitates was verified by incubation with anti HA antibody. The graphs indicated the ratio of ubiquitination of the immunoprecipitate calculated the ratio of the ubiquitination signal and flag signal from IN-1 treated samples (+) and control (-).

Next we asked whether LRRK2 kinase activity negatively affects overall UPS efficiency or instead specifically impairs NSF ubiquitination. To solve this issue, we exploited a cell-free ubiquitination assay. Briefly, we purified NSF and LRRK2 from cell expressing respectively Strep-FLAG-NSF or FLAG LRRK G2019S. Purified NSF and LRRK2 were combined 1:2 in kinase permissive condition in the presence or not of IN-1 2μM. Subsequently NSF was isolated on streptavidin resin and then incubated with lysate obtained from cell over-expressing Myc-ubiquitin. The incubation was performed in a dedicated buffer

allowing ubiquitination (Antrobus and Borner 2011). Reactions were stopped after 30 minutes and proteins were resolved on SDS-PAGE. Ubiquitination level was evaluated by anti-Myc immunoblotting. Interestingly, we observed that NSF ubiquitination patter was reduced upon LRRK2 phosphorylation and that the treatment with IN-1 restored the ubiquitination levels to the ones of NSF exposed to the ubiquitination reaction without the presence of LRRK2.

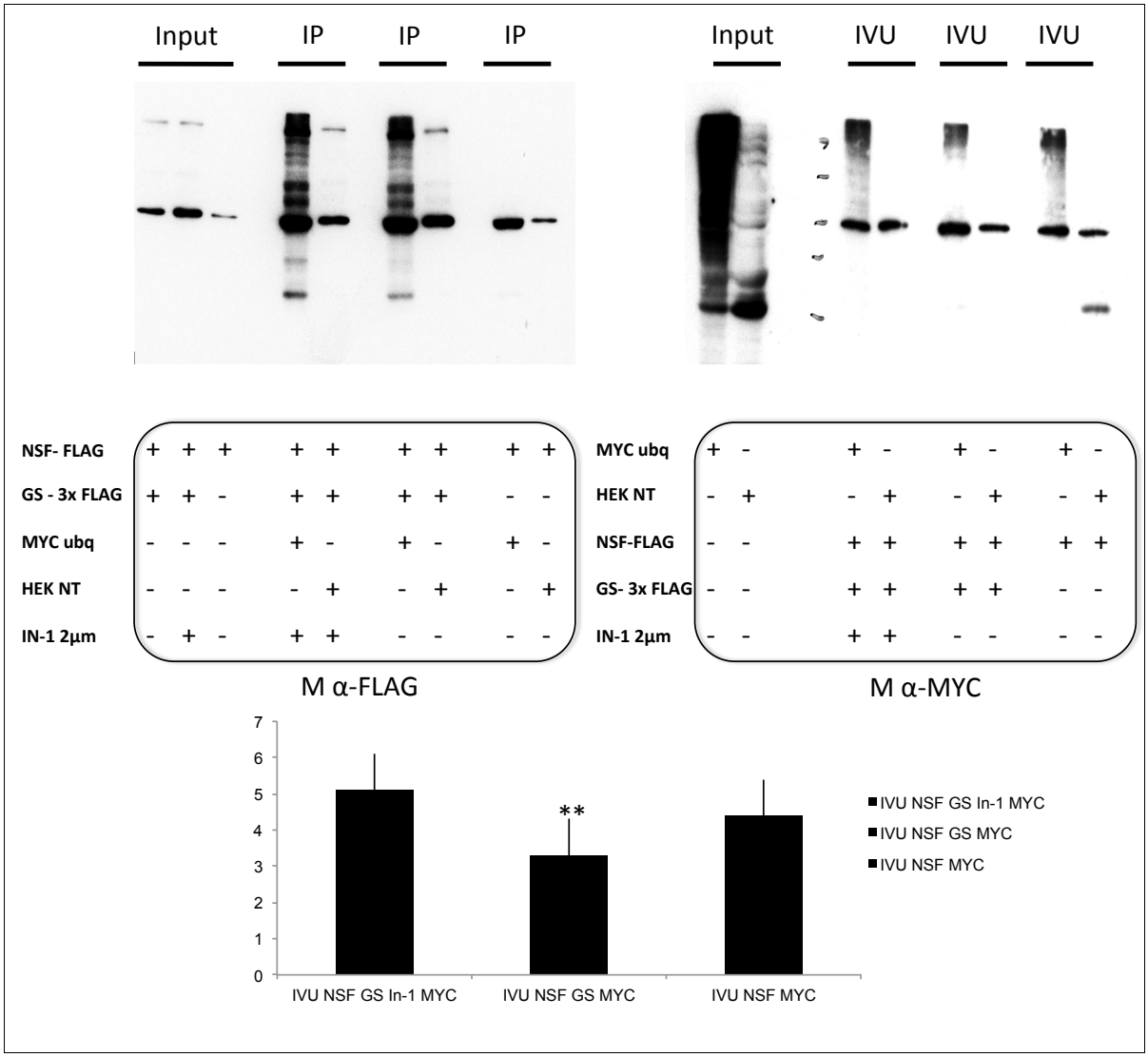

Figure 15. In vitro ubiquitination assay. Strep- FLAG NSF and 3X-FLAG LRRK2 proteins were purified from HEK293 cells upon 48 hours transfection on FLAG-beads. NSF and LRRK2 purified proteins were incubated in a ratio of 1:2 in presence of 10mM ATP at 37°C to promote NSF phosphorylation by LRRK2. The impact on NSF ubiquitination of LRRK2 kinase activity or presence of the LRRK2 protein was tested by running the phosphorylation reaction also in presence of IN-1 10µM or in absence of LRRK2. The phosphorylated NSF was then trapped on Strep beads and incubated with 20 mg of Myc-ubiquin expressing HEK lysate (MYC ubq) or not transfected HEK lysate (HEK NT) donors of ubiquitin-proteasome substrates in the in vitro ubiquitination mix and 10mM ATP. The proteasome activity was inhibited by adding 10µM MG-132 to the in vitro ubiquitination reaction. After 30 min, we stopped the reaction in Laemmli Buffer. We resolved the protein on SDS-PAGE. As shown by the blots we evaluated the immunoprecipitation (IP) and ubiquitination of NSF yield (IVU) via western-blotting with anti-Flg and anti-Myc antibodies. The graph indicates the ubiquitination signal of immunoprecipitated NSF in presence of kinase inhibited LRRK2 (IVU NSF GS In-1 MYC), active LRRK2 (IVU NSF GS MYC) and in absence of LRRK2 protein (IVU NSF MYC). Data are expressed as mean ± SEM, n=5 **p< 0.001, T-test.

These data confirm that NSF ubiquitination is regulated by LRRK2 and that LRRK2 kinase activity directly controls it.

8 Reduced NSF clearance is toxic for G2019S neurons

Protein aggregation is thought as one of the main cause of cytotoxicity that lead to the neuronal death in most of neurodegenerative diseases. For this, we asked whether NSF accumulation induces similar effects and, in case, if such effect depends on LRRK2 kinase activity. To answer this question, we analyzed the morphology of GS and Wild-type cortical neurons overexpressing FLAG-NSF- wild-type or FLAG-NSF T645A together with GFP. The neurites were tracked automatically using the GFP signal by Neuron Studio software. The reduction of neurites number is a marker of neuronal toxicity (Piccoli et al 2014). We confirm our previous observation of impaired neurite outgrowth in the GS neurons respect to the wild-type ones but we report that the overexpression of wild-type NSF is toxic for the GS neurons as the numbers of neurites is significantly reduced compared to the GS neurons transfected only with GFP (Fig 16 NT lane). Moreover the overexpression of NSF in wild-type neurons does not induce any significant alteration in the total neurite number, thus does wild type neurons does not overt NSF toxicity.

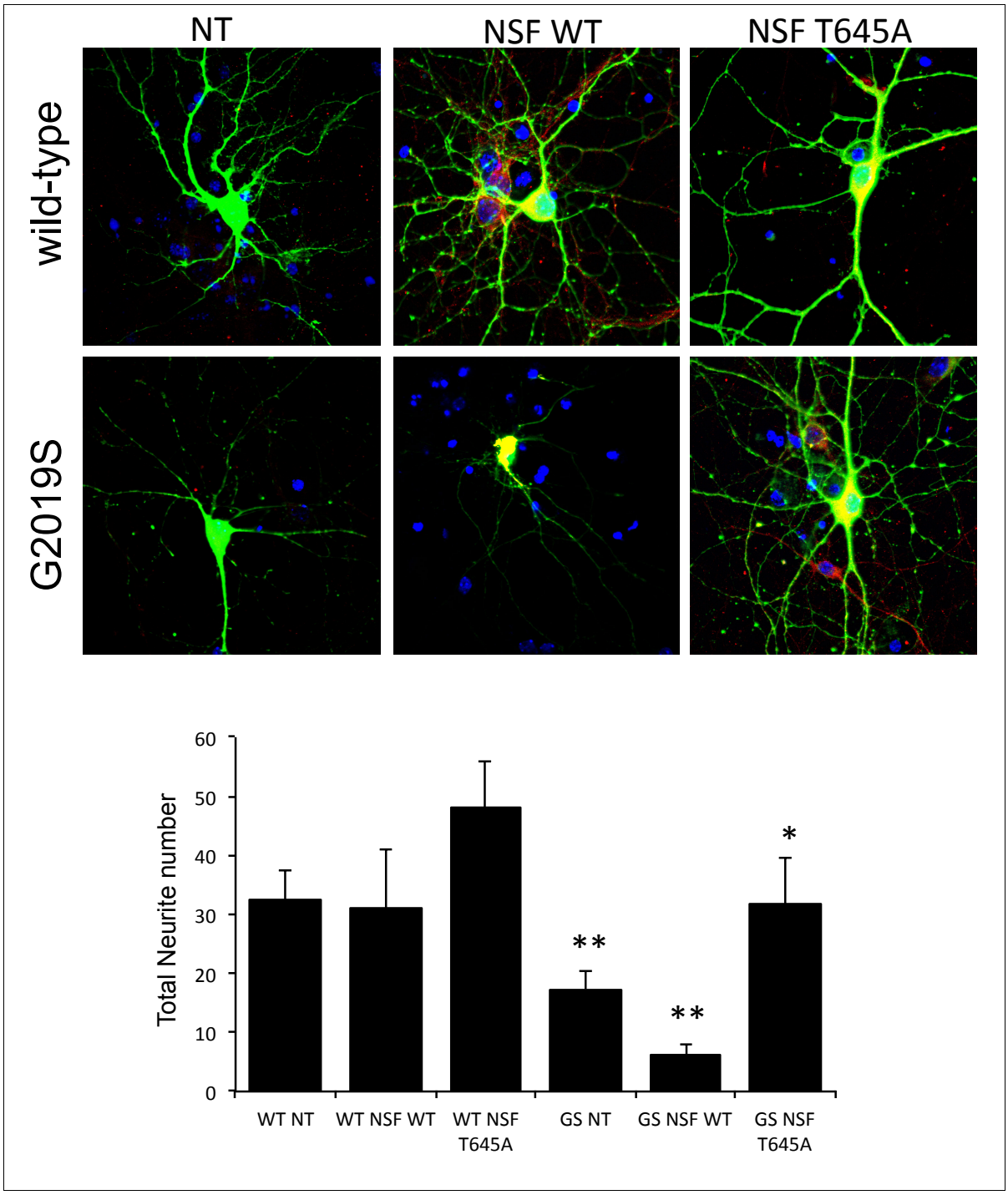

Figure 16. NSF induced toxity was tested in wild-type and BAC hG2019S cortical neurons. The neurons were transfected at DIV 4 with GFP alone, FLAG-NSF wild-type plus GFP, FLAG-NSF T645A plus GFP and imaged at DIV 14 post staining with NSF specific antibody. The neurites were tracked automatically using the GFP signal by Neuron Studio software. The graph shows the total neurite number of wild-type neurons transfected with GFP (WT NT), NSF wild type - GFP (WT NSF WT), NSF T654A –GFP (WT NSF T645A) and BAC hG2019S (GS) neurons transfected with GFP (GS NT), NSF wild type - GFP (GS NSF WT), NSF T654A –GFP (GS NSF T645A). Data are expressed as mean ± SEM, n=3 **p< 0.001, T-test.

Moreover, when we overexpressed in GS neurons, NSF T645A, resistant to LRRK2 phosphorylation, we did report a significant recovery of neurite tree. This evidence suggests that the cytotoxic effect is dependent on NSF phosphorylation by LRRK2. All together these results suggest that NSF over-expression is toxic for GS neurons and that this effect is dependent on LRRK2 kinase activity.

9 Trehalose reduces NSF aggregates and ameliorates motor phenotype in BAC hG2019S mice

Protein deposition can be attenuated by autophagy induction. Trehalose is a disaccharide that prevents aggregation of denatured proteins inducing their degradation via autophagy (Sarkar et al. 2007) and has been used successfully in reducing protein aggregation in a rodent model of Parkin-PD (Rodríguez-Navarro et al. 2010).

Aged match wild-type and G2019S mice were offered water or water with 1% trehalose for 2 months. At the end of the treatment, we studied NSF deposition by immunohistochemistry striatal specimen from wild-type and G2019S 12-months mice treated or not with trehalose. Interestingly we noticed that in the GS trehalose-treated samples, NSF aggregates disappear, and NSF distribution is comparable to the wild-type. (Fig 17).

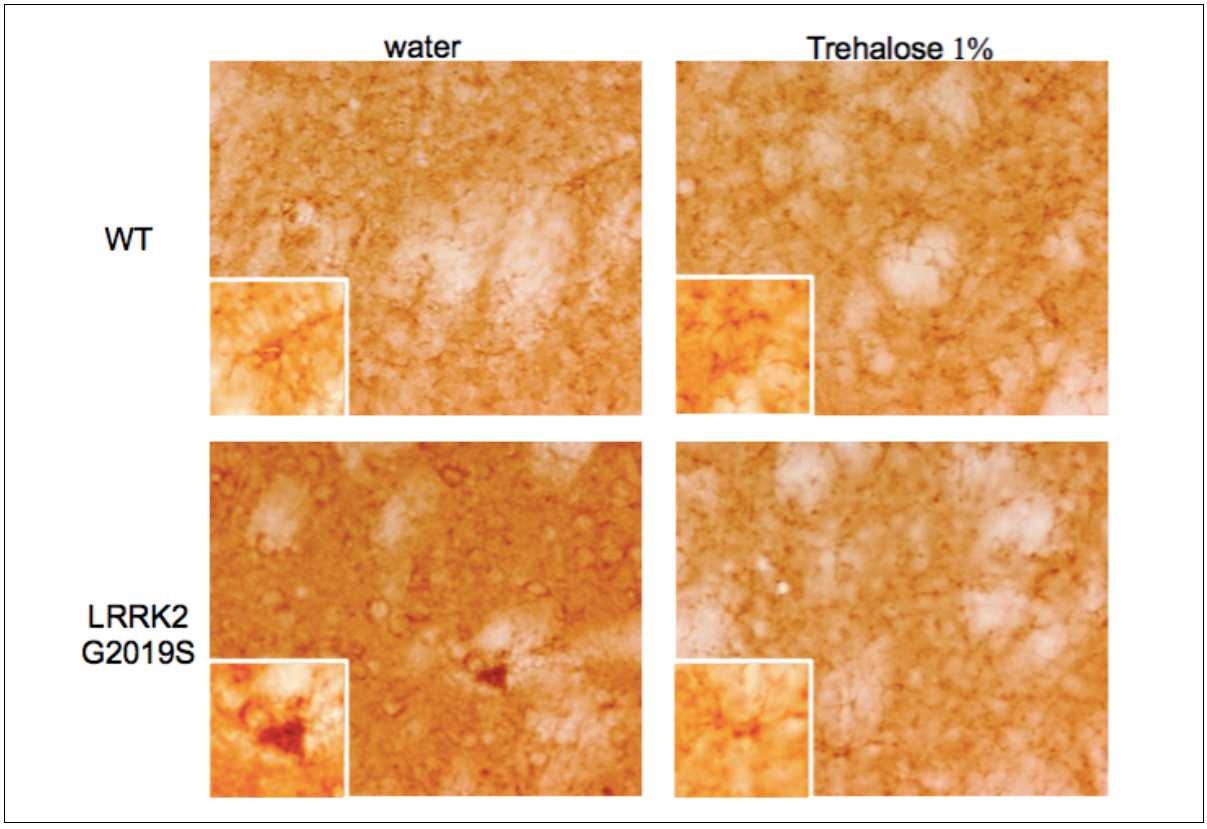

Figure 17. Presence of NSF aggregates was analyzed in the striatum of 12 months old wild and BAC hLRRK2 G2019S mice treated for 2 months with aqueous solution of 1% Trehalose or water as control. Images show the staining with NSF specific antibody on 30µm free floating coronal sections revealed by DAB.

Next we investigated the impact of LRRK2 mutation on motor and cognitive performances in 6 and 12 months old GS and wild-type mice. Motor coordination was evaluated by means of balance beam, pole and rotarod resistance test, while the episodic memory was analyzed by novel object recognition test. Specifically balance beam test on 6 and 12 months of age wild –type and GS mice, was performed on 12mm beam and on 6mm

beam (fig.18). When the 6 months mice performed the test on 12mm beam, Two way Anova revealed a significant difference among the two genotypes (F(1,48) =5.61, P=0.02) but not for genotype (F(1,48)=0.47, P=0.49) and treatment (F(1,48) =0.16, P=0.68). Post hoc analysis revealed a significant difference between GS mice and their littermates only when treated with vehicle. Also when 6 months mice were tested on 6mm beam, Two way Anova revealed a significant difference among the two genotypes (F(1,48) =5.45, P=0.02) but not for genotype (F(1,48)=0.33, P=0.56) and treatment (F(1,48) =0.24, P=0.62). Bonferroni test revealed that GS mice took longer time to cross the beam compared to wild-type; when treated with trehalose, GS mice spent less time compared to their GS littermates treated with vehicle. This result indicates a partial recovery of the motor impairment of GS mice following the trehalose treatment. When tested in Balance Beam test at the age of 12 months (fig 18), Two way Anova did not revealed any significant differences among wild-type and GS mice although it indicates a significant difference among the wild-type treated or not with trehalose treatment (F(1,53) =4.63, P=0.03). Post hoc analysis revealed a significant decrease in time spent by wild-type treated with trehalose to cross the beam compared to their wild-type littermates treated with vehicle. Finally, when tested at the age of 12 months on 12mm beam, two way Anova did not reveal any significant differences (genotype: (F(1,53) =0.62, P=0.43; treatment: (F(1,53) =0.42, P=0.51; genotype x treatment interaction: (F(1,53) =0.46, P=0.49).

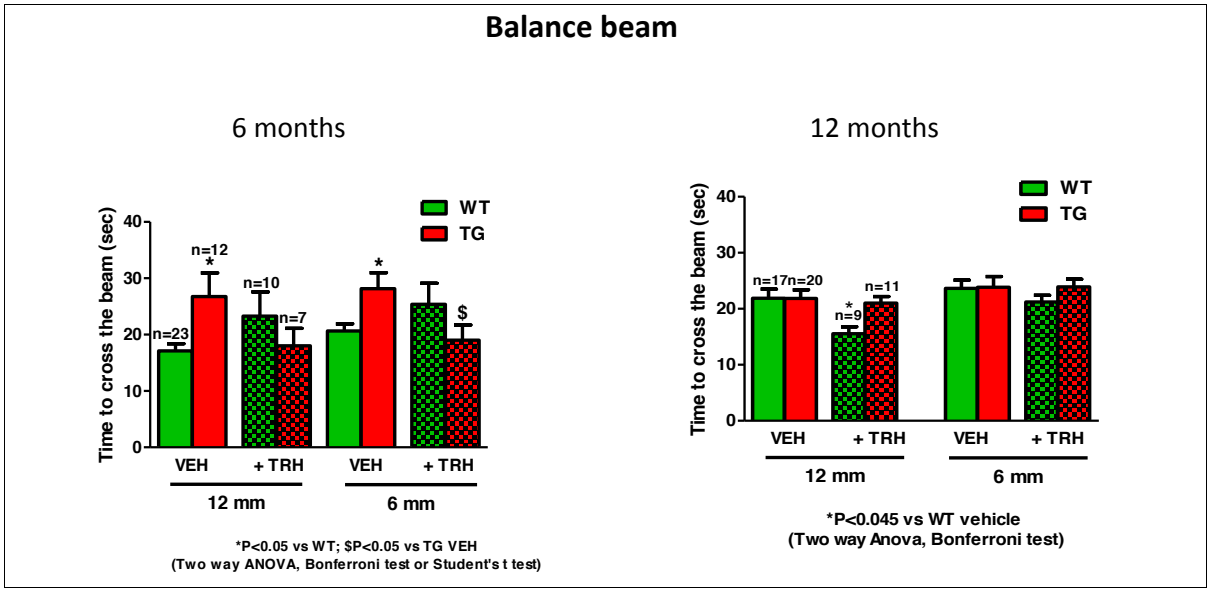

Figure 18. Motor coordination analyses evaluated by balance beam test of 6 and 12 months old wild-type and BAC hLRRK2 G2019S treated for 2 months with 1% Trehalose aqueous solution (TRH) or water (VEH).

The Fig 19 shows the results of Pole test. At 6 months, Two way Anova, revealed a significant difference among GS and wild-type mice ($F_{(1,45)}$ =14.27, P=0.0005) but none for

the genotype and treatment interaction ($F_{(1,45)}$ =0.67, P=0.41). Post hoc analysis revealed a significant increase of the time request by GS mice treated with vehicle to complete the test, compared to corresponding wild-type mice. At 12 months, Two way Anova did not showed a significant difference among the genotype, nonetheless Bonferroni test revealed that GS mice, treated with trehalose, took longer time to complete the task compared to wild-type with the same treatment.

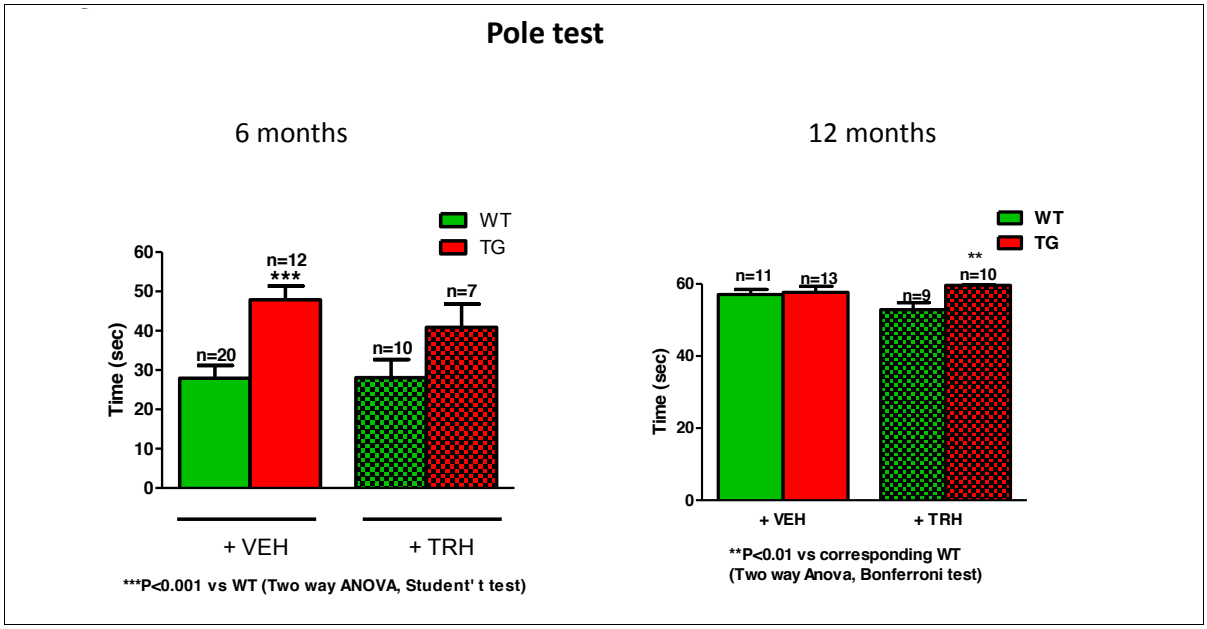

Figure 19. Episodic memory analyses of 6 and 12 months old wild-type and BAC hLRRK2 G2019S treated for 2 months with 1% Trehalose aqueous solution (TRH) or water (VEH).

In Fig 20 the Rotarod 32 rpm results are shown. At the age of 6 months, Two way Anova, revealed a significant difference of treatment as between subject factor ($F_{(3,172)}$ =8.71, P<0.0001), of time ($F_{(3,172)}$=4.11, P=0.007) but not time x treatment interaction ($F_{(3,172)}$ =0.67, P<0.0001). Post hoc analysis revealed a significant decrease of time in vehicle treated GS mice at all tested trials while trehalose treatment significantly rescued the performance of GS mice. At 12 months, Two way Anova, revealed a significant difference of treatment as between subject factor ($F_{(3,96)}$ =18.22, P<0.0001), of time ($F_{(3,96)}$=5.61, P=0.001) but not time x treatment interaction ($F_{(9,96)}$ =1.71, P=0.001). Post hoc analysis revealed a significant improvement of performance, after treatment, in GS mice only at the 2° and 3° trial.

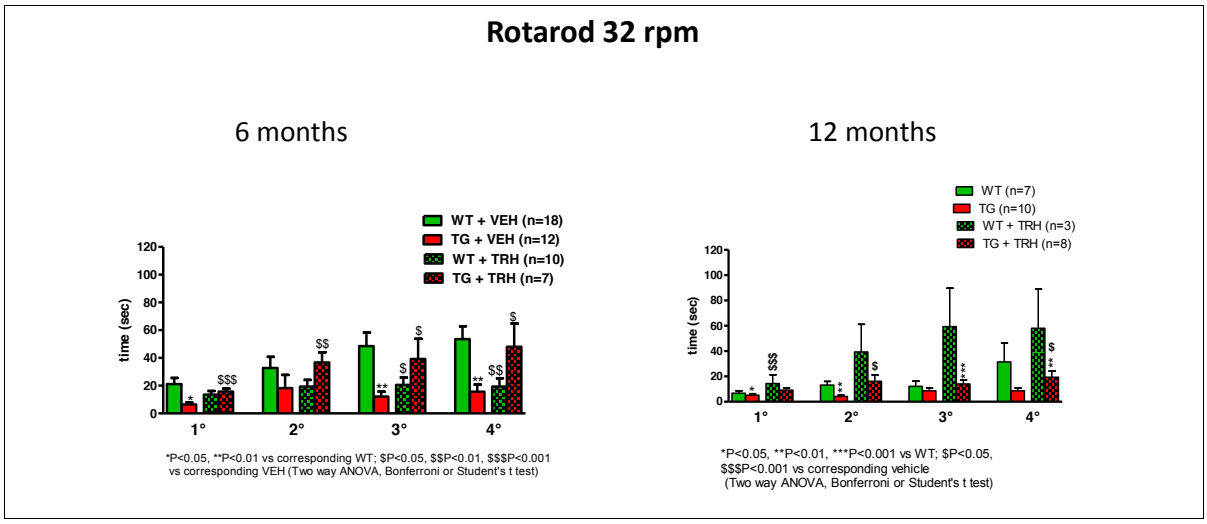

Figure 20. Motor coordination analyses evaluated by rotarod 32 rpm of 6 and 12 months old wild-type and BAC hLRRK2 G2019S treated for 2 months with 1% Trehalose aqueous solution (TRH) or water (VEH).

When tested in the Novel Object Recognition test (Fig 21), at the age of 6 months, Two way Anova revealed a significant difference of treatment as between subject factor ($F_{(3,129)}$ =14.47, P<0.0001), but not of time ($F_{(2,129)}$=0.26, P=0.76) and of time x treatment interaction ($F_{(6,129)}$ =1.05, P=0.39). Post hoc analysis revealed a significant reduction of index in vehicle GS mice at all the tested intervals compared to corresponding wild-type; trehalose treatment rescued at all the tested times but significantly only at 120 min. At age of 12 months similar pattern was shown [two way anova: treatment as between subject factor ($F_{(3,120)}$ =20.35, P<0.0001), but not of time ($F_{(2,120)}$=1.08, P=0.34) and of time x treatment interaction ($F_{(6,120)}$ =0.72, P=0.63)]. Post hoc analysis revealed a significant reduction of index in vehicle TG mice at all the tested intervals compared to corresponding wild-type; trehalose treatment significantly rescued at all the tested times.

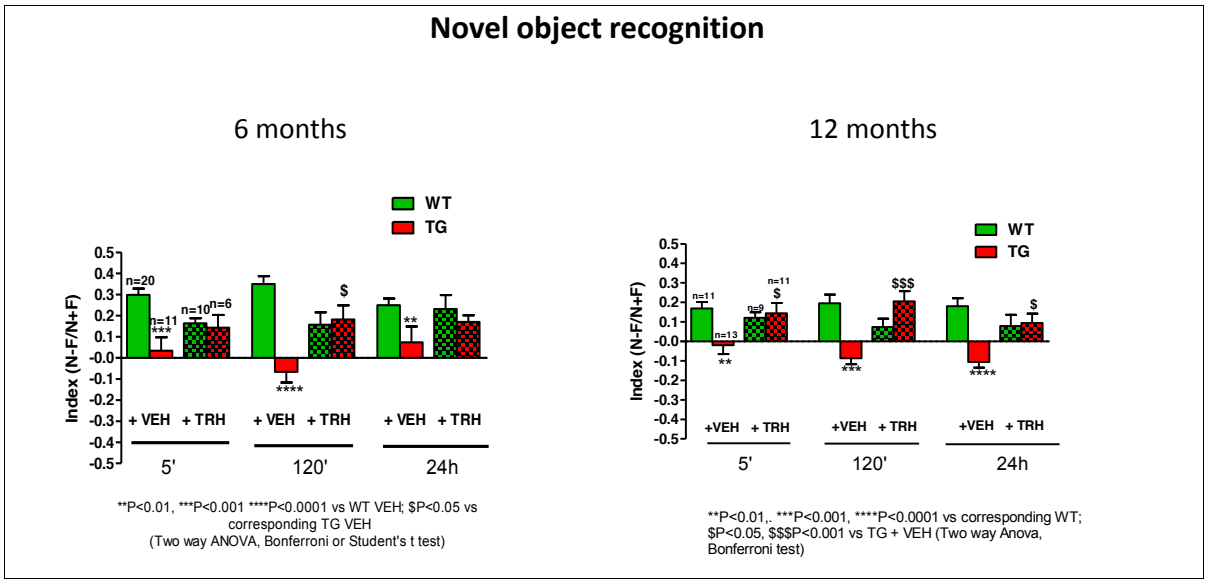

Figure 21. Episodic memory analyses of 6 and 12 months old wild-type and BAC hLRRK2 G2019S treated for 2 months with 1% Trehalose aqueous solution (TRH) or water (VEH).

Summarizing, the results of rotarod at 32 rpm evidentiate a motor impairment of GS mice both at 6 and 12 months compared to wild type ones, whereas the balance beam and pole test results depicts a motor coordination of the GS mice already at 6 months of age. These motor deficits were rescued by the treatment with trehalose indicating a crutial role of the protein aggregation in the development of the motor defects. Moreover, we report also a cognivite impairment of the GS mice at both 6 and 12 months that is completely rescued by the trehalose treatment.

Hence, this evidence suggests that autophagy induction via trehalose might protect from the NSF aggregation and motor and cognitive impairment observed in G2019S animals.

5 Discussion

Despite being responsible for most of the case of familial PD, the physiological function of LRRK2 is far from being understood. In this study, we focused on the role of LRRK2 kinase activity. In particular, we characterized the impact of LRRK2 G2019S mutation on SV dynamics and neuronal morphology, and on NSF clearance.

Accumulating evidence has pointed out how LRRK2 plays a role in the regulation of presynaptic activity. Severe neurotransmission defects have been observed in different LRRK2 models (Y. Li et al. 2009; X. Li et al. 2010; Tong et al. 2012). The R1441C LRRK2 homozygous knock-in mice and the R1441C LRRK2 BAC (bacterial artificial chromosome) transgenic mice display impairments in nigrostriatal dopaminergic innervation and degeneration of the nigrostriatal projections (X. Li et al. 2010; Tong et al. 2009). Interestingly, the G2019S BAC transgenic mice show deficiencies in striatal dopamine release and increased striatal tau immunoreactivity without dopaminergic neuron loss in the SNpc (X. Li et al. 2010; Melrose et al. 2010). Previous studies of our group suggested that the presence of LRRK2 is mandatory or the proper neuronal electrophysiological activity, vesicular trafficking and spatial distribution of the presynaptic pool. We identified LRRK2 as a molecular hub, connecting synaptic vesicles to cytoskeletal elements via a complex panel of protein-protein interactions and described how the pharmacological inhibition of LRRK2 kinase activity alters synaptic function (Piccoli et al 2014, Cirnaru et al 2014). Many studies report that LRRK2 might regulate SV dynamics by phosphorylation of presynaptic proteins such as endophilin and snapin (Matta et al. 2012; Yun et al. 2013). Recently we have identified NSF as LRRK2 interactor and substrate. NSF phosphorylation on threonine 645**,** an important site for NSF oligomerization, increases NSF ATPase activity and increases the disassembly rate of SNARE complexes. It is important to mention that wild-type LRRK2 has a reduced kinase activity and that the gain of function conferred by th**e** mutation G2019S might perturb proper neurotransmitter release. Indeed, our present data report a fast endocytosis in the LRRK2 hG2019S BAC cortical neurons, which is in line with the increase in the glutamate release that has been reported in LRRK2 G2019S knock-in mice. nonetheless our observation is in contrast with the reduced dopamine release observed in the G2019S BAC mice. This might be due to different regulation in the release of the dopaminergic dense core vesicles with respect to the glutamate one. For this we believe

further analysis of the DA synapse must be done using dopaminergic neurons, as we believe that the alteration of the intracellular trafficking might depict the starting point in the PD pathogenesis. Nonetheless the quantity of dopamine released depends also on the number of releasing sites available. As recently reported, SNc dopaminergic neurons have a massive and highly-tortuous axonal arborisation along which more 200 000 synapse are distributed towards the striatum (Matsuda et al. 2009; Hunn et al. 2015) . Decrease in the neurite tree complexity directly lead to reduce of the number of releasing sites and consequentially in quantity of neurotransmitter. In this study, we report the impact of both LRRK2 protein levels and kinase activity on the neuronal morphology of LRRK2 BAC hG2019S mice cortical culture neurons, indicating how the two act in the same direction generating a cumulative negative effect in the neurites outgrowth. Interestingly, chronic pharmacological inhibition of the kinase activity produced the same effects as the removal of the endogenous murine LRRK2 (olig 6 condition), highlighting also the specific contribution of LRRK2 increase activity to the phenotype that remained impaired respect to the Wt. This was further proved by rescue noticed in the olig 6 condition, which is similar to a knock-in LRRK2 hG2019S, upon chronic treatment with LRRK2 kinase inhibitor. Altogether, these data indicate that LRRK2 protein as well as its kinase activity controls the neurites outgrowth. Speculating on the observation of the study of Stewart et al. that report pronounced overgrowth of the neuromuscular junction of Drosophila that express a dominant negative genetically modified NSF, NSF2 ($NSF^{E/Q}$) that is still able to bind MgATP but it hydrolysis ATP less (Stewart et al. 2002; Nunes et al. 2006) we are tempted to think that the reduced complexity of the neurite tree of the G2019S mice neurons might be mediated by a hyper-phosphorylated NSF that hydrolysis more ATP. Moreover, we believe that through these observation we could explain the reduce in the dopamine release observed in the BAC G2019S mice, revealing two distinct mechanism that can lead to the early development of PD: alteration in SV dynamics and reduction of complexity of the neuronal processes. Nonetheless, further investigation is needed using a more appropriate disease model, such as the patient derived neuronal precursors that can be efficiently differentiate to dopaminergic neurons (Reinhardt et al. 2013).

On the other hand, our data show that LRRK2 kinase activity might contribute also to a late pathological mechanism via impaired NSF protein clearance. We identified NSF aggregates that co-localize with alpha synuclein in the basal ganglia of LRRK2 G2019S PD patients as well as in the striatum of aged mice that over express hLRRK2 G2019S variant. These observations are in line with other post-mortem brain investigations that have shown that LRRK2 G2019S kindred most often show synucleinopathy, occasionally tauopathy,

suggesting a role for LRRK2 in protein inclusion pathology (Taymans and Cookson 2010). Recent studies showed that LRRK2 overexpression led to proteins accumulation without affecting the catalytic activity of the proteasome or expression levels of proteasomal core sub complexes (Lichtenberg et al. 2011). Indeed, our results indicate that the proteasome activity of the aged GS mouse is similar to the Wild-type ones. Thus, LRRK2 might control protein fate acting upstream of the proteasome, in particular influencing their ubiquitination. We reported here that LRRK2 G2019S aberrant kinase activity negatively correlates with NSF ubiquitination and subsequent degradation via proteasome. In particular, our data suggest that LRRK2 kinase activity directly impair ubiquitination of NSF rather than interfere with the proteasomal degradation system. As previously discussed, LRRK2 specifically phosphorylates NSF on Thr645 a site that is crucial for NSF oligomerization and catalytic activity (Belluzzi et al. 2015 appendix). Our hypothesis is that LRRK2 phosphorylation of NSF on the threonin 645 residue might impair via steric hindrance the addition of ubiquitin tagging on flanking lysine, impairing NSF ubiquitination. In fact, it will be of great interest to perform structural studies and analyse whether the phosphorylstion of this site may disturb via steric or elettric hyndrance the transfer of a ubiquitin chain to near-by lysine residue.

Considering that wild-type LRRK2 has a low kinase activity, and that the protein bears multiple domains that mediate protein-protein interaction it is possible that the main function of LRRK2 is as a scaffolding protein with the residual kinase activity, important to regulate omophylic binding (Berger, Smith, and Lavoie 2010; Greggio et al. 2008). This might suggest that only upon mutation LRRK2 gains the capability of phosphorylating other proteins. In particular, despite the low stoichiometry characterizing LRRK2 G2019S enzymatic activity, we argue that LRRK2 phosphorylation of NSF might shift the equilibrium between ubiquitinated and not ubiquitinated NSF. This event might impair NSF clearance via proteasome and eventually induce its cytosolic aggregation. The proper turnover of NSF is crucial for the correct functioning of the presynaptic processes as NSF is a key component of presynaptic machinery, allowing the first step of SV recycling (Pallanck et al. 1995). Numerous studies have shown that depletion of cytosolic NSF impair membrane fusion machinery (Rothman 1994) and results in accumulation of intracellular vesicles (Malhotra et al. 1988; Mohtashami et al. 2001). Interestingly, experimental ischemia induces NSF aggregation into Triton-X 100 insoluble inclusions that sequester synaptic vesicle (Liu and Hu 2004)(Liu and Hu, 2004). Therefore, NSF aggregation might affect the presynaptic fusion machinery, determining a reduction of the neurotransmitter exocytosis that might explain the early stage or preclinical manifestation of PD in animal model (Melrose et al. 2010) or in LRRK2 G2019S carriers (Sossi et al. 2010). Protein clearance plays an important role in the

homeostasis of the neuronal cells, particular sensitive to abnormal proteins accumulation as they do not regenerate and lose the proteasomal activity with aging. Thus, impairment in NSF clearance might explain also the neuronal loss in the substantia nigra reported in late phase of the disease. Indeed, our experimental data suggests that NSF accumulation in cytoplasmic aggregates is toxic. Moreover, we report that NSF aggregation cytotoxicity is dependent on LRRK2 kinase activity. Altogether, this evidence could leave space for a therapeutic strategy targeting LRRK2 kinase activity. Several brain penetrant LRRK2 selective inhibitors have been identified (Deng et al. 2011; Reith et al. 2012; Sheng et al. 2012); however, the wide expression of LRRK2 in other organs apart from the central nervous system, including lung, kidney and the immune system raised issues about side effects. Last but not least, our recent data describing a functional role of endogenous LRRK2 enzymatic activity at the synaptic site (Cirnaru et al. 2014) and the severe kidney abnormality reported upon chronic inhibition (Herzig et al. 2011) reduce the feasibility of pharmacological strategy targeting LRRK2 kinase activity. The pharmacological modulation of protein clearance is instead an achievable goal: the degradation of protein misfolding can be improved by induction of the autophagic pathway (Ebrahimi-Fakhari, Wahlster, and McLean 2012). A number of report suggests that autophagy itself might be involved in LRRK2 physiological and pathological role, but the mechanism underlined is almost unclear [reviewed in (Manzoni 2012)]. The investigation of *LRRK2*-deficient mice displayed a biphasic alteration in autophagy in the kidney (Tong et al. 2012); however, similar studies in an independent *LRRK2*-knock out mouse line demonstrated an accumulation of secondary lysosomes in the kidney without a major involvement of autophagy (Herzig et al. 2011). Even more complex is the state-of-art describing autophagy in LRRK2 disease context. In fact a number of authors conclude that G2019S mutation increases autophagy in different model, including stable cell line (Gómez-Suaga et al. 2014; Plowey et al. 2008)8), fibroblast (Yakhine-Diop et al. 2014), iPS derived neurons (Bravo-San Pedro et al. 2013), *C.Elegans* (Ferree et al. 2012) and mice (Ramonet et al. 2011). However others studies have reported that the same mutation reduces (Manzoni et al. 2013) Oxidative stress including DNA damage, increased lipid and protein oxidation, are important features of aging and neurodegeneration suggesting that endogenous antioxidant protective pathways are inadequate or overwhelmed. Importantly, oxidative protein damage contributes to age-dependent accumulation of dysfunctional mitochondria or protein aggregates. In addition, environmental toxins such as rotenone and paraquat, which are risk factors for the pathogenesis of neurodegenerative diseases, also promote protein oxidation. The obvious approach of supplementing the primary antioxidant systems designed to suppress the initiation of oxidative stress has been tested in animal models and positive

results were obtained. However, these findings have not been effectively translated to treating human patients, and clinical trials for antioxidant therapies using radical scavenging molecules such as α-tocopherol, ascorbate and coenzyme Q have met with limited success, highlighting several limitations to this approach. These could include: (1) radical scavenging antioxidants cannot reverse established damage to proteins and organelles; (2) radical scavenging antioxidants are oxidant specific, and can only be effective if the specific mechanism for neurodegeneration involves the reactive species to which they are targeted and (3) since reactive species play an important role in physiological signaling, suppression of endogenous oxidants maybe deleterious. Therefore, alternative approaches that can circumvent these limitations are needed. While not previously considered an antioxidant system we propose that the autophagy-lysosomal activities, may serve this essential function in neurodegenerative diseases by removing damaged or dysfunctional proteins and organelle (Giordano, Darley-Usmar, and Zhang 2014)or at least does not affect (Sánchez-Danés et al., 2012) autophagy. Thus it is still matter of debate if G2019S mutation correlates with an increased or a decreased degradative pathway. Even accepting the idea that G2019S correlates with an increased autophagic activity, remains open question if G2019S impact on autophagy comes as a direct result of kinase hyperactivation or instead is as cellular response aiming at rescuing LRRK2 toxicity. In any case, the stimulation of autophagy might compensate for low functional UPS and reduce oxidative stress in damaged neurons (Giordano, Darley-Usmar, and Zhang 2014). Trehalose is a disaccharide that prevents aggregation of denatured proteins inducing their degradation via autophagy. Treatment with trehalose demonstrated to be protective in models of Huntington disease, Spinocerebellar ataxia and Parkin-PD(Sarkar et al. 2007; Rodríguez-Navarro et al. 2010). Indeed enhancing protein degradation via autophagy induction might prove to be a double-edged sword, since both reduced and excessive protein degradation can result neurotoxic. Furthermore, the exact role and nature of protein aggregates or Lewy bodies in neurodegeneration remains unclear. In fact it has been proposed that aggregate form in neurons as a protective mechanism to scavenge soluble toxic forms and prolong cellular survival ((Arrasate et al. 2004). Thus, the overall consequences of preventing, dissolving or removing mature aggregates are uncertain. Notwithstanding all these concerns, we reported here that chronic trehalose treatment reduced NSF aggregation and partially ameliorated motor phenotype in aged G2019S mice. The pharmacodynamics and the therapeutic profile of trehalose is well established for human treatment: thus we deem our results could be translated into the clinical management of PD patients.

Conclusions

In this study, we describe how the kinase activating G2019S mutation affects neuronal functions and NSF protein accumulation. We depict a scenario where alteration of SV dynamics and reduction of the neurite tree accounts for early onset PD symptoms while NSF aggregation correlates with late onset defects such as motor deficits. Moreover, we report that the chronic treatment with trehalose, an autophagy-inducing molecule, partially recovered the motor phenotype and NSF aggregation proposing it as an interesting therapeutic strategy.

References

Abeliovich, A., Y. Schmitz, I. Fariñas, D. Choi-Lundberg, W. H. Ho, P. E. Castillo, N. Shinsky, et al. 2000. "Mice Lacking Alpha-Synuclein Display Functional Deficits in the Nigrostriatal Dopamine System." *Neuron* 25 (1): 239–52.

Adams, John R., Hinke van Netten, Michael Schulzer, Edwin Mak, Jessamyn Mckenzie, Audrey Strongosky, Vesna Sossi, et al. 2005. "PET in LRRK2 Mutations: Comparison to Sporadic Parkinson's Disease and Evidence for Presymptomatic Compensation." *Brain: A Journal of Neurology* 128 (Pt 12): 2777–85. doi:10.1093/brain/awh607.

Alegre-Abarrategui, Javier, Helen Christian, Michele M. P. Lufino, Ruxandra Mutihac, Lara Lourenço Venda, Olaf Ansorge, and Richard Wade-Martins. 2009. "LRRK2 Regulates Autophagic Activity and Localizes to Specific Membrane Microdomains in a Novel Human Genomic Reporter Cellular Model." *Human Molecular Genetics* 18 (21): 4022–34. doi:10.1093/hmg/ddp346.

Alvarez-Erviti, Lydia, Maria C. Rodriguez-Oroz, J. Mark Cooper, Cristina Caballero, Isidro Ferrer, Jose A. Obeso, and Anthony H. V. Schapira. 2010. "Chaperone-Mediated Autophagy Markers in Parkinson Disease Brains." *Archives of Neurology* 67 (12): 1464–72. doi:10.1001/archneurol.2010.198.

Anand, Vasanti S., and Steven P. Braithwaite. 2009. "LRRK2 in Parkinson's Disease: Biochemical Functions." *The FEBS Journal* 276 (22): 6428–35. doi:10.1111/j.1742-4658.2009.07341.x.

Anheim, M., A. Elbaz, S. Lesage, A. Durr, C. Condroyer, F. Viallet, P. Pollak, et al. 2012. "Penetrance of Parkinson Disease in Glucocerebrosidase Gene Mutation Carriers." *Neurology* 78 (6): 417–20. doi:10.1212/WNL.0b013e318245f476.

Antrobus, Robin, and Georg H. H. Borner. 2011. "Improved Elution Conditions for Native Co-Immunoprecipitation." *PloS One* 6 (3): e18218. doi:10.1371/journal.pone.0018218.

Ariga, Hiroyoshi, Kazuko Takahashi-Niki, Izumi Kato, Hiroshi Maita, Takeshi Niki, and Sanae M. M. Iguchi-Ariga. 2013. "Neuroprotective Function of DJ-1 in Parkinson's Disease." *Oxidative Medicine and Cellular Longevity* 2013: 683920. doi:10.1155/2013/683920.

Arrasate, Montserrat, Siddhartha Mitra, Erik S. Schweitzer, Mark R. Segal, and Steven Finkbeiner. 2004. "Inclusion Body Formation Reduces Levels of Mutant Huntingtin and the Risk of Neuronal Death." *Nature* 431 (7010): 805–10. doi:10.1038/nature02998.

Bandopadhyay, Rina, Ann E. Kingsbury, Mark R. Cookson, Andrew R. Reid, Ian M. Evans, Andrew D. Hope, Alan M. Pittman, et al. 2004. "The Expression of DJ-1 (PARK7) in Normal Human CNS and Idiopathic Parkinson's Disease." *Brain: A Journal of Neurology* 127 (Pt 2): 420–30. doi:10.1093/brain/awh054.

Bardien, Soraya, Suzanne Lesage, Alexis Brice, and Jonathan Carr. 2011. "Genetic Characteristics of Leucine-Rich Repeat Kinase 2 (LRRK2) Associated Parkinson's Disease." *Parkinsonism & Related Disorders* 17 (7): 501–8. doi:10.1016/j.parkreldis.2010.11.008.

Bartels, Tim, Joanna G. Choi, and Dennis J. Selkoe. 2011. "α-Synuclein Occurs Physiologically as a Helically Folded Tetramer That Resists Aggregation." *Nature* 477 (7362): 107–10. doi:10.1038/nature10324.

Belluzzi, Elisa, Elisa Greggio, and Giovanni Piccoli. 2012. "Presynaptic Dysfunction in Parkinson's Disease: A Focus on LRRK2." *Biochemical Society Transactions* 40 (5): 1111–16. doi:10.1042/BST20120124.

Benamer, Hani T. S., and Rajith de Silva. 2010. “LRRK2 G2019S in the North African Population: A Review.” *European Neurology* 63 (6): 321–25. doi:10.1159/000279653.

Bentivoglio, A. R., P. Cortelli, E. M. Valente, T. Ialongo, A. Ferraris, A. Elia, P. Montagna, and A. Albanese. 2001. “Phenotypic Characterisation of Autosomal Recessive PARK6-Linked Parkinsonism in Three Unrelated Italian Families.” *Movement Disorders: Official Journal of the Movement Disorder Society* 16 (6): 999–1006.

Berger, Zdenek, Kelsey A. Smith, and Matthew J. Lavoie. 2010. “Membrane Localization of LRRK2 Is Associated with Increased Formation of the Highly Active LRRK2 Dimer and Changes in Its Phosphorylation.” *Biochemistry* 49 (26): 5511–23. doi:10.1021/bi100157u.

Bonifati, Vincenzo. 2014. “Genetics of Parkinson’s Disease--State of the Art, 2013.” *Parkinsonism & Related Disorders* 20 Suppl 1 (January): S23–28. doi:10.1016/S1353-8020(13)70009-9.

Bonifati, V., P. Rizzu, F. Squitieri, E. Krieger, N. Vanacore, J. C. van Swieten, A. Brice, et al. 2003. “DJ-1(PARK7), a Novel Gene for Autosomal Recessive, Early Onset Parkinsonism.” *Neurological Sciences: Official Journal of the Italian Neurological Society and of the Italian Society of Clinical Neurophysiology* 24 (3): 159–60. doi:10.1007/s10072-003-0108-0.

Bravo-San Pedro, José M., Mireia Niso-Santano, Rubén Gómez-Sánchez, Elisa Pizarro-Estrella, Ana Aiastui-Pujana, Ana Gorostidi, Vicente Climent, et al. 2013. “The LRRK2 G2019S Mutant Exacerbates Basal Autophagy through Activation of the MEK/ERK Pathway.” *Cellular and Molecular Life Sciences: CMLS* 70 (1): 121–36. doi:10.1007/s00018-012-1061-y.

Burré, Jacqueline, Sandro Vivona, Jiajie Diao, Manu Sharma, Axel T. Brunger, and Thomas C. Südhof. 2013. “Properties of Native Brain α-Synuclein.” *Nature* 498 (7453): E4–6; discussion E6–7. doi:10.1038/nature12125.

Calabresi, Paolo, Barbara Picconi, Alessandro Tozzi, Veronica Ghiglieri, and Massimiliano Di Filippo. 2014. “Direct and Indirect Pathways of Basal Ganglia: A Critical Reappraisal.” *Nature Neuroscience* 17 (8): 1022–30. doi:10.1038/nn.3743.

Canet-Avilés, Rosa M., Mark A. Wilson, David W. Miller, Rili Ahmad, Chris McLendon, Sourav Bandyopadhyay, Melisa J. Baptista, Dagmar Ringe, Gregory A. Petsko, and Mark R. Cookson. 2004. “The Parkinson’s Disease Protein DJ-1 Is Neuroprotective due to Cysteine-Sulfinic Acid-Driven Mitochondrial Localization.” *Proceedings of the National Academy of Sciences of the United States of America* 101 (24): 9103–8. doi:10.1073/pnas.0402959101.

Chen, Yun, and Gerald W. Dorn. 2013. “PINK1-Phosphorylated Mitofusin 2 Is a Parkin Receptor for Culling Damaged Mitochondria.” *Science (New York, N.Y.)* 340 (6131): 471–75. doi:10.1126/science.1231031.

Cherra, Salvatore J., and Charleen T. Chu. 2008. “Autophagy in Neuroprotection and Neurodegeneration: A Question of Balance.” *Future Neurology* 3 (3): 309–23. doi:10.2217/14796708.3.3.309.

Chu, Charleen T. 2006. “Autophagic Stress in Neuronal Injury and Disease.” *Journal of Neuropathology and Experimental Neurology* 65 (5): 423–32. doi:10.1097/01.jnen.0000229233.75253.be.

Cirnaru, Maria D., Antonella Marte, Elisa Belluzzi, Isabella Russo, Martina Gabrielli, Francesco Longo, Ludovico Arcuri, et al. 2014. “LRRK2 Kinase Activity Regulates Synaptic Vesicle Trafficking and Neurotransmitter Release through Modulation of LRRK2 Macro-Molecular Complex.” *Frontiers in Molecular Neuroscience* 7: 49. doi:10.3389/fnmol.2014.00049.

Civiero, Laura, Renée Vancraenenbroeck, Elisa Belluzzi, Alexandra Beilina, Evy Lobbestael, Lauran Reyniers, Fangye Gao, et al. 2012. “Biochemical Characterization of Highly Purified Leucine-Rich Repeat Kinases 1 and 2 Demonstrates Formation of Homodimers.” *PloS One* 7 (8): e43472. doi:10.1371/journal.pone.0043472.

Cookson, Mark R. 2012. “Evolution of Neurodegeneration.” *Current Biology: CB* 22 (17): R753–61.

doi:10.1016/j.cub.2012.07.008.

———. 2015. “LRRK2 Pathways Leading to Neurodegeneration.” *Current Neurology and Neuroscience Reports* 15 (7): 42. doi:10.1007/s11910-015-0564-y.

Cully, Megan, Han You, Arnold J. Levine, and Tak W. Mak. 2006. “Beyond PTEN Mutations: The PI3K Pathway as an Integrator of Multiple Inputs during Tumorigenesis.” *Nature Reviews. Cancer* 6 (3): 184–92. doi:10.1038/nrc1819.

Dachsel, J. C., C. Wider, C. Vilariño-Güell, J. O. Aasly, A. Rajput, A. H. Rajput, T. Lynch, et al. 2011. “Death-Associated Protein Kinase 1 Variation and Parkinson’s Disease.” *European Journal of Neurology* 18 (8): 1090–93. doi:10.1111/j.1468-1331.2010.03255.x.

Deng, Xianming, Nicolas Dzamko, Alan Prescott, Paul Davies, Qingsong Liu, Qingkai Yang, Jiing-Dwan Lee, et al. 2011. “Characterization of a Selective Inhibitor of the Parkinson’s Disease Kinase LRRK2.” *Nature Chemical Biology* 7 (4): 203–5. doi:10.1038/nchembio.538.

de Vries, Rosa L. A., and Serge Przedborski. 2013. “Mitophagy and Parkinson’s Disease: Be Eaten to Stay Healthy.” *Molecular and Cellular Neurosciences* 55 (July): 37–43. doi:10.1016/j.mcn.2012.07.008.

Ebrahimi-Fakhari, Darius, Lara Wahlster, and Pamela J. McLean. 2012. “Protein Degradation Pathways in Parkinson’s Disease: Curse or Blessing.” *Acta Neuropathologica* 124 (2): 153–72. doi:10.1007/s00401-012-1004-6.

Ehlers, Michael D. 2003. “Activity Level Controls Postsynaptic Composition and Signaling via the Ubiquitin-Proteasome System.” *Nature Neuroscience* 6 (3): 231–42. doi:10.1038/nn1013.

Ferree, Andrew, Maria Guillily, Hu Li, Katelyn Smith, Aki Takashima, Rachel Squillace, Manfred Weigele, James J. Collins, and Benjamin Wolozin. 2012. “Regulation of Physiologic Actions of LRRK2: Focus on Autophagy.” *Neuro-Degenerative Diseases* 10 (1-4): 238–41. doi:10.1159/000332599.

Funayama, Manabu, Kazuko Hasegawa, Hisayuki Kowa, Masaaki Saito, Shoji Tsuji, and Fumiya Obata. 2002. “A New Locus for Parkinson’s Disease (PARK8) Maps to Chromosome 12p11.2-q13.1.” *Annals of Neurology* 51 (3): 296–301.

Garcia-Reitböck, Pablo, Oleg Anichtchik, Arianna Bellucci, Mariangela Iovino, Chiara Ballini, Elena Fineberg, Bernardino Ghetti, et al. 2010. “SNARE Protein Redistribution and Synaptic Failure in a Transgenic Mouse Model of Parkinson’s Disease.” *Brain: A Journal of Neurology* 133 (Pt 7): 2032–44. doi:10.1093/brain/awq132.

Gardet, Agnès, Yair Benita, Chun Li, Bruce E. Sands, Isabel Ballester, Christine Stevens, Joshua R. Korzenik, et al. 2010. “LRRK2 Is Involved in the IFN-Gamma Response and Host Response to Pathogens.” *Journal of Immunology (Baltimore, Md.: 1950)* 185 (9): 5577–85. doi:10.4049/jimmunol.1000548.

Gilks, William P., Patrick M. Abou-Sleiman, Sonia Gandhi, Shushant Jain, Andrew Singleton, Andrew J. Lees, Karen Shaw, et al. 2005. “A Common LRRK2 Mutation in Idiopathic Parkinson’s Disease.” *Lancet (London, England)* 365 (9457): 415–16. doi:10.1016/S0140-6736(05)17830-1.

Giordano, Samantha, Victor Darley-Usmar, and Jianhua Zhang. 2014. “Autophagy as an Essential Cellular Antioxidant Pathway in Neurodegenerative Disease.” *Redox Biology* 2: 82–90. doi:10.1016/j.redox.2013.12.013.

Girotto, Stefania, Laura Cendron, Marco Bisaglia, Isabella Tessari, Stefano Mammi, Giuseppe Zanotti, and Luigi Bubacco. 2014. “DJ-1 Is a Copper Chaperone Acting on SOD1 Activation.” *The Journal of Biological Chemistry* 289 (15): 10887–99. doi:10.1074/jbc.M113.535112.

Goedert, Michel, Maria Grazia Spillantini, Kelly Del Tredici, and Heiko Braak. 2012. “100 Years of Lewy Pathology.” *Nature Reviews Neurology* 9 (1): 13–24. doi:10.1038/nrneurol.2012.242.

Goldberg, Matthew S., Sheila M. Fleming, James J. Palacino, Carlos Cepeda, Hoa A. Lam, Anushree Bhatnagar, Edward G. Meloni, et al. 2003. "Parkin-Deficient Mice Exhibit Nigrostriatal Deficits but Not Loss of Dopaminergic Neurons." *The Journal of Biological Chemistry* 278 (44): 43628–35. doi:10.1074/jbc.M308947200.

Gómez-Suaga, P., E. Fdez, B. Fernández, M. Martínez-Salvador, M. Blanca Ramírez, J. Madero-Pérez, P. Rivero-Ríos, J. M. Fuentes, and S. Hilfiker. 2014. "Novel Insights into the Neurobiology Underlying LRRK2-Linked Parkinson's Disease." *Neuropharmacology* 85 (October): 45–56. doi:10.1016/j.neuropharm.2014.05.020.

Greene, Andrew W., Karl Grenier, Miguel A. Aguileta, Stephanie Muise, Rasoul Farazifard, M. Emdadul Haque, Heidi M. McBride, David S. Park, and Edward A. Fon. 2012. "Mitochondrial Processing Peptidase Regulates PINK1 Processing, Import and Parkin Recruitment." *EMBO Reports* 13 (4): 378–85. doi:10.1038/embor.2012.14.

Greggio, Elisa, Ibardo Zambrano, Alice Kaganovich, Alexandra Beilina, Jean-Marc Taymans, Veronique Daniëls, Patrick Lewis, et al. 2008. "The Parkinson Disease-Associated Leucine-Rich Repeat Kinase 2 (LRRK2) Is a Dimer That Undergoes Intramolecular Autophosphorylation." *The Journal of Biological Chemistry* 283 (24): 16906–14. doi:10.1074/jbc.M708718200.

Hattori, N., T. Kitada, H. Matsumine, S. Asakawa, Y. Yamamura, H. Yoshino, T. Kobayashi, et al. 1998. "Molecular Genetic Analysis of a Novel Parkin Gene in Japanese Families with Autosomal Recessive Juvenile Parkinsonism: Evidence for Variable Homozygous Deletions in the Parkin Gene in Affected Individuals." *Annals of Neurology* 44 (6): 935–41. doi:10.1002/ana.410440612.

Herbert, Megan K., Jorine M. Eeftens, Marjolein B. Aerts, Rianne A. J. Esselink, Bastiaan R. Bloem, H. Bea Kuiperij, and Marcel M. Verbeek. 2014. "CSF Levels of DJ-1 and Tau Distinguish MSA Patients from PD Patients and Controls." *Parkinsonism & Related Disorders* 20 (1): 112–15. doi:10.1016/j.parkreldis.2013.09.003.

Hertz, Nicholas T., Amandine Berthet, Martin L. Sos, Kurt S. Thorn, Al L. Burlingame, Ken Nakamura, and Kevan M. Shokat. 2013. "A Neo-Substrate That Amplifies Catalytic Activity of Parkinson's-Disease-Related Kinase PINK1." *Cell* 154 (4): 737–47. doi:10.1016/j.cell.2013.07.030.

Herzig, Martin C., Carine Kolly, Elke Persohn, Diethilde Theil, Tatjana Schweizer, Thomas Hafner, Christine Stemmelen, et al. 2011. "LRRK2 Protein Levels Are Determined by Kinase Function and Are Crucial for Kidney and Lung Homeostasis in Mice." *Human Molecular Genetics* 20 (21): 4209–23. doi:10.1093/hmg/ddr348.

Hristova, Ventzislava A., Steven A. Beasley, R. Jane Rylett, and Gary S. Shaw. 2009. "Identification of a Novel Zn2+-Binding Domain in the Autosomal Recessive Juvenile Parkinson-Related E3 Ligase Parkin." *The Journal of Biological Chemistry* 284 (22): 14978–86. doi:10.1074/jbc.M808700200.

Hunn, Benjamin H. M., Stephanie J. Cragg, J. Paul Bolam, Maria-Grazia Spillantini, and Richard Wade-Martins. 2015. "Impaired Intracellular Trafficking Defines Early Parkinson's Disease." *Trends in Neurosciences* 38 (3): 178–88. doi:10.1016/j.tins.2014.12.009.

Inoue, Takao, Yanru Wang, Kevin Jefferies, Jie Qi, Ayana Hinton, and Michael Forgac. 2005. "Structure and Regulation of the V-ATPases." *Journal of Bioenergetics and Biomembranes* 37 (6): 393–98. doi:10.1007/s10863-005-9478-8.

Ishikawa, Shizuma, Takahiro Taira, Kazuko Takahashi-Niki, Takeshi Niki, Hiroyoshi Ariga, and Sanae M. M. Iguchi-Ariga. 2010. "Human DJ-1-Specific Transcriptional Activation of Tyrosine Hydroxylase Gene." *The Journal of Biological Chemistry* 285 (51): 39718–31. doi:10.1074/jbc.M110.137034.

Janda, Elzbieta, Ciro Isidoro, Cristina Carresi, and Vincenzo Mollace. 2012. "Defective Autophagy in Parkinson's Disease: Role of Oxidative Stress." *Molecular Neurobiology* 46 (3): 639–61. doi:10.1007/s12035-012-8318-1.

Janezic, Stephanie, Sarah Threlfell, Paul D. Dodson, Megan J. Dowie, Tonya N. Taylor, Dawid

Potgieter, Laura Parkkinen, et al. 2013. “Deficits in Dopaminergic Transmission Precede Neuron Loss and Dysfunction in a New Parkinson Model.” *Proceedings of the National Academy of Sciences of the United States of America* 110 (42): E4016–25. doi:10.1073/pnas.1309143110.

Kane, Lesley A., Michael Lazarou, Adam I. Fogel, Yan Li, Koji Yamano, Shireen A. Sarraf, Soojay Banerjee, and Richard J. Youle. 2014. “PINK1 Phosphorylates Ubiquitin to Activate Parkin E3 Ubiquitin Ligase Activity.” *The Journal of Cell Biology* 205 (2): 143–53. doi:10.1083/jcb.201402104.

Kapp, W. 1992. “The History of Drugs for the Treatment of Parkinson’s Disease.” *Journal of Neural Transmission. Supplementum* 38: 1–6.

Kawakami, Fumitaka, Takatoshi Yabata, Etsuro Ohta, Tatsunori Maekawa, Naoki Shimada, Minori Suzuki, Hiroko Maruyama, Takafumi Ichikawa, and Fumiya Obata. 2012. “LRRK2 Phosphorylates Tubulin-Associated Tau but Not the Free Molecule: LRRK2-Mediated Regulation of the Tau-Tubulin Association and Neurite Outgrowth.” *PloS One* 7 (1): e30834. doi:10.1371/journal.pone.0030834.

Kazlauskaite, Agne, Chandana Kondapalli, Robert Gourlay, David G. Campbell, Maria Stella Ritorto, Kay Hofmann, Dario R. Alessi, Axel Knebel, Matthias Trost, and Miratul M. K. Muqit. 2014. “Parkin Is Activated by PINK1-Dependent Phosphorylation of Ubiquitin at Ser65.” *The Biochemical Journal* 460 (1): 127–39. doi:10.1042/BJ20140334.

Kinumi, Tomoya, Junko Kimata, Takahiro Taira, Hiroyoshi Ariga, and Etsuo Niki. 2004. “Cysteine-106 of DJ-1 Is the Most Sensitive Cysteine Residue to Hydrogen Peroxide-Mediated Oxidation in Vivo in Human Umbilical Vein Endothelial Cells.” *Biochemical and Biophysical Research Communications* 317 (3): 722–28. doi:10.1016/j.bbrc.2004.03.110.

Kitada, T., S. Asakawa, N. Hattori, H. Matsumine, Y. Yamamura, S. Minoshima, M. Yokochi, Y. Mizuno, and N. Shimizu. 1998. “Mutations in the Parkin Gene Cause Autosomal Recessive Juvenile Parkinsonism.” *Nature* 392 (6676): 605–8. doi:10.1038/33416.

Kong, Stephanie M. Y., Brian K. K. Chan, Jin-Sung Park, Kathryn J. Hill, Jade B. Aitken, Louise Cottle, Hovik Farghaian, et al. 2014. “Parkinson’s Disease-Linked Human PARK9/ATP13A2 Maintains Zinc Homeostasis and Promotes α-Synuclein Externalization via Exosomes.” *Human Molecular Genetics* 23 (11): 2816–33. doi:10.1093/hmg/ddu099.

Koyano, Fumika, Kei Okatsu, Hidetaka Kosako, Yasushi Tamura, Etsu Go, Mayumi Kimura, Yoko Kimura, et al. 2014. “Ubiquitin Is Phosphorylated by PINK1 to Activate Parkin.” *Nature* 510 (7503): 162–66. doi:10.1038/nature13392.

Krebiehl, Guido, Sabine Ruckerbauer, Lena F. Burbulla, Nicole Kieper, Brigitte Maurer, Jens Waak, Hartwig Wolburg, et al. 2010. “Reduced Basal Autophagy and Impaired Mitochondrial Dynamics due to Loss of Parkinson’s Disease-Associated Protein DJ-1.” *PloS One* 5 (2): e9367. doi:10.1371/journal.pone.0009367.

Krebs, Catharine E., Siamak Karkheiran, James C. Powell, Mian Cao, Vladimir Makarov, Hossein Darvish, Gilbert Di Paolo, et al. 2013. “The Sac1 Domain of SYNJ1 Identified Mutated in a Family with Early-Onset Progressive Parkinsonism with Generalized Seizures.” *Human Mutation* 34 (9): 1200–1207. doi:10.1002/humu.22372.

Lazarou, Michael, Seok Min Jin, Lesley A. Kane, and Richard J. Youle. 2012. “Role of PINK1 Binding to the TOM Complex and Alternate Intracellular Membranes in Recruitment and Activation of the E3 Ligase Parkin.” *Developmental Cell* 22 (2): 320–33. doi:10.1016/j.devcel.2011.12.014.

Lees, Andrew J. 2007. “Unresolved Issues Relating to the Shaking Palsy on the Celebration of James Parkinson’s 250th Birthday.” *Movement Disorders: Official Journal of the Movement Disorder Society* 22 Suppl 17 (September): S327–34. doi:10.1002/mds.21684.

Leroy, E., D. Anastasopoulos, S. Konitsiotis, C. Lavedan, and M. H. Polymeropoulos. 1998. “Deletions in the Parkin Gene and Genetic Heterogeneity in a Greek Family with Early Onset Parkinson’s Disease.” *Human Genetics* 103 (4): 424–27.

Lev, Nirit, Yael Barhum, Tali Ben-Zur, Eldad Melamed, Israel Steiner, and Daniel Offen. 2013.

"Knocking out DJ-1 Attenuates Astrocytes Neuroprotection against 6-Hydroxydopamine Toxicity." *Journal of Molecular Neuroscience: MN* 50 (3): 542–50. doi:10.1007/s12031-013-9984-9.

Lichtenberg, M., A. Mansilla, V. R. Zecchini, A. Fleming, and D. C. Rubinsztein. 2011. "The Parkinson's Disease Protein LRRK2 Impairs Proteasome Substrate Clearance without Affecting Proteasome Catalytic Activity." *Cell Death & Disease* 2: e196. doi:10.1038/cddis.2011.81.

Liu, C., and B. Hu. 2004. "Alterations of N-Ethylmaleimide-Sensitive Atpase Following Transient Cerebral Ischemia." *Neuroscience* 128 (4): 767–74. doi:10.1016/j.neuroscience.2004.07.025.

Li, Xianting, Jyoti C. Patel, Jing Wang, Marat V. Avshalumov, Charles Nicholson, Joseph D. Buxbaum, Gregory A. Elder, Margaret E. Rice, and Zhenyu Yue. 2010. "Enhanced Striatal Dopamine Transmission and Motor Performance with LRRK2 Overexpression in Mice Is Eliminated by Familial Parkinson's Disease Mutation G2019S." *The Journal of Neuroscience: The Official Journal of the Society for Neuroscience* 30 (5): 1788–97. doi:10.1523/JNEUROSCI.5604-09.2010.

Li, Yanping, Wencheng Liu, Tinmarla F. Oo, Lei Wang, Yi Tang, Vernice Jackson-Lewis, Chun Zhou, et al. 2009. "Mutant LRRK2(R1441G) BAC Transgenic Mice Recapitulate Cardinal Features of Parkinson's Disease." *Nature Neuroscience* 12 (7): 826–28. doi:10.1038/nn.2349.

Lobbestael, Evy, Veerle Baekelandt, and Jean-Marc Taymans. 2012. "Phosphorylation of LRRK2: From Kinase to Substrate." *Biochemical Society Transactions* 40 (5): 1102–10. doi:10.1042/BST20120128.

Luzio, J. Paul, Michael D. J. Parkinson, Sally R. Gray, and Nicholas A. Bright. 2009. "The Delivery of Endocytosed Cargo to Lysosomes." *Biochemical Society Transactions* 37 (Pt 5): 1019–21. doi:10.1042/BST0371019.

MacLeod, David A., Herve Rhinn, Tomoki Kuwahara, Ari Zolin, Gilbert Di Paolo, Brian D. McCabe, Brian D. MacCabe, et al. 2013. "RAB7L1 Interacts with LRRK2 to Modify Intraneuronal Protein Sorting and Parkinson's Disease Risk." *Neuron* 77 (3): 425–39. doi:10.1016/j.neuron.2012.11.033.

Malhotra, V., L. Orci, B. S. Glick, M. R. Block, and J. E. Rothman. 1988. "Role of an N-Ethylmaleimide-Sensitive Transport Component in Promoting Fusion of Transport Vesicles with Cisternae of the Golgi Stack." *Cell* 54 (2): 221–27.

Mandemakers, Wim, An Snellinx, Michael J. O'Neill, and Bart de Strooper. 2012. "LRRK2 Expression Is Enriched in the Striosomal Compartment of Mouse Striatum." *Neurobiology of Disease* 48 (3): 582–93. doi:10.1016/j.nbd.2012.07.017.

Manzoni, Claudia. 2012. "LRRK2 and Autophagy: A Common Pathway for Disease." *Biochemical Society Transactions* 40 (5): 1147–51. doi:10.1042/BST20120126.

Manzoni, Claudia, Adamantios Mamais, Sybille Dihanich, Phillip McGoldrick, Michael J. Devine, Julia Zerle, Eleanna Kara, et al. 2013. "Pathogenic Parkinson's Disease Mutations across the Functional Domains of LRRK2 Alter the Autophagic/lysosomal Response to Starvation." *Biochemical and Biophysical Research Communications* 441 (4): 862–66. doi:10.1016/j.bbrc.2013.10.159.

Mata, Ignacio F., Harvey Checkoway, Carolyn M. Hutter, Ali Samii, John W. Roberts, Hojoong M. Kim, Pinky Agarwal, et al. 2012. "Common Variation in the LRRK2 Gene Is a Risk Factor for Parkinson's Disease." *Movement Disorders: Official Journal of the Movement Disorder Society* 27 (14): 1822–25. doi:10.1002/mds.25226.

Mata, Ignacio F., William J. Wedemeyer, Matthew J. Farrer, Julie P. Taylor, and Kathleen A. Gallo. 2006. "LRRK2 in Parkinson's Disease: Protein Domains and Functional Insights." *Trends in Neurosciences* 29 (5): 286–93. doi:10.1016/j.tins.2006.03.006.

Matsuda, Wakoto, Takahiro Furuta, Kouichi C. Nakamura, Hiroyuki Hioki, Fumino Fujiyama, Ryohachi Arai, and Takeshi Kaneko. 2009. "Single Nigrostriatal Dopaminergic Neurons Form Widely Spread and Highly Dense Axonal Arborizations in the Neostriatum." *The Journal of Neuroscience: The Official Journal of the Society for Neuroscience* 29 (2): 444–53.

doi:10.1523/JNEUROSCI.4029-08.2009.

Matta, Samer, Kristof Van Kolen, Raquel da Cunha, Geert van den Bogaart, Wim Mandemakers, Katarzyna Miskiewicz, Pieter-Jan De Bock, et al. 2012. "LRRK2 Controls an EndoA Phosphorylation Cycle in Synaptic Endocytosis." *Neuron* 75 (6): 1008–21. doi:10.1016/j.neuron.2012.08.022.

Matteoli, M., K. Takei, M. S. Perin, T. C. Südhof, and P. De Camilli. 1992. "Exo-Endocytotic Recycling of Synaptic Vesicles in Developing Processes of Cultured Hippocampal Neurons." *The Journal of Cell Biology* 117 (4): 849–61.

McCall, Bridget. 2003. "Young-Onset Parkinson's Disease: A Guide to Care and Support." *Nursing Times* 99 (30): 28–31.

McNaught, Kevin St P., Lars M. Björklund, Roger Belizaire, Ole Isacson, Peter Jenner, and C. Warren Olanow. 2002. "Proteasome Inhibition Causes Nigral Degeneration with Inclusion Bodies in Rats." *Neuroreport* 13 (11): 1437–41.

Meissner, Cathrin, Holger Lorenz, Andreas Weihofen, Dennis J. Selkoe, and Marius K. Lemberg. 2011. "The Mitochondrial Intramembrane Protease PARL Cleaves Human Pink1 to Regulate Pink1 Trafficking." *Journal of Neurochemistry* 117 (5): 856–67. doi:10.1111/j.1471-4159.2011.07253.x.

Melrose, H. L., J. C. Dächsel, B. Behrouz, S. J. Lincoln, M. Yue, K. M. Hinkle, C. B. Kent, et al. 2010. "Impaired Dopaminergic Neurotransmission and Microtubule-Associated Protein Tau Alterations in Human LRRK2 Transgenic Mice." *Neurobiology of Disease* 40 (3): 503–17. doi:10.1016/j.nbd.2010.07.010.

Meulener, Marc C., Charles L. Graves, Deepak M. Sampathu, Cecilia E. Armstrong-Gold, Nancy M. Bonini, and Benoit I. Giasson. 2005. "DJ-1 Is Present in a Large Molecular Complex in Human Brain Tissue and Interacts with Alpha-Synuclein." *Journal of Neurochemistry* 93 (6): 1524–32. doi:10.1111/j.1471-4159.2005.03145.x.

Miesenböck, G., D. A. De Angelis, and J. E. Rothman. 1998. "Visualizing Secretion and Synaptic Transmission with pH-Sensitive Green Fluorescent Proteins." *Nature* 394 (6689): 192–95. doi:10.1038/28190.

Mohtashami, M., B. A. Stewart, G. L. Boulianne, and W. S. Trimble. 2001. "Analysis of the Mutant Drosophila N-Ethylmaleimide Sensitive Fusion-1 Protein in Comatose Reveals Molecular Correlates of the Behavioural Paralysis." *Journal of Neurochemistry* 77 (5): 1407–17.

Moore, Darren J. 2008. "The Biology and Pathobiology of LRRK2: Implications for Parkinson's Disease." *Parkinsonism & Related Disorders* 14 Suppl 2: S92–98. doi:10.1016/j.parkreldis.2008.04.010.

Morel, Nicolas, and Sandrine Poëa-Guyon. 2015. "The Membrane Domain of Vacuolar H(+)ATPase: A Crucial Player in Neurotransmitter Exocytotic Release." *Cellular and Molecular Life Sciences: CMLS* 72 (13): 2561–73. doi:10.1007/s00018-015-1886-2.

Murphy, Karen E., Amanda M. Gysbers, Sarah K. Abbott, Nahid Tayebi, Woojin S. Kim, Ellen Sidransky, Antony Cooper, Brett Garner, and Glenda M. Halliday. 2014. "Reduced Glucocerebrosidase Is Associated with Increased α-Synuclein in Sporadic Parkinson's Disease." *Brain: A Journal of Neurology* 137 (Pt 3): 834–48. doi:10.1093/brain/awt367.

Nagakubo, D., T. Taira, H. Kitaura, M. Ikeda, K. Tamai, S. M. Iguchi-Ariga, and H. Ariga. 1997. "DJ-1, a Novel Oncogene Which Transforms Mouse NIH3T3 Cells in Cooperation with Ras." *Biochemical and Biophysical Research Communications* 231 (2): 509–13. doi:10.1006/bbrc.1997.6132.

Narendra, Derek, Atsushi Tanaka, Der-Fen Suen, and Richard J. Youle. 2008. "Parkin Is Recruited Selectively to Impaired Mitochondria and Promotes Their Autophagy." *The Journal of Cell Biology* 183 (5): 795–803. doi:10.1083/jcb.200809125.

Nichols, W. C., V. E. Elsaesser, N. Pankratz, M. W. Pauciulo, D. K. Marek, C. A. Halter, A. Rudolph,

C. W. Shults, T. Foroud, and Parkinson Study Group-PROGENI Investigators. 2007. “LRRK2 Mutation Analysis in Parkinson Disease Families with Evidence of Linkage to PARK8.” *Neurology* 69 (18): 1737–44. doi:10.1212/01.wnl.0000278115.50741.4e.

Nunes, Paula, Nicola Haines, Venkat Kuppuswamy, David J. Fleet, and Bryan A. Stewart. 2006. “Synaptic Vesicle Mobility and Presynaptic F-Actin Are Disrupted in a N-Ethylmaleimide-Sensitive Factor Allele of Drosophila.” *Molecular Biology of the Cell* 17 (11): 4709–19. doi:10.1091/mbc.E06-03-0253.

Nuytemans, Karen, Guney Bademci, Vanessa Inchausti, Amy Dressen, Daniel D. Kinnamon, Arpit Mehta, Liyong Wang, et al. 2013. “Whole Exome Sequencing of Rare Variants in EIF4G1 and VPS35 in Parkinson Disease.” *Neurology* 80 (11): 982–89. doi:10.1212/WNL.0b013e31828727d4.

Okatsu, Kei, Midori Uno, Fumika Koyano, Etsu Go, Mayumi Kimura, Toshihiko Oka, Keiji Tanaka, and Noriyuki Matsuda. 2013. “A Dimeric PINK1-Containing Complex on Depolarized Mitochondria Stimulates Parkin Recruitment.” *The Journal of Biological Chemistry* 288 (51): 36372–84. doi:10.1074/jbc.M113.509653.

Olanow, C. Warren, and Patrik Brundin. 2013. “Parkinson’s Disease and Alpha Synuclein: Is Parkinson’s Disease a Prion-like Disorder?” *Movement Disorders: Official Journal of the Movement Disorder Society* 28 (1): 31–40. doi:10.1002/mds.25373.

Olanow, C. Warren, and Kevin St P. McNaught. 2006. “Ubiquitin-Proteasome System and Parkinson’s Disease.” *Movement Disorders: Official Journal of the Movement Disorder Society* 21 (11): 1806–23. doi:10.1002/mds.21013.

Ordureau, Alban, Shireen A. Sarraf, David M. Duda, Jin-Mi Heo, Mark P. Jedrychowski, Vladislav O. Sviderskiy, Jennifer L. Olszewski, et al. 2014. “Quantitative Proteomics Reveal a Feedforward Mechanism for Mitochondrial PARKIN Translocation and Ubiquitin Chain Synthesis.” *Molecular Cell* 56 (3): 360–75. doi:10.1016/j.molcel.2014.09.007.

Paisán-Ruíz, Coro, Shushant Jain, E. Whitney Evans, William P. Gilks, Javier Simón, Marcel van der Brug, Adolfo López de Munain, et al. 2004. “Cloning of the Gene Containing Mutations That Cause PARK8-Linked Parkinson’s Disease.” *Neuron* 44 (4): 595–600. doi:10.1016/j.neuron.2004.10.023.

Paisán-Ruiz, Coro, Abi Li, Susanne A. Schneider, Janice L. Holton, Robert Johnson, Desmond Kidd, Jeremy Chataway, et al. 2012. “Widespread Lewy Body and Tau Accumulation in Childhood and Adult Onset Dystonia-Parkinsonism Cases with PLA2G6 Mutations.” *Neurobiology of Aging* 33 (4): 814–23. doi:10.1016/j.neurobiolaging.2010.05.009.

Pallanck, L., R. W. Ordway, M. Ramaswami, W. Y. Chi, K. S. Krishnan, and B. Ganetzky. 1995. “Distinct Roles for N-Ethylmaleimide-Sensitive Fusion Protein (NSF) Suggested by the Identification of a Second Drosophila NSF Homolog.” *The Journal of Biological Chemistry* 270 (32): 18742–44.

Parisiadou, Loukia, Jia Yu, Carmelo Sgobio, Chengsong Xie, Guoxiang Liu, Lixin Sun, Xing-Long Gu, et al. 2014. “LRRK2 Regulates Synaptogenesis and Dopamine Receptor Activation through Modulation of PKA Activity.” *Nature Neuroscience* 17 (3): 367–76. doi:10.1038/nn.3636.

Park, Jin-Sung, Nicholas F. Blair, and Carolyn M. Sue. 2015. “The Role of ATP13A2 in Parkinson’s Disease: Clinical Phenotypes and Molecular Mechanisms.” *Movement Disorders: Official Journal of the Movement Disorder Society* 30 (6): 770–79. doi:10.1002/mds.26243.

Piccoli, Giovanni, Steven B. Condliffe, Matthias Bauer, Florian Giesert, Karsten Boldt, Silvia De Astis, Andrea Meixner, et al. 2011. “LRRK2 Controls Synaptic Vesicle Storage and Mobilization within the Recycling Pool.” *The Journal of Neuroscience: The Official Journal of the Society for Neuroscience* 31 (6): 2225–37. doi:10.1523/JNEUROSCI.3730-10.2011.

Piccoli, Giovanni, Franco Onofri, Maria Daniela Cirnaru, Christoph J. O. Kaiser, Pravinkumar Jagtap, Andreas Kastenmüller, Francesca Pischedda, et al. 2014. “Leucine-Rich Repeat Kinase 2 Binds to Neuronal Vesicles through Protein Interactions Mediated by Its C-Terminal WD40 Domain.” *Molecular and Cellular Biology* 34 (12): 2147–61. doi:10.1128/MCB.00914-13.

Plowey, Edward D., Salvatore J. Cherra, Yong-Jian Liu, and Charleen T. Chu. 2008. "Role of Autophagy in G2019S-LRRK2-Associated Neurite Shortening in Differentiated SH-SY5Y Cells." *Journal of Neurochemistry* 105 (3): 1048–56. doi:10.1111/j.1471-4159.2008.05217.x.

Pountney, Dean L., Mark J. Raftery, Fariba Chegini, Peter C. Blumbergs, and Wei Ping Gai. 2008. "NSF, Unc-18-1, Dynamin-1 and HSP90 Are Inclusion Body Components in Neuronal Intranuclear Inclusion Disease Identified by Anti-SUMO-1-Immunocapture." *Acta Neuropathologica* 116 (6): 603–14. doi:10.1007/s00401-008-0437-4.

Pungaliya, Pooja P., Yuchen Bai, Kerri Lipinski, Vasanti S. Anand, Saurabh Sen, Eugene L. Brown, Brian Bates, et al. 2010. "Identification and Characterization of a Leucine-Rich Repeat Kinase 2 (LRRK2) Consensus Phosphorylation Motif." *PloS One* 5 (10): e13672. doi:10.1371/journal.pone.0013672.

Ramirez, Alfredo, André Heimbach, Jan Gründemann, Barbara Stiller, Dan Hampshire, L. Pablo Cid, Ingrid Goebel, et al. 2006. "Hereditary Parkinsonism with Dementia Is Caused by Mutations in ATP13A2, Encoding a Lysosomal Type 5 P-Type ATPase." *Nature Genetics* 38 (10): 1184–91. doi:10.1038/ng1884.

Ramonet, David, João Paulo L. Daher, Brian M. Lin, Klodjan Stafa, Jaekwang Kim, Rebecca Banerjee, Marie Westerlund, et al. 2011. "Dopaminergic Neuronal Loss, Reduced Neurite Complexity and Autophagic Abnormalities in Transgenic Mice Expressing G2019S Mutant LRRK2." *PloS One* 6 (4): e18568. doi:10.1371/journal.pone.0018568.

Reinhardt, Peter, Michael Glatza, Kathrin Hemmer, Yaroslav Tsytsyura, Cora S. Thiel, Susanne Höing, Sören Moritz, et al. 2013. "Derivation and Expansion Using Only Small Molecules of Human Neural Progenitors for Neurodegenerative Disease Modeling." *PloS One* 8 (3): e59252. doi:10.1371/journal.pone.0059252.

Reith, Alastair D., Paul Bamborough, Karamjit Jandu, Daniele Andreotti, Lucy Mensah, Pamela Dossang, Hwan Geun Choi, et al. 2012. "GSK2578215A; a Potent and Highly Selective 2-Arylmethyloxy-5-Substitutent-N-Arylbenzamide LRRK2 Kinase Inhibitor." *Bioorganic & Medicinal Chemistry Letters* 22 (17): 5625–29. doi:10.1016/j.bmcl.2012.06.104.

Rinaldi, Débora E., Gerardo R. Corradi, Lucía Martínez Cuesta, Hugo P. Adamo, and Felicitas de Tezanos Pinto. 2015. "The Parkinson-Associated Human P5B-ATPase ATP13A2 Protects against the Iron-Induced Cytotoxicity." *Biochimica Et Biophysica Acta* 1848 (8): 1646–55. doi:10.1016/j.bbamem.2015.04.008.

Rizo, Josep, and Thomas C. Südhof. 2012. "The Membrane Fusion Enigma: SNAREs, Sec1/Munc18 Proteins, and Their Accomplices--Guilty as Charged?" *Annual Review of Cell and Developmental Biology* 28: 279–308. doi:10.1146/annurev-cellbio-101011-155818.

Rockenstein, Edward, Silke Nuber, Cassia R. Overk, Kiren Ubhi, Michael Mante, Christina Patrick, Anthony Adame, et al. 2014. "Accumulation of Oligomer-Prone α-Synuclein Exacerbates Synaptic and Neuronal Degeneration in Vivo." *Brain: A Journal of Neurology* 137 (Pt 5): 1496–1513. doi:10.1093/brain/awu057.

Rodríguez-Navarro, Jose A., Laura Rodríguez, María J. Casarejos, Rosa M. Solano, Ana Gómez, Juan Perucho, Ana María Cuervo, Justo García de Yébenes, and María A. Mena. 2010. "Trehalose Ameliorates Dopaminergic and Tau Pathology in Parkin Deleted/tau Overexpressing Mice through Autophagy Activation." *Neurobiology of Disease* 39 (3): 423–38. doi:10.1016/j.nbd.2010.05.014.

Rothman, J. E. 1994. "Mechanisms of Intracellular Protein Transport." *Nature* 372 (6501): 55–63. doi:10.1038/372055a0.

Rudzińska, M., S. Bukowczan, J. Stożek, K. Zajdel, E. Mirek, W. Chwała, M. Wójcik-Pędziwiatr, K. Banaszkiewicz, and A. Szczudlik. 2013. "The Incidence and Risk Factors of Falls in Parkinson Disease: Prospective Study." *Neurologia I Neurochirurgia Polska* 47 (5): 431–37.

Rusmini, Paola, Valeria Crippa, Elisa Giorgetti, Alessandra Boncoraglio, Riccardo Cristofani, Serena

Carra, and Angelo Poletti. 2013. “Clearance of the Mutant Androgen Receptor in Motoneuronal Models of Spinal and Bulbar Muscular Atrophy.” *Neurobiology of Aging* 34 (11): 2585–2603. doi:10.1016/j.neurobiolaging.2013.05.026.

Sankaranarayanan, S., D. De Angelis, J. E. Rothman, and T. A. Ryan. 2000. “The Use of pHluorins for Optical Measurements of Presynaptic Activity.” *Biophysical Journal* 79 (4): 2199–2208. doi:10.1016/S0006-3495(00)76468-X.

Sarkar, Sovan, Janet E. Davies, Zebo Huang, Alan Tunnacliffe, and David C. Rubinsztein. 2007. “Trehalose, a Novel mTOR-Independent Autophagy Enhancer, Accelerates the Clearance of Mutant Huntingtin and Alpha-Synuclein.” *The Journal of Biological Chemistry* 282 (8): 5641–52. doi:10.1074/jbc.M609532200.

Sarraf, Shireen A., Malavika Raman, Virginia Guarani-Pereira, Mathew E. Sowa, Edward L. Huttlin, Steven P. Gygi, and J. Wade Harper. 2013. “Landscape of the PARKIN-Dependent Ubiquitylome in Response to Mitochondrial Depolarization.” *Nature* 496 (7445): 372–76. doi:10.1038/nature12043.

Schapansky, Jason, Jonathan D. Nardozzi, Fredrik Felizia, and Matthew J. LaVoie. 2014. “Membrane Recruitment of Endogenous LRRK2 Precedes Its Potent Regulation of Autophagy.” *Human Molecular Genetics* 23 (16): 4201–14. doi:10.1093/hmg/ddu138.

Schulte, Eva C., Brit Mollenhauer, Alexander Zimprich, Benjamin Bereznai, Peter Lichtner, Dietrich Haubenberger, Walter Pirker, et al. 2012. “Variants in Eukaryotic Translation Initiation Factor 4G1 in Sporadic Parkinson’s Disease.” *Neurogenetics* 13 (3): 281–85. doi:10.1007/s10048-012-0334-9.

Seirafi, Marjan, Guennadi Kozlov, and Kalle Gehring. 2015. “Parkin Structure and Function.” *The FEBS Journal* 282 (11): 2076–88. doi:10.1111/febs.13249.

Senior, Steven L., Natalia Ninkina, Robert Deacon, David Bannerman, Vladimir L. Buchman, Stephanie J. Cragg, and Richard Wade-Martins. 2008. “Increased Striatal Dopamine Release and Hyperdopaminergic-like Behaviour in Mice Lacking Both Alpha-Synuclein and Gamma-Synuclein.” *The European Journal of Neuroscience* 27 (4): 947–57. doi:10.1111/j.1460-9568.2008.06055.x.

Sen, Saurabh, Philip J. Webber, and Andrew B. West. 2009. “Dependence of Leucine-Rich Repeat Kinase 2 (LRRK2) Kinase Activity on Dimerization.” *The Journal of Biological Chemistry* 284 (52): 36346–56. doi:10.1074/jbc.M109.025437.

Shendelman, Shoshana, Alan Jonason, Cecile Martinat, Thomas Leete, and Asa Abeliovich. 2004. “DJ-1 Is a Redox-Dependent Molecular Chaperone That Inhibits Alpha-Synuclein Aggregate Formation.” *PLoS Biology* 2 (11): e362. doi:10.1371/journal.pbio.0020362.

Sheng, Zejuan, Shuo Zhang, Daisy Bustos, Tracy Kleinheinz, Claire E. Le Pichon, Sara L. Dominguez, Hilda O. Solanoy, et al. 2012. “Ser1292 Autophosphorylation Is an Indicator of LRRK2 Kinase Activity and Contributes to the Cellular Effects of PD Mutations.” *Science Translational Medicine* 4 (164): 164ra161. doi:10.1126/scitranslmed.3004485.

Shimura, H., N. Hattori, S. i Kubo, Y. Mizuno, S. Asakawa, S. Minoshima, N. Shimizu, et al. 2000. “Familial Parkinson Disease Gene Product, Parkin, Is a Ubiquitin-Protein Ligase.” *Nature Genetics* 25 (3): 302–5. doi:10.1038/77060.

Shin, Narae, Hyerhan Jeong, Jungsun Kwon, Hye Young Heo, Jung June Kwon, Hye Jin Yun, Cy-Hyun Kim, et al. 2008. “LRRK2 Regulates Synaptic Vesicle Endocytosis.” *Experimental Cell Research* 314 (10): 2055–65. doi:10.1016/j.yexcr.2008.02.015.

Sidransky, Ellen, Ted Samaddar, and Nahid Tayebi. 2009. “Mutations in GBA Are Associated with Familial Parkinson Disease Susceptibility and Age at Onset.” *Neurology* 73 (17): 1424–25, author reply 1425–26. doi:10.1212/WNL.0b013e3181b28601.

Skibinski, Gaia, Ken Nakamura, Mark R. Cookson, and Steven Finkbeiner. 2014. “Mutant LRRK2 Toxicity in Neurons Depends on LRRK2 Levels and Synuclein but Not Kinase Activity or Inclusion Bodies.” *The Journal of Neuroscience: The Official Journal of the Society for Neuroscience* 34 (2): 418–33. doi:10.1523/JNEUROSCI.2712-13.2014.

Sossi, Vesna, Raul de la Fuente-Fernández, Ramachandiran Nandhagopal, Michael Schulzer, Jessamyn McKenzie, Thomas J. Ruth, Jan O. Aasly, Matthew J. Farrer, Zbigniew K. Wszolek, and Jon A. Stoessl. 2010. "Dopamine Turnover Increases in Asymptomatic LRRK2 Mutations Carriers." *Movement Disorders: Official Journal of the Movement Disorder Society* 25 (16): 2717–23. doi:10.1002/mds.23356.

Stewart, Bryan A., Mahmood Mohtashami, Patricia Rivlin, David L. Deitcher, William S. Trimble, and Gabrielle L. Boulianne. 2002. "Dominant-Negative NSF2 Disrupts the Structure and Function of Drosophila Neuromuscular Synapses." *Journal of Neurobiology* 51 (4): 261–71.

Sundal, Christina, Shinsuke Fujioka, Ryan J. Uitti, and Zbigniew K. Wszolek. 2012. "Autosomal Dominant Parkinson's Disease." *Parkinsonism & Related Disorders* 18 Suppl 1 (January): S7–10. doi:10.1016/S1353-8020(11)70005-0.

Taira, Takahiro, Yoshiro Saito, Takeshi Niki, Sanae M. M. Iguchi-Ariga, Kazuhiko Takahashi, and Hiroyoshi Ariga. 2004. "DJ-1 Has a Role in Antioxidative Stress to Prevent Cell Death." *EMBO Reports* 5 (2): 213–18. doi:10.1038/sj.embor.7400074.

Taymans, Jean-Marc, and Mark R. Cookson. 2010. "Mechanisms in Dominant Parkinsonism: The Toxic Triangle of LRRK2, Alpha-Synuclein, and Tau." *BioEssays: News and Reviews in Molecular, Cellular and Developmental Biology* 32 (3): 227–35. doi:10.1002/bies.200900163.

Tokuda, T., M. M. Qureshi, M. T. Ardah, S. Varghese, S. a. S. Shehab, T. Kasai, N. Ishigami, A. Tamaoka, M. Nakagawa, and O. M. A. El-Agnaf. 2010. "Detection of Elevated Levels of α-Synuclein Oligomers in CSF from Patients with Parkinson Disease." *Neurology* 75 (20): 1766–72. doi:10.1212/WNL.0b013e3181fd613b.

Tong, Youren, Emilie Giaime, Hiroo Yamaguchi, Takaharu Ichimura, Yumin Liu, Huiqing Si, Huaibin Cai, Joseph V. Bonventre, and Jie Shen. 2012. "Loss of Leucine-Rich Repeat Kinase 2 Causes Age-Dependent Bi-Phasic Alterations of the Autophagy Pathway." *Molecular Neurodegeneration* 7: 2. doi:10.1186/1750-1326-7-2.

Tong, Youren, Antonio Pisani, Giuseppina Martella, Maha Karouani, Hiroo Yamaguchi, Emmanuel N. Pothos, and Jie Shen. 2009. "R1441C Mutation in LRRK2 Impairs Dopaminergic Neurotransmission in Mice." *Proceedings of the National Academy of Sciences of the United States of America* 106 (34): 14622–27. doi:10.1073/pnas.0906334106.

Turner, K. M., R. D. Burgoyne, and A. Morgan. 1999. "Protein Phosphorylation and the Regulation of Synaptic Membrane Traffic." *Trends in Neurosciences* 22 (10): 459–64.

Usenovic, Marija, Adam L. Knight, Arpita Ray, Victoria Wong, Kevin R. Brown, Guy A. Caldwell, Kim A. Caldwell, Igor Stagljar, and Dimitri Krainc. 2012. "Identification of Novel ATP13A2 Interactors and Their Role in α-Synuclein Misfolding and Toxicity." *Human Molecular Genetics* 21 (17): 3785–94. doi:10.1093/hmg/dds206.

Valente, E. M., A. R. Bentivoglio, P. H. Dixon, A. Ferraris, T. Ialongo, M. Frontali, A. Albanese, and N. W. Wood. 2001. "Localization of a Novel Locus for Autosomal Recessive Early-Onset Parkinsonism, PARK6, on Human Chromosome 1p35-p36." *American Journal of Human Genetics* 68 (4): 895–900.

Valente, E. M., F. Brancati, V. Caputo, E. A. Graham, M. B. Davis, A. Ferraris, M. M. B. Breteler, et al. 2002. "PARK6 Is a Common Cause of Familial Parkinsonism." *Neurological Sciences: Official Journal of the Italian Neurological Society and of the Italian Society of Clinical Neurophysiology* 23 Suppl 2 (September): S117–18. doi:10.1007/s100720200097.

Valente, Enza Maria, Sergio Salvi, Tamara Ialongo, Roberta Marongiu, Antonio Emanuele Elia, Viviana Caputo, Luigi Romito, Alberto Albanese, Bruno Dallapiccola, and Anna Rita Bentivoglio. 2004. "PINK1 Mutations Are Associated with Sporadic Early-Onset Parkinsonism." *Annals of Neurology* 56 (3): 336–41. doi:10.1002/ana.20256.

van der Merwe, Celia, Zahra Jalali Sefid Dashti, Alan Christoffels, Ben Loos, and Soraya Bardien.

2015. “Evidence for a Common Biological Pathway Linking Three Parkinson’s Disease-Causing Genes: Parkin, PINK1 and DJ-1.” *The European Journal of Neuroscience* 41 (9): 1113–25. doi:10.1111/ejn.12872.

Verstraeten, Aline, Jessie Theuns, and Christine Van Broeckhoven. 2015. “Progress in Unraveling the Genetic Etiology of Parkinson Disease in a Genomic Era.” *Trends in Genetics: TIG* 31 (3): 140–49. doi:10.1016/j.tig.2015.01.004.

Vilariño-Güell, Carles, Christian Wider, Owen A. Ross, Justus C. Dachsel, Jennifer M. Kachergus, Sarah J. Lincoln, Alexandra I. Soto-Ortolaza, et al. 2011. “VPS35 Mutations in Parkinson Disease.” *American Journal of Human Genetics* 89 (1): 162–67. doi:10.1016/j.ajhg.2011.06.001.

Waak, Jens, Stephanie S. Weber, Karin Görner, Christoph Schall, Hidenori Ichijo, Thilo Stehle, and Philipp J. Kahle. 2009. “Oxidizable Residues Mediating Protein Stability and Cytoprotective Interaction of DJ-1 with Apoptosis Signal-Regulating Kinase 1.” *The Journal of Biological Chemistry* 284 (21): 14245–57. doi:10.1074/jbc.M806902200.

Wang, Xinnan, Dominic Winter, Ghazaleh Ashrafi, Julia Schlehe, Yao Liang Wong, Dennis Selkoe, Sarah Rice, Judith Steen, Matthew J. LaVoie, and Thomas L. Schwarz. 2011. “PINK1 and Parkin Target Miro for Phosphorylation and Degradation to Arrest Mitochondrial Motility.” *Cell* 147 (4): 893–906. doi:10.1016/j.cell.2011.10.018.

Waragai, Masaaki, Masaaki Nakai, Jianshe Wei, Masayo Fujita, Hideya Mizuno, Gilbert Ho, Eliezer Masliah, Hiroyasu Akatsu, Fusako Yokochi, and Makoto Hashimoto. 2007. “Plasma Levels of DJ-1 as a Possible Marker for Progression of Sporadic Parkinson’s Disease.” *Neuroscience Letters* 425 (1): 18–22. doi:10.1016/j.neulet.2007.08.010.

West, Andrew B., Darren J. Moore, Saskia Biskup, Artem Bugayenko, Wanli W. Smith, Christopher A. Ross, Valina L. Dawson, and Ted M. Dawson. 2005. “Parkinson’s Disease-Associated Mutations in Leucine-Rich Repeat Kinase 2 Augment Kinase Activity.” *Proceedings of the National Academy of Sciences of the United States of America* 102 (46): 16842–47. doi:10.1073/pnas.0507360102.

Whaley, N. R., R. J. Uitti, D. W. Dickson, M. J. Farrer, and Z. K. Wszolek. 2006. “Clinical and Pathologic Features of Families with LRRK2-Associated Parkinson’s Disease.” *Journal of Neural Transmission. Supplementum*, no. 70: 221–29.

Winner, B., H. L. Melrose, C. Zhao, K. M. Hinkle, M. Yue, C. Kent, A. T. Braithwaite, et al. 2011. “Adult Neurogenesis and Neurite Outgrowth Are Impaired in LRRK2 G2019S Mice.” *Neurobiology of Disease* 41 (3): 706–16. doi:10.1016/j.nbd.2010.12.008.

Wiznerowicz, Maciej, and Didier Trono. 2003. “Conditional Suppression of Cellular Genes: Lentivirus Vector-Mediated Drug-Inducible RNA Interference.” *Journal of Virology* 77 (16): 8957–61.

Xiong, Yulan, Candice E. Coombes, Austin Kilaru, Xiaojie Li, Aaron D. Gitler, William J. Bowers, Valina L. Dawson, Ted M. Dawson, and Darren J. Moore. 2010. “GTPase Activity Plays a Key Role in the Pathobiology of LRRK2.” *PLoS Genetics* 6 (4): e1000902. doi:10.1371/journal.pgen.1000902.

Yakhine-Diop, Sokhna M. S., José M. Bravo-San Pedro, Rubén Gómez-Sánchez, Elisa Pizarro-Estrella, Mario Rodríguez-Arribas, Vicente Climent, Ana Aiastui, Adolfo López de Munain, José M. Fuentes, and Rosa A. González-Polo. 2014. “G2019S LRRK2 Mutant Fibroblasts from Parkinson’s Disease Patients Show Increased Sensitivity to Neurotoxin 1-Methyl-4-Phenylpyridinium Dependent of Autophagy.” *Toxicology* 324 (October): 1–9. doi:10.1016/j.tox.2014.07.001.

Yamano, Koji, and Richard J. Youle. 2013. “PINK1 Is Degraded through the N-End Rule Pathway.” *Autophagy* 9 (11): 1758–69. doi:10.4161/auto.24633.

Yun, Hye Jin, Joohyun Park, Dong Hwan Ho, Heyjung Kim, Cy-Hyun Kim, Hakjin Oh, Inhwa Ga, et al. 2013. “LRRK2 Phosphorylates Snapin and Inhibits Interaction of Snapin with SNAP-25.” *Experimental & Molecular Medicine* 45: e36. doi:10.1038/emm.2013.68.

Zarranz, Juan J., Javier Alegre, Juan C. Gómez-Esteban, Elena Lezcano, Raquel Ros, Israel Ampuero,

Lídice Vidal, et al. 2004. “The New Mutation, E46K, of Alpha-Synuclein Causes Parkinson and Lewy Body Dementia.” *Annals of Neurology* 55 (2): 164–73. doi:10.1002/ana.10795.

Zavodszky, Eszter, Matthew N. J. Seaman, and David C. Rubinsztein. 2014. “VPS35 Parkinson Mutation Impairs Autophagy via WASH.” *Cell Cycle (Georgetown, Tex.)* 13 (14): 2155–56. doi:10.4161/cc.29734.

Zhang, Nan-Yan, Zhiyong Tang, and Chang-Wei Liu. 2008. “Alpha-Synuclein Protofibrils Inhibit 26 S Proteasome-Mediated Protein Degradation: Understanding the Cytotoxicity of Protein Protofibrils in Neurodegenerative Disease Pathogenesis.” *The Journal of Biological Chemistry* 283 (29): 20288–98. doi:10.1074/jbc.M710560200.

Zhao, Tianna, Lies-Anne Severijnen, Marcel van der Weiden, Ping Pin Zheng, Ben A. Oostra, Renate K. Hukema, Rob Willemsen, Johan M. Kros, and Vincenzo Bonifati. 2013. “FBXO7 Immunoreactivity in α-Synuclein-Containing Inclusions in Parkinson Disease and Multiple System Atrophy.” *Journal of Neuropathology and Experimental Neurology* 72 (6): 482–88. doi:10.1097/NEN.0b013e318293c586.

Zhou, Wenbo, and Curt R. Freed. 2005. “DJ-1 up-Regulates Glutathione Synthesis during Oxidative Stress and Inhibits A53T Alpha-Synuclein Toxicity.” *The Journal of Biological Chemistry* 280 (52): 43150–58. doi:10.1074/jbc.M507124200.

Zigmond, Michael J., Teresa G. Hastings, and Ruth G. Perez. 2002. “Increased Dopamine Turnover after Partial Loss of Dopaminergic Neurons: Compensation or Toxicity?” *Parkinsonism & Related Disorders* 8 (6): 389–93.

Zimprich, Alexander, Anna Benet-Pagès, Walter Struhal, Elisabeth Graf, Sebastian H. Eck, Marc N. Offman, Dietrich Haubenberger, et al. 2011. “A Mutation in VPS35, Encoding a Subunit of the Retromer Complex, Causes Late-Onset Parkinson Disease.” *American Journal of Human Genetics* 89 (1): 168–75. doi:10.1016/j.ajhg.2011.06.008.

Zimprich, Alexander, Saskia Biskup, Petra Leitner, Peter Lichtner, Matthew Farrer, Sarah Lincoln, Jennifer Kachergus, et al. 2004. “Mutations in LRRK2 Cause Autosomal-Dominant Parkinsonism with Pleomorphic Pathology.” *Neuron* 44 (4): 601–7. doi:10.1016/j.neuron.2004.11.005.

Appendix

Molecular Neurodegeneration

LRRK2 phosphorylates pre-synaptic N-ethylmaleimide sensitive fusion (NSF) protein enhancing its ATPase activity and SNARE complex disassembling rate

--Manuscript Draft--

Manuscript Number:	MOND-D-15-00066R2
Full Title:	LRRK2 phosphorylates pre-synaptic N-ethylmaleimide sensitive fusion (NSF) protein enhancing its ATPase activity and SNARE complex disassembling rate
Article Type:	Research article
Funding Information:	Michael J. Fox Foundation for Parkinson's Research (US) — Dr Franco Onofri, Dr Giovanni Piccoli, Dr. Elisa Greggio Fondazione Telethon (IT) (GGP12237) — Dr. Elisa Greggio Progetto di Ateneo CPDA University pf Padova (124045/12) — Dr Mariano Beltramini Regione Lombardia (18099/RCC) — Dr Giovanni Piccoli
Abstract:	Background Lrrk2, a gene linked to Parkinson's disease, encodes a large scaffolding protein with kinase and GTPase activities implicated in vesicle and cytoskeletal-related processes. At the presynaptic site, LRRK2 associates with synaptic vesicles through interaction with a panel of presynaptic proteins. Results Here, we show that LRRK2 kinase activity influences the dynamics of synaptic vesicle fusion. We therefore investigated whether LRRK2 phosphorylates component(s) of the exo/endocytosis machinery. We have previously observed that LRRK2 interacts with NSF, a hexameric AAA+ ATPase that couples ATP hydrolysis to the disassembling of SNARE proteins allowing them to enter another fusion cycle during synaptic exocytosis. Here, we demonstrate that NSF is a substrate of LRRK2 kinase activity. LRRK2 phosphorylates full-length NSF at threonine 645 in the ATP binding pocket of D2 domain. Functionally, NSF phosphorylated by LRRK2 displays enhanced ATPase activity and increased rate of SNARE complex disassembling. Substitution of threonine 645 with alanine abrogates LRRK2-mediated increased ATPase activity. Conclusions Given that the most common Parkinson's disease LRRK2 G2019S mutation displays increased kinase activity, our results suggest that mutant LRRK2 may impair synaptic vesicle dynamics via aberrant phosphorylation of NSF.
Corresponding Author:	Elisa Greggio ITALY
Corresponding Author Secondary Information:	
Corresponding Author's Institution:	
Corresponding Author's Secondary Institution:	
First Author:	Elisa Belluzzi
First Author Secondary Information:	
Order of Authors:	Elisa Belluzzi Adriano Gonnelli Maria-Daniela Cirnaru

	Antonella Marte
	Nicoletta Plotegher
	Isabella Russo
	Laura Civiero
	Susanna Cogo
	Maria Perèz Carrion
	Cinzia Franchin
	Giorgio Arrigoni
	Mariano Beltramini
	Luigi Bubacco
	Franco Onofri
	Giovanni Piccoli
	Elisa Greggio
Order of Authors Secondary Information:	
Response to Reviewers:	Dear Professor Nielsen, Please find enclosed our revised manuscript MOND-D-15-00066R1 entitled: “LRRK2 phosphorylates pre-synaptic N-ethylmaleimide sensitive fusion (NSF) protein enhancing its ATPase activity and SNARE complex disassembling rate”. We would like to thank the reviewers for the positive feedback on our revisions. Attached to this letter you can find a point-by-point response to the remaining concerns. We hope that you will find our revised work now suitable for publication in Molecular Neurodegeneration. Sincerely, Elisa Greggio Response to reviewers. Reviewer #1: I am satisfied with the efforts made by the authors to improve the manuscript. Nice article, will be of interest to the LRRk2 field. We thank this reviewer for the positive feedback on our revisions. Reviewer #2: The authors did a very good job at revising the manuscript. The authors are asked to add the following minor stylistic modifications to their manuscript: P3, line 14/15: "as a pharmacological target" P3, line 16/17: "LRRK2's kinase activity" P3, line 42: "an alpha-helical" P4, line 16/17: please change sentence to "primary cortical cultures in the presence or absence of the LRRK2 inhibitor […]" P4, line 40: "while 300 AP is sufficient" P5, line 2: please change 'infected' to 'transduced' P6, line 38: "at a 1:10 ratio" P8, line 22: "as a bona fide" I would like to thank the authors for properly and diligently addressing all previously raised comments and concerns.

	We thank the reviewer for the positive feedback and for helping in improving the manuscript. All the suggested stylistic modifications have been made. Reviewer #3: I have looked over the rebuttal and the responses address my questions. There is however still one remaining issue that I have substantial trouble with: The synaptophluorin data at the beginning of the paper are still very weak. Essential controls are not there and more importantly, they are not connected to the rest of the work. The authors characterize a connection between LRRK2 and NSF but they are not testing this interaction in the context of the synaptophluorin assay. As I stated in my first review I am not asking them to perform these experiments, but I think that at this junction it is not helpful to include those data in the paper. I would remove these data as they do not add to the central point. If the authors do so I am happy to recommend publication. First of all, we thank this reviewer for the general positive feedback. Concerning figure 1, we completely agree with the reviewer. Our data suggest a role for LRRK2 in controlling synaptic vesicle exo/endocytosis. In particular, we propose that LRRK2 kinase activity influences vesicle endocytosis. However, it is indeed true that the experiment proposed does not prove the implication of NSF by itself. To this purpose, it will be necessary to first abolish the putative phosphosite within NSF. Accordingly, we are developing a CRISPR/Cas9 gene editing strategy to mutate endogenous NSF. The outcome of such analysis will be the focus of future studies. We would like to point that in this revised version of the manuscript, we repeated the assays taking advantage of a more specific LRRK2 inhibitor (GSK2578215A compound). Furthermore we included in our analysis primary cultures obtained from mice expressing hyperactive (G2019S) LRRK2. We deem that the overall results are coherent with a role played by LRRK2 kinase activity in controlling synaptic vesicle exo/endocytosis. To our knowledge, this is the first report where a dynamic assay monitoring vesicle trafficking is used in the contest of inhibited and enhanced LRRK2 kinase activity. Moreover, given the positive feedback of reviewers 1 and 2 on the revised SypHy experiments, we feel that removing figure 1 might weaken the biological meaning of our findings.

LRRK2 phosphorylates pre-synaptic N-ethylmaleimide sensitive fusion (NSF) protein enhancing its ATPase activity and SNARE complex disassembling rate

Elisa Belluzzi[1,§,*], Adriano Gonnelli[1,§], Maria-Daniela Cirnaru[2], Antonella Marte[3], Nicoletta Plotegher[1,¶], Isabella Russo[1], Laura Civiero[1], Susanna Cogo[1], Maria Perèz Carrion[2], Cinzia Franchin[4,5], Giorgio Arrigoni[4,5], Mariano Beltramini[1], Luigi Bubacco[1], Franco Onofri[3], Giovanni Piccoli[2,6], Elisa Greggio[1,CA]

[1] Department of Biology, University of Padova, Padova, Italy

[2] San Raffaele Scientific Park & University Vita-Salute San Raffaele, Milan, Italy

[3] Department of Experimental Medicine, University of Genova, Genova, Italy

[4] Department of Biomedical Sciences, University of Padova, Padova, Italy

[5] Proteomics Center of Padova University, Padova, Italy

[6] IN-CNR Milano

[§]Equal contribution

[¶]Present Address: Department of Cell and Developmental Biology, University College London, London WC1E 6BT, UK

*Present Address: Rheumatology Unit, Department of Medicine – DIMED, University Hospital of Padova, Italy

Email addresses:
elisa.belluzzi@gmail.com, adriano.gonnelli@bio.unipd.it, Cirnaru.mariadaniela@hsr.it antonella.marte@unige.it, n.plotegher@ucl.ac.uk, isabella.russo@unipd.it, laura.civiero@unipd.it, susanna.cogo@studenti.unipd.it, mdolores.perez.carrion@gmail.com, cinzia.franchin@unipd.it, giorgio.arrigoni@unipd.it, mariano.beltramini@unipd.it, luigi.bubacco@unipd.it, franco.onofri@unige.it, piccoli.giovanni@hsr.it, elisa.greggio@unipd.it

[CA] To whom the correspondence should be addressed:
Elisa Greggio PhD, Department of Biology, via Ugo Bassi 58/B, University of Padova, 35131, Padova, Italy. Email: elisa.greggio@unipd.it

Abstract

Background

Lrrk2, a gene linked to Parkinson's disease, encodes a large scaffolding protein with kinase and GTPase activities implicated in vesicle and cytoskeletal-related processes. At the presynaptic site, LRRK2 associates with synaptic vesicles through interaction with a panel of presynaptic proteins.

Results

Here, we show that LRRK2 kinase activity influences the dynamics of synaptic vesicle fusion. We therefore investigated whether LRRK2 phosphorylates component(s) of the exo/endocytosis machinery. We have previously observed that LRRK2 interacts with NSF, a hexameric AAA+ ATPase that couples ATP hydrolysis to the disassembling of SNARE proteins allowing them to enter another fusion cycle during synaptic exocytosis. Here, we demonstrate that NSF is a substrate of LRRK2 kinase activity. LRRK2 phosphorylates full-length NSF at threonine 645 in the ATP binding pocket of D2 domain. Functionally, NSF phosphorylated by LRRK2 displays enhanced ATPase activity and increased rate of SNARE complex disassembling. Substitution of threonine 645 with alanine abrogates LRRK2-mediated increased ATPase activity.

Conclusions

Given that the most common Parkinson's disease LRRK2 G2019S mutation displays increased kinase activity, our results suggest that mutant LRRK2 may impair synaptic vesicle dynamics *via* aberrant phosphorylation of NSF.

Keywords

Parkinson's disease, Leucine-rich repeat kinase 2, N-ethylmaleimide sensitive fusion, presynapse, phosphorylation

Background

Leucine-rich repeat kinase 2 (LRRK2) is a large kinase with protein-to-protein interaction domains and dual enzymatic activities. The catalytic core includes a ROC (Ras Of Complex) domain with GTPase activity, followed by a COR (C-terminus Of ROC) domain likely involved in protein dimerization, and a serine-threonine kinase domain [1-3]. Mutations in *Lrrk2* cause late-onset autosomal dominant Parkinson's disease (PD) [4,5], whereas more common variants around the *Lrrk2* locus act as risk factors for disease [6,7]. As the most common G2019S mutation increases kinase activity *in vitro* and *in vivo* by ~3 fold, LRRK2 is being intensively explored as a pharmacological target for the treatment of PD [8]. Several substrates of LRRK2's kinase activity have been reported, however few of these have been extensively validated at a physiological level [9]. There is, therefore, an increasing interest in identifying LRRK2 substrates and cellular pathways compromised during pathological conditions that could serve as therapeutic alternatives to directly targeting LRRK2 kinase activity. LRRK2 has been found associated with various membrane structures, including synaptic vesicles (SV) [10-15]. Multiple studies on different experimental models support a role for LRRK2 at the synapse. Mutant LRRK2 rodent models display defects in neurotransmission [16-19], and LRRK2 overexpression or knockdown results in impaired SV endocytosis/exocytosis [15,20]. We recently showed that LRRK2 binds SV *via* interaction with a number of presynaptic proteins [21] and that its kinase activity modulates these interactions and impacts on SV dynamics [22]. Among the LRRK2 interactors identified, we found N-ethylmaleimide sensitive factor (NSF), which is involved in the fusion of SV orchestrated by SNARE (Soluble NSF-Attachment protein REceptor) proteins. During membrane fusion, vesicular and target SNAREs assemble into an alpha-helical trans-SNARE complex that juxtaposes the two membranes together to catalyze membrane fusion. NSF is the ATPase that catalyzes the release of SNARE complexes, thus allowing SV endocytosis and the next cycle of fusion [23]. Notably, NSF activity is tightly controlled by phosphorylation/dephosphorylation [24-26]. In the present study, using dynamic assays of SV cycling, we found that SV fusion is altered by LRRK2 kinase function, suggesting components of the exo/endocytic machinery may be a target of LRRK2 kinase activity. Given that LRRK2 interacts with NSF, we assessed whether NSF is a substrate for LRRK2 kinase activity. We found that LRRK2 can efficiently phosphorylate NSF *in vitro,* with phosphorylation primarily occurring at T645. Importantly, phosphorylated NSF displays enhanced ATPase activity and increased rate of SNARE complex disassembling *in vitro*. Our data implicate LRRK2 kinase activity in the regulation

of SV exo/endocytosis by phospho-modulation of NSF activity and suggest that pathological LRRK2 may disturb SV dynamics *via* aberrant phosphorylation of NSF.

Results

LRRK2 kinase activity influences synaptic vesicle dynamics

We recently reported that inhibition of LRRK2 kinase activity causes impairment in synaptic vesicles (SV) dynamics, indicating a role for LRRK2 catalytic activity in SV fusion cycle [22]. To further determine the role of LRRK2 kinase activity at the presynapse, we performed dynamic assays of SV taking advantage of the sypHy assay in two complementary models: a) primary cortical cultures in the presence or absence of the LRRK2 inhibitor GSK2578215A (GSK in, 0.2 μM, 2h), a brain penetrant, selective LRRK2 inhibitor (IC_{50} 10 nM) [27]; b) primary cortical neurons obtained from BAC hG2019S mice characterized by higher LRRK2 kinase activity [28]. GSK treatment induced LRRK2 dephosphorylation at Ser935, as predicted (Fig. S1-b), but did not cause protein destabilization (Fig. S1a-c), whereas BAC hG2019S neurons displayed increased LRRK2 expression due to the presence of the transgene (Fig. S1a-b-c). Synaptophysin-pHluorin (sypHy) is a pH-sensitive fluorescent reporter that, by analogy with the original synaptopHluorin (synaptobrevin-pHluorin), is quenched in the acidic intracellular space of the SV and will only become fluorescent upon SV fusion, when the contents of the SV is exposed to the more basic pH of the extracellular space [29]. As shown in figure 1, at the onset of the stimulus, exocytosis caused a rapid increase in sypHy fluorescence, which after cessation of the stimulus, slowly returned to baseline (Fig. 1a-b). The first stimulus, 40 AP, is predicted to mobilize SV belonging to the ready releasable pool, while 300 AP is sufficient to trigger the fusion of SV belonging to the total recycling pool [29]. Furthermore, the kinetics describing the on-set and the decay of the fluorescence are correlated to the efficiency of the exocytotic and endocytotic mechanism, respectively [29]. Interestingly, while we measured a significant impairment of SV fusion (decreased fluorescence) in the presence of GSK upon either 40 or 300 AP stimuli, BAC hG2019S neurons were characterized by a higher answer following the two stimulations (ΔF40/F0 and ΔF300/F0 respectively, fig. 1c). Furthermore, while upon acute pharmacological inhibition the time taken for fluorescence decay was extended, τ decay was decreased in hG2019S cells (Tau decay, fig. 1c). To further assess a role for LRRK2 in the SV cycle, we took advantage of the exo/endocytic assay previously reported [20,21]. Using this approach, we previously demonstrated that acute pharmacological blockade of LRRK2 kinase activity

impairs SV recycling [22]. Building upon these data, BAC hG2019S cortical cultures were transduced at DIV4 with control viruses co-expressing GFP to track neuronal processes and assayed at DIV14. Briefly, we exposed living cultures to rabbit polyclonal antibodies directed against the intravesicular domain of synaptotagmin1, which are internalized inside the vesicle lumen upon SV recycling [30]. Vesicles within GFP positive processes were then monitored *via* laser confocal microscopy. The vesicles appeared as clusters either synaptotagmin and synaptophysin positive (i.e. cycling vesicles) or only synaptophysin positive (Fig. 1d). The analysis showed that BAC hG2019S cultures are characterized by a significant increase in the number of synaptotagmin and synaptophysin positive clusters (Fig. 1e). The total number of synaptic contacts, however, remained unaltered despite any pharmacological treatments (Fig. S1d). Taken together, these results indicate that LRRK2 kinase activity is involved in the regulation of SV fusion.

LRRK2 interacts with NSF

Having found that LRRK2 kinase activity influences SV fusion, we next asked what the molecular mechanisms behind this phenotype might be. We had previously demonstrated that LRRK2 interacts with the vesicle fusing ATPase NSF through its WD40 domain [21].

We first confirmed LRRK2 and NSF interaction at the endogenous level in synaptosomal preparations. Using co-immunoprecipitation with endogenous proteins from rat synaptosomes, we observed that LRRK2 efficiently co-precipitates NSF (Fig. 2a). Next, we dissected the domain(s) of NSF involved in binding LRRK2. To this aim, we cloned human full-length NSF (aa 1-744) and its different domains, namely N domain (aa 1-205), D1 domain (aa 206-487) and D2 domain (aa 488-744) in fusion with a N-terminal Flag-tag and purified the proteins from HEK293T cells. Proteins bounds to Flag-conjugated beads were adjusted to equal molar concentrations and subsequently incubated with a mouse brain lysate. As shown in figure 2b, full-length NSF pulls-down endogenous LRRK2. Interestingly, N and D2 domains, but not D1, also pull-down endogenous LRRK2 (Fig. 2b). To further confirm the interaction between LRRK2 and NSF, we used size exclusion chromatography (SEC) to fractionate HEK293T lysates expressing Flag-NSF or co-expressing Flag-NSF and 2xMyc-LRRK2, followed by dot blot analysis. As shown in figure 2c, NSF elutes between 11 mL and 17.5 mL. Interestingly, in the presence of LRRK2, NSF elution profile shifts toward shorter retention times (elution peak between 10 mL and 16.5 mL) suggesting the formation of a complex with higher molecular weight than NSF alone (Fig. 2c). We also evaluated the cellular localization of endogenous NSF and LRRK2 in

primary neuronal cultures and found that the two proteins largely co-localize, and co-localization is enriched within clusters along the neurites (Fig. 2d). Collectively these data indicate that LRRK2 and NSF form a complex in the cell.

LRRK2 phosphorylates NSF in D2 domain

LRRK2 affects SV dynamics *via* its kinase activity (Fig. 1a-c) [22]. Therefore, we hypothesized that NSF could be a substrate of LRRK2 and, as such, be involved in the LRRK2 kinase dependent regulation of SV. To test this hypothesis, we performed *in vitro* kinase assays using recombinant LRRK2 and NSF purified from mammalian cells. We first validated recombinant human NSF biochemically. NSF purified as described in the methods section folds into hexamers when loaded with 1 mM ATP as evidenced by negative-stain transmission electron microscopy (TEM) (Fig. S2a). Of interest, Flag-tagged NSF purified with Flag affinity resin co-precipitates endogenous NSF as indicated by the presence of a band corresponding to endogenous NSF (Fig. S2b), further supporting the notion that Flag-NSF forms oligomers. To verify that purified NSF is functional, we measured ATP to ADP hydrolysis rate by isocratic reverse-phase HPLC (Fig. S2c-d) and malachite green colorimetric assay (Fig. S2e). NSF efficiently hydrolyzes ATP to ADP over time under these purification and assay conditions.

Having validated recombinant human full-length NSF, we next purified soluble 3xFlag-LRRK2 wild-type, the hyperactive clinical mutant G2019S and the kinase dead K1906M from HEK293T cells and subsequently incubated these purified proteins with full-length NSF in kinase assay conditions [31]. As shown in figure 3a, at a 1:10 ratio of LRRK2:NSF, we observe robust phosphorylation of NSF by LRRK2. Importantly, in the presence of LRRK2 K1906M or upon addition of 1 μM LRRK2 IN-1 inhibitor, NSF phosphorylation corresponds to the background levels observed for NSF alone, confirming that the incorporation of radioactive phosphate is genuinely due to LRRK2 kinase activity (Fig. 3a). We confirmed LRRK2-mediated phosphorylation of NSF using the hyperactive G2019S-LRRK2$^{970\text{-}2527}$ fragment (Fig. 3b). The stoichiometry of phosphate incorporation, measured using a calibration curve with different concentrations of ^{33}P-ATP, is approximately 0.04 moles of phosphate per mole of monomeric NSF in the presence of LRRK2 wild-type, 0.1 in the presence of G2019S and 0.4 with an artificial truncated variant characterized by higher activity, G2019S-LRRK2$^{970\text{-}2527}$ (Fig. 3c). The low value for this stoichiometry, when taken in the context of a hexameric NSF complex, is sufficient to imply the presence of at least one phosphorylated monomer per hexamer. The reaction reached a plateau after 1-

hour incubation (Fig. S3a-b), likely due to inactivation of LRRK2 under assay conditions as previously reported [32].

To define the region(s) of NSF phosphorylated by LRRK2, we performed kinase assays in the presence of NSF full-length or isolated domains. While we failed to detect any phosphorylation when N and D1 domains were incubated with G2019S-LRRK2$^{970-2527}$, we were able to measure phosphate incorporation in the D2 domain (Fig. 3d). Importantly, NSF is not a substrate of the cognate protein LRRK1 under these assay conditions (Fig. 3e), suggesting that this phosphorylation event is specific to LRRK2. *In toto,* these results indicate that LRRK2 likely phosphorylates the D2 domain of NSF.

LRRK2 phosphorylates NSF at threonine 645.

We next set out to identify NSF phosphorylation site(s) targeted by LRRK2. To achieve this, we used phospho-peptide enrichment coupled with liquid chromatography/tandem mass spectrometry (LC-MS/MS) analysis on purified NSF pretreated with alkaline phosphatase to eliminate possible cellular phosphorylation sites, and subsequently phosphorylated by LRRK2 *in vitro*. Under the experimental conditions used, we were able to achieve ≈80% NSF sequence coverage (Fig. S4a) and identified the peptide ^{639}KLLIIGTTSR^{648} as a *bona fide* phospho substrate. The MS analysis could not discriminate whether single/multiple phosphorylation occurred at T645, T646 or S647 or whether these sites may be multi-phosphorylated (Fig. S4b). This phosphopeptide was enriched following incubation with wild-type and G2019S LRRK2, but not in control samples (LRRK2 kinase dead or in the presence of 1 μM IN-1) indicating it contains specific LRRK2 phosphorylation site(s). We next validated the MS data by site-direct mutagenesis and *in vitro* kinase assays. Wild-type and phospho-deficient NSF mutants T645A, T646A and S647A were expressed and purified in HEK293T cells and subsequently incubated *in vitro* with catalytically active LRRK2 under phosphorylation permissive conditions. T645A displayed ~50% reduction of ^{33}P incorporation compared to NSF wild-type, T646A and S647A (**p<0.01, One-Way ANOVA with Bonferroni's post-test). Since NSF is also phosphorylated by PKC but within a different residue (S237) [26], we next assessed whether PKC is able to phosphorylate NSF at T645 to rule out any promiscuous effect. As shown in figure S5, we confirm that PKC efficiently phosphorylates NSF *in vitro,* but NSF^{T645A} exhibits similar ^{33}P incorporation as NSF wild-type, suggesting that T645 is a LRRK2 specific phospho-site. Overall, our data indicate that T645 is a LRRK2 phosphorylation site within NSF.

LRRK2-mediated phosphorylation increases NSF ATPase activity

We next investigated whether LRRK2 mediated phosphorylation of NSF has a functional consequence on its ATPase activity. We first identified the optimal detergent concentrations at which both LRRK2 and NSF display maximal catalytic activity (0.007% of polysorbate 20, the critical micelle concentration of the detergent; Fig. S6). Subsequently, full-length NSF was exposed to LRRK2-G2019S$^{970\text{-}2527}$ or buffer in kinase assays conditions (with 50 µM ATP to minimize interference with the subsequent ATPase assay) for 30 min. As shown in figure 5a, NSF phosphorylated by LRRK2 exhibits increased ATPase activity (K_m=355±50 µM; k_{cat}=40±11 min^{-1}; V_{max}=0.95±0.22 µmol/min, from n=4 independent purifications) compared to unphosphorylated NSF (K_m=178±12 µM; k_{cat}=19±4 min^{-1}; V_{max}=0.37±0.07 µmol/min, from n=4 independent purifications). Given that we identified threonine 645 as a *bona fide* LRRK2 target, we next assessed the ATPase activity of NSF^{T645A}, along with NSF wild-type, NSF^{T646A} and NSF^{S647A}, pre-treated with LRRK2-G2019S$^{970\text{-}2527}$ or buffer control in kinase assay conditions. As shown in figure 5b, NSF^{T645A} displays impaired ability to hydrolyze ATP and, importantly, activity could not be restored when NSF^{T645A} is pre-phosphorylated by LRRK2. Interestingly, the neighboring T646 mutated to alanine also exhibits impaired ATPase activity that cannot be recovered by LRRK2 phosphorylation, whereas NSF^{S647A}, two residues apart from T645, displays ATPase activity similar to wild-type, and this activity is enhanced by LRRK2 phosphorylation. These results strongly indicate that T645 and T646 are critical for NSF catalytic activity. To rule out that NSF^{T645A} impaired activity was due to partial unfolding, we used circular dichroism (CD) and fluorescence spectroscopy to compare the secondary structures of NSF wild-type and NSF^{T645A}. Tryptophan fluorescence is similar among wild-type and NSF^{T645A} (Fig. S7a). CD spectra also confirm that the overall folding is maintained (Fig. S7b). In addition, TEM imaging confirms that NSF^{T645A} retains the ability to form hexamers (Fig. S7c). Taken together, these data indicate that NSF phosphorylated by LRRK2 possesses enhanced ATPase activity and T645 is a crucial site for enzymatic catalysis.

LRRK2-mediated phosphorylation of NSF increases the rate of SNARE complex disassembling

NSF-mediated ATP hydrolysis promotes disassembly of the SNARE complex [33]. Given that NSF phosphorylation by LRRK2 increases its ATPase activity (Fig. 5), we next

postulated that this also impacts upon the rate of SNARE complex dissociation. To test this, we monitored the kinetic of SNARE complex disassembling *in vitro* as previously described [34,35]. We co-expressed in *E. coli* recombinant soluble syntaxin, SNAP-25 and 6xHis-VAMP and purified the assembled complex by IMAC affinity purification followed by size exclusion chromatography [35]. As shown in figure S8, the complex elutes as single band corresponding to the expected molecular weight for the soluble SNARE complex (68 kDa), which is dissociated into the three SNARE components upon heating. To assess whether LRRK2 phosphorylation on NSF impacts the rate of SNARE complex disassembling *in vitro*, we incubated SNARE complex (480 nM) with 1.5 µM of alpha-SNAP, an essential co-factor, and 24 nM of NSF (phosphorylated or not by LRRK2) in the presence of 2 mM of ATP, and subsequently analyzed the kinetic of SNARE complex disappearance over 150 minutes. Under these assay conditions, NSF phosphorylated by LRRK2 displayed a markedly increased efficiency in disassembling SNARE complex compared to non-phosphorylated NSF (Fig. 6a-b). These data further support the notion that LRRK2-mediated phosphorylation increases NSF catalytic activity with consequent acceleration of the disassembly of SNARE complexes *in vitro*.

Discussion

Identification of heterologous substrates of LRRK2 kinase activity is essential for understanding the cellular pathways deregulated in PD caused by mutations in this gene [3]. Here we provided evidence that the presynaptic ATPase NSF is a substrate of LRRK2 kinase activity, and that phosphorylated NSF displays enhanced ATP hydrolysis and SNARE complex dissociation activity *in vitro*.

Multiple lines of evidence support a role of LRRK2 at the presynaptic compartment. We previously found that LRRK2 controls SV storage and mobilization within the recycling pool [20] and that this process is dependent on LRRK2 kinase activity [22]. Synaptosomes treated with LRRK2 inhibitors exhibit decreased evoked glutamate release [22] whereas elevated glutamate release and synaptic transmission were observed in LRRK2 G2019S knock-in mice [16]. Altogether, these data indicate that LRRK2 kinase may play an important role in modulating a step of the exo-endocytic pathway. LRRK2 is a complex kinase with several protein interaction domains, which was shown to assemble multiprotein complexes during signal transduction [11]. At the presynapse, LRRK2 interacts with several proteins [21]. Moreover, accumulating literature suggests that LRRK2 regulates SV dynamics *via* phosphorylation of presynaptic proteins, such as

Snapin, and EndophilinA [36-38]. The present work provides evidence that NSF is not only an interactor but also a substrate of LRRK2 *in vitro*. Recently, another LRRK2 interactor, the ribosomal protein s15, has been shown to serve as LRRK2 substrate [39], further emphasizing the value of examining LRRK2 interacting proteins as potential kinase substrates.

Here, we demonstrated that LRRK2 phosphorylates NSF at T645. The functional consequence of this is that NSF hydrolyses ATP faster when phosphorylated by LRRK2 at this residue. The physiological relevance of this finding is further supported by the observed increased rate of SNARE complex disassembling in the presence of phosphorylated NSF. Indeed, we found T645A is characterized by a reduced endogenous ATPase activity. Given that T645 is located within the D2 domain of NSF, which is thought to be important for NSF oligomerization *via* ATP binding [40], these results are consistent with our current understanding of NSF function. Specifically, T645 is part of the beta strand S4 (aa 639-646), which stabilizes the hexamer through interaction with the neighboring alpha-helix H5 [41]. Therefore, T645 is predicted to be a key residue for protein oligomerization, which impacts the ability of the D1 domain to hydrolyze ATP. Clearly, further investigation is merited to determine whether LRRK2 phosphorylation at T645 directly alters NSF oligomerization.

Translating these findings into the neuronal context, these data imply that LRRK2 may play a role in tuning the kinetics of SV fusion by accelerating SNARE complex dissociation *via* NSF phosphorylation. Previous studies reported NSF as substrate of other serine-threonine kinases: NSF is phosphorylated by Pctaire1 at S569 in the D2 domain, and this phosphorylation reduces NSF oligomerization [25]; NSF is also phosphorylated by PKC *in vitro* at Ser-237 of the catalytic D1 domain which negatively regulate NSF binding to alpha-SNAP-SNARE complexes (Fig. S5) [26]. Therefore, both Pctaire1 and PKC appear to switch off NSF activity. In our current study, we report multiple strands of evidence that suggest that NSF phosphorylated by LRRK2 is more active *in vitro*, however it is still unknown whether this is replicated *in vivo*. Wild-type LRRK2 is characterized by a low basal activity that may become pathologically relevant in the presence of gain of function mutations. We predict that in the presence of pathological hyperactive LRRK2 variant, SV endocytosis may be abnormally fast. Such alteration could result in 1) increased neurotransmitter release or 2) impaired neurotransmitter release by accelerating SV endocytosis. While the second hypothesis would fit with the reduced dopamine release observed in mice expressing LRRK2 G2019S selectively in midbrain dopaminergic

neurons [42], increased glutamate release has been reported in G2019S knock-in neurons [16] – consistent with the first hypothesis. Thus, additional research is needed to clearly identify the best representative model of LRRK2 function and dysfunction in the neuron.

We also provide robust evidence that the kinase activity of LRRK2 affects SV dynamics using two complementary models: LRRK2 inhibition and hyperactive LRRK2 (BAC hG2019S) in primary cortical neurons. The strong impairment of SV exo-endocytosis observed in the presence of pharmacological inhibition (Fig. 1, [22]) suggests that a consequence of therapeutic LRRK2 kinase inhibition might be alterations in the biology of the presynaptic compartment, likely impairing neurotransmitter release and synaptic function. These observations, together with the reported side effects in peripheral organs [43] suggest that additional strategies should be considered to target pathological LRRK2 function.

Conclusions

In the present study, we report LRRK2 kinase as a positive regulator of NSF activity and SNARE complex disassembling *in vitro*. Future studies should also be directed at understanding whether this phosphorylation is relevant in the pathogenesis of PD.

Methods

Animals, neuron cultures and drugs.

Housing and handling of mice were carried out in compliance with the guidelines established by the European Community Council (Directive 2010/63/EU of March 4th, 2014) and approved by the Italian Ministry of Health (IACUC 625). Non-transgenic wild-type and LRRK2 BAC hG2019S mice, back-crossed on a C57BL/6J strain, were obtained from Mayo Clinic (Jacksonville, FL, USA) through a collaboration with Dr. Heather Melrose [28]. Animals were kept following guidelines of Ministry of Education, Universities and Research (MIUR). Neuron cultures were prepared from either mouse cortexes or hippocampi obtained from embryonic day 15.5-16.5 mice (C57BL/6J). High-density (750-1000 cells/mm^2) and medium-density (150–200 cells/mm^2) neuron cultures were plated and grown as described on 12-well plastic tissue culture plates (Iwaki; Bibby Sterilin Staffordshire, UK) or on 12 mm diameter coverslips put into 24-well plastic tissue culture plates (Iwaki) [44]. GSK-2578215A compound (Tocris Bioscience, Bristol, UK) or DMSO were added to culture media at the concentrations indicated through the text. For

immunocytochemistry, primary cultured neurons were fixed with 4% paraformaldehyde and probed with primary rabbit anti-NSF (1:200, D31C7, Cell Signaling, Danvers, MA, USA) and mouse anti-LRRK2 (1:200 N231B/34, NeuroMab, Davis, CA, USA) and secondary anti-mouse Alexa Fluor 488 and anti-rabbit Alexa Fluor 568 (Thermo Fisher, Waltham, MA USA).

Plasmids and constructs

pCHMWS 3xFlag-tagged LRRK2 wild-type, K1906M and G2019S, 2x-Myc LRRK2 constructs have been previously described [31]. NSF constructs (full-length and domains) were cloned into p3XFLAG-CMV-7.1 vector (Sigma-Aldrich, St. Louis, MO, USA). NSF domains were amplified using forward primers with NotI overhang and reverse primers with KpnI overhang as following:

N-Domain (1-205): forward 5'-AAGCTTGCGGCCGCCTTCGCGGGCCGGAGC-3' and reverse 5'-TCGACTGGTACCTTAGCGATTTTCCTTGGTTTT-3'

D1 domain (206-477aa): forward 5'-AAGCTTGCGGCCGCCCAATCAATTATCAATC-3' and reverse 5'-TCGACTGGTACCTTATCTCGTCACTTGCAGGC-3'

D2 domain (478-744aa): forward 5'-AAGCTTGCGGCCGCCGGAGACTTCCTTGCTTC-3' and reverse 5'-TCGACTGGTACCTCAATCAAAATCAAGGGG-3'.

NSF mutants were generated using the QuickChange mutagenesis kit (Agilent Technologies, CA, USA) according to the manufacturer's instructions. All plasmids were validated by restriction analysis and DNA sequencing.

Cell culture and transfection

Human embryonic kidney cells (HEK293T) were cultured in Dulbecco's modified Eagle's medium (DMEM, Thermo Fisher, Waltham, MA USA) supplemented with 10% fetal bovine serum (FBS, Thermo Fisher, Waltham, MA USA) at 37°C and 5% CO_2. HEK293T were transiently transfected using linear polyethylenimine (PEI, Polysciences) with ratio DNA:PEI 1:2. 40 μ g of DNA were dissolved in 1ml of OPTI-MEM (Thermo Fisher, Waltham, MA USA) and 80 μl of PEI (40 μM) were added to 1ml of OPTI-MEM. After 5 minutes of incubation the two solutions were mixed together and incubated for 20 minutes to allow the formation of DNA/PEI complexes. Then, the mix was added directly to the cells in Petri dishes of 15 cm^2 and used after 48-72 hours.

Antibodies, SDS-PAGE and western blot analysis

Antibodies used for western blotting were as follows: anti-Flag M2 (1:10000, Sigma-Aldrich, St. Louis, MO, USA); anti-NSF (1:500, Cell Signaling, Danvers, MA, USA); anti-LRRK2 (1:1000, C41-2, Abcam, Cambridge, UK); anti-Synaptobrevin, anti-synaptophysin and anti-Synaptotagmin 1 (1:1000, Synaptic System, Göttingen, Germany).

Between 10 and 20 µg of protein samples were dissolved in 4-20% Tris-glycine polyacrylamide gels (Biorad) in SDS/Tris-glycine running buffer. Precision Plus molecular weight markers (Biorad) were used for size estimation. Solubilized proteins were then transferred to polyvinylidenedifluoride (PVDF) membranes in transfer buffer containing 10% methanol. The PVDF sheets were blocked in Tris-buffered saline plus 0.1% Triton (TBS-T) plus 5% nonfat dry milk for 1 hour at 4°C and then incubated overnight at 4°C with primary antibody in TBS-T plus 5% non-fat dry milk. The PVDF membranes were washed in TBS-T (3x10 min) at room temperature (RT) followed by incubation for 1 h at RT with horseradish peroxidase-conjugated anti-mouse IgG. Blots were then washed in TBS-T (4x10 min) at RT and rinsed in TBS, and immunoreactive proteins were visualized using enhanced chemiluminescence plus (ECL+, GE Healthcare, Waukesha, WI, USA). Densitometric analysis was carried out using Image J software.

Protein purification

Human NSF with a N-terminal Flag tag or NSF domains were purified from HEK293T cells after transient transfection as described above. Cells were resuspended in 1 ml of a lysis buffer (20 mM Tris-HCl pH 7.5, 150 mM NaCl, 1 mM EDTA, 2.5 mM $Na_4P_2O_7$, 1 mM beta-glycerophosphate, 1mM Na_3VO_4, Protease Inhibitor Mixture (Sigma-Aldrich, St. Louis, MO, USA)) and then lysed with 5 cycles of freezing and thawing in liquid nitrogen. The cell lysate was collected after centrifugation at 18000xg for 40 minutes at 4°C. The supernatant was incubate overnight with 40 µl of Anti-Flag M2 Affinity gel (Sigma-Aldrich, St. Louis, MO, USA) at 4°C. After centrifugation, the supernatant was discarded and the beads with human NSF were washed with 1 ml of different buffers: WB1 (20 mM Tris-HCl pH 7.5, 500 mM NaCl) twice, WB2 (20 mM Tris-HCl pH 7.5, 350 mM NaCl) twice, WB3 (20 mM Tris-HCl pH 7.5, 150 mM NaCl) six times. The protein was then eluted by incubating the beads with 200 µl of 20 mM Tris-HCl pH 7.5, 150 mM NaCl or directly in the kinase assay buffer (25 mM Tris-HCl pH 7.5, 5 mM beta-glycerophosphate, 2 mM DTT, 0,1 mM Na_3VO_4, 10 mM $MgCl_2$) with 150 ng/µl 3xFlag peptide and mixing the sample for about 2 hours. The sample was centrifuged to pellet the resin and the supernatant was collected. Note that all the purification steps were carried out in the absence of detergent, a condition

that resulted essential to maintain NSF folding and to detect specific phosphorylation by LRRK2. Purified human NSF was separated on SDS-PAGE and quantified by comparison with different concentrations of BSA (Bovine Serum Albumin). Proteins were electrophoretically resolved on 4–20% Tris-glycine polyacrylamide gels (Biorad) using SDS/Tris-glycine running buffer. To estimate the molecular weight of proteins Precision Plus molecular weight marker (Biorad) was used. After the run, proteins were stained with Coomassie Brillant blue to enable the quantification with ImageJ software.

Synaptosomes preparation and immunoprecipitation

Brains from adult rats were quickly removed and the cerebral cortex dissected out at 4°C. Purified synaptosomes were prepared on Percoll gradients (Sigma-Aldrich, St Louis, MO, USA) essentially according to Nakamura et al. with minor modifications [45]. Briefly, the tissue was homogenized in 14 volumes of 0.32 M sucrose, Tris–HCl pH 7.4, using a glass-teflon tissue grinder (clearance 0.25 mm, 12 up–down strokes in about 1 min). The homogenate was centrifuged (5 min, 1000g at 4°C) to remove nuclei and debris and the supernatant was gently stratified on a discontinuous Percoll gradient (2%, 6%, 10%, and 20% v/v in Tris-buffered sucrose) and centrifuged at 33500g for 5 min at 4°C.

The layer between 10% and 20% Percoll (synaptosomal fraction) was collected, washed by centrifugation and resuspended in RIPA buffer (NaCl 150mM, Tris 50mM (pH 7.4), NP40 (1%v/v), SDS (0.1%v/v) and protease inhibitors). To precipitate the immunocomplexes the extract was incubated for 2h at RT with anti-LRRK2 antibodies (10µg/sample; MJFF C41-2, Abcam, Cambridge, UK) or a control rabbit IgG (10µg/sample; Sigma-Aldrich, St. Louis, MO, USA) conjugated with 25µl of settled prewashed protein G-Sepharose beads (GE-Healthcare, Waukesha, WI, USA). The eluted proteins were separated by SDS-PAGE, transferred onto nitrocellulose membrane (GE-Healthcare, Waukesha, WI, USA) and analyzed by western-blotting with anti-LRRK2 and anti-NSF (Cell Signaling, Danvers, MA, USA) antibodies. Western-blotting with anti-synaptotagmin 1, anti-synaptophysin and anti-synaptobrevin were performed to confirm purity of synaptosomal preparation.

Pull-down assays

NSF domains and full length NSF were purified after transient transfection from HEK293T cells. Cells were harvested in 500 µl of Lysis buffer (50 mM Tris-HCl pH 7.5, 1 mM EDTA, 2.5 mM $Na_4P_2O_7$, 1 mM beta-glycerophosphate, 1 mM Na_3VO_4, 0.27 M Sucrose, 1% Triton

X-100, Protease Inhibitor Mixture (Sigma-Aldrich, St. Louis, MO, USA)). The cell lysate was then centrifuged at 18000xg for 30 minutes at 4°C. Subsequently, the lysate was incubated overnight with 20 µl of Anti-Flag M2 Affinity gel (Sigma-Aldrich, St. Louis, MO, USA) at 4°C. After centrifugation, the supernatant was discarded and the beads with NSF proteins were washed 3 times with 1 ml of a Washing buffer (50 mM Tris-HCl pH 7.5, 1 mM EDTA, 0.27 M Sucrose, 250 mM NaCl, 0.02% Triton X-100) and resuspended in 100 µl of the same buffer. Proteins were loaded on an SDS-PAGE gel and their concentration was quantified measuring the intensity of the band against known BSA standards with ImageJ software.

Proteins were subsequently adjusted to the same concentration (2 µM) and incubated with 600 µl mouse brain lysate (2.5 mg/ml concentrated) overnight at 4°C. The day after, resins were boiled with sample buffer, loaded into a SDS-PAGE gel and transferred onto PVDF membranes.

Size Exclusion Chromatography (SEC) and dot blot analysis

Flag-NSF alone or Flag-NSF and 2xmyc-LRRK2 transfected HEK293T cells were lysed in 500 µl of lysis buffer containing 0.06 % (v/v) Triton X-100 and centrifuged. Cell lysates clarified were separated on a Superose 6 10/300 column (Ge Healthcare, Waukesha, WI, USA) pre-equilibrated with 20 mM Tris-HCl pH 7.5, 150 mM NaCl and 0.06% (v/v) Triton X-100. The flow rate used was 0.5 ml/min. A calibration curve was produced using the following proteins and relative elution volumes: 7.5 ml for Blue Dextran (void volume), 11.5 ml for hemocyanin from *Carcinus aestuarii* (900 kDa), 12 ml for thyroglobulin (669 kDa), 14 ml for ferritin (440 kDa) and 12.5 ml for catalase (232 kDa). Fractions of 0.25 ml were collected and spotted onto a nitrocellulose membrane and analyzed by dot blot. The membrane was blocked with 10% milk in TTBS and incubated with mouse monoclonal anti-Flag M2-peroxidase (Sigma-Aldrich, St. Louis, MO, USA) or anti-myc (Roche) in TTBS with 10% milk. A secondary rabbit antibody (Sigma-Aldrich, St. Louis, MO, USA) was used to stain the anti-myc. Immunoproteins were visualized using ECL (GE, Healthcare, Waukesha, WI, USA).

Electron microscopy

Purified NSF proteins were incubated with 1mM ATP and 2 mM $MgCl_2$. A total of 15 ng of protein was adsorbed few minutes to a glow-discharged carbon-coated copper grid, washed with deionized water, and stained with 1% uranyl acetate. Images were collected

using a Fei Tecnai T12 electron microscope equipped with a LaB6 filament and operated at an acceleration voltage of 100 kV.

In vitro Kinase Assay

Purified NSFs eluted in kinase assay buffer were incubated with LRRK2 proteins dissolved in kinase buffer for 1 hour at 30 °C in the presence of ^{33}P-ATP (1 µCi) and 10 µM cold ATP as previously described [31].

Incorporated ^{33}P-ATP was detected by autoradiography or by Phospho-Imager system (Cyclone, Perkin-Elmer). The same membranes were probed with anti-Flag antibody for total protein loading and analyzed using ImageJ software.

SypHy assay

We infected DIV4 primary neurons with viruses expressing sypHy, a fusion construct of synaptophysin and super ecliptic pHluorin [29]. At DIV14 neurons were treated with DMSO (control) or GSK2578215A (0.2 µM, 2 hours). Syphy positive boutons were assayed in a stimulation chamber on the stage of a Zeiss Axiovert 200M equipped with a mono-chromator (Poly V) and a cooled CCD camera (PCO, Imago QE), both from TILL photonics (Gräfelfing, Germany). The assay was carried out as described previously [46]. Briefly, cells were submerged in 500 µl of KRH buffer (125 mM NaCl, 5 mM KCl, 1.8 mM $CaCl_2$ 2.6 mM $MgSO_4$ 5 mM Hepes, pH 7.2) in presence of APV (2µM, Sigma-Aldrich, St. Louis, MO, USA) and CNQX (2µM, Sigma-Aldrich, St. Louis, MO, USA). SypHy was excited at 475 nm and its fluorescence emission collected at 525 nm using a 60X, 1.1 NA water immersion objective. Images were acquired every second for 200 seconds using TillVision software (TILL Photonics). At frame 30, cells were stimulated with 40 action potential (AP, 20Hz) then at frame 70 with 300 AP (20 Hz). Total fluorescence was measured upon incubation with 50 mM NH_4Cl. Quantitative measurements of the fluorescence intensity at individual boutons were obtained by averaging a selected area of pixel intensities using ImageJ. Net fluorescence changes (ΔF) were obtained by subtracting the average intensity of the first 15 frames (F0) from the intensity of each frame (Ft) for individual boutons and normalized F0 (ΔF/F0). The fluorescence increase and decay, reflect exo- and endocytosis, respectively [29]. Both the fluorescence upstroke and decay were fitted with a single exponential τ ($\tau_{upstroke}$ and τ_{decay} respectively). Data are expressed as mean ± SEM and statistical significance was assessed by unpaired two-tailed Student's t test (GraphPad Prism).

Exo/endocytotic assay

The endocytosis assay to monitor SV recycling was performed using rabbit polyclonal antibodies directed against the intravesicular domain of synaptotagmin1 (Synaptic System), applied for 5 min at RT on the cultures, as described previously [30]. Incubations with the antibody (1:400) were performed in Tyrode solution containing 124 mM NaCl, 5mM KCl, 2mM $MgCl_2$, 30mM glucose, 25 mM HEPES, pH 7.4 and 2mM $CaCl_2$. After fixation and permeabilization, a synaptophysin counter staining with mouse anti synaptophysin, 1:400 (Sigma-Aldrich) visualized the totality of synaptic vesicles. Acquired images were processed and quantitatively analyzed with ImageJ software as previously described [47]. Briefly, cultures were infected at DIV4 with GPF expressing viruses and assayed at DIV14 as in [22]. GFP positive processes were manually tracked and the number of synaptotagmin and synaptophysin positive clusters and synaptophysin positive clusters present in the region of interest were automatically counted.

Proteins digestion

Approximately 2 µg of purified NSF pre-dephosphorylated with alkaline phosphatase (Promega) and subsequently phosphorylated or not with LRRK2 in the presence of 100 µM ATP were loaded into a SDS-precasted gel (Biorad). Gel slices corresponding to purified NSF were excised, cut in smaller pieces, dehydrated with 100 µl of acetonitrile (ACN) for 10 minutes, then dried under vacuum. A protein reduction step was performed with 100 µl of freshly prepared 10 mM Dithiothreitol (DTT, Fluka) in 50 mM NH_4HCO_3, at 56°C. After 1 h DTT solution was discarded and 100 µl of a freshly prepared solution of 55 mM iodoacetamide (Sigma-Aldrich, St. Louis, MO, USA) in 50 mM NH_4HCO_3 was added to the gel pieces for 45 min at room temperature and in the dark. Gel pieces were washed 4 times (ten minutes each) alternating 100 µl of 25 mM NH_4HCO_3 and 100 µl of ACN, dried under vacuum, and suspended in 20 µl of a sequencing grade modified trypsin solution (Promega, 12.5 ng/mL in 25 mM NH_4HCO_3). Digestion was performed overnight at 37°C. Peptides were extracted with 3 changes (50 µl each) of 50% ACN/0.1% formic acid (FA, Fluka). Samples were dried under vacuum and stored at -20 °C till the phosphopeptide enrichment procedure was performed.

Enrichment of Phosphopeptides

Phosphopeptides were enriched with home made micro-columns of TiO_2 as previously described [48]. TiO_2 micro-columns were conditioned twice with 50 µl of ACN and twice with loading buffer (80% ACN/6% trifluoroacetic acid (TFA, Riedel-de Haën)). Samples were suspended in 50 µl of loading buffer and slowly loaded into the columns, which were then washed twice with 50 µl of loading buffer and twice with washing buffer (0.1% TFA). Phosphopeptides bound to TiO_2 were eluted with 50 µl of freshly prepared 5% NH_4OH and subsequently with 50 µl of 50% ACN/0.1% FA. Samples were immediately acidified by adding 5 µl of 100% FA and dried under vacuum.

Mass spectrometry analysis

Mass spectrometry analysis of phosphopeptides was performed with a LTQ-Orbitrap XL mass spectrometer (Thermo Fisher Scientific) coupled online with a nano-HPLC Ultimate 3000 (Dionex-Thermo Fisher Scientific). Samples were dissolved in 30 µl of 3% ACN/0.1% FA and for every analysis 8 µl of sample were loaded at a flow rate of 8 µl/min into a trap column (300 mm I.D., 300 Å, C18, 3 mm; SGE Analytical Science). Samples were injected into a home-made 10 cm pico-frit capillary column (75 µm I.D., 15 µm tip; New Objective) packed with C18 material (Aeris Peptide 3.6 um XB-C18, Phenomenex). Peptides were separated using a linear gradient from 3% to 40% of ACN/0.1 FA in 20 min at a flow rate of 250 nl/min.

To increase the confidence in the identification of phosphopeptides, the MS analysis of each sample was performed with 3 different acquisition methods, as reported in [49]. A MS^2 data dependent acquisition (1 full-MS scan in the range 300-1700 Da on the Orbitrap with a resolution of 60000, followed by MS/MS spectra acquired in the linear ion trap for the 10 most abundant ions); a MS^3 neutral loss-triggered dependent acquisition (1 full-MS scan on the Orbitrap, followed by MS/MS scans on the 3 most intense ions and by MS^3 upon detection of neutral loss of phosphoric acid in MS^2 spectra); a Multi Stage Acquisition (MSA) (1 full-MS scan at a resolution of 60000 followed by MS/MS scans on the 3 most abundant ions with the activation of neutral loss product without an additional isolation cycle).

Raw data files were analyzed with Proteome Discoverer software (version 1.4, Thermo Fisher Scientific) connected to a Mascot Server version 2.2.4 (Matrix Science, UK) and a SequestHT search engine version 28.0 (Thermo Fisher Scientific) against the Uniprot Human Database (version 2013.11.13 used by SequestHT, version 2014.04.16 used by Mascot). Trypsin was set as digesting enzyme with up to 2 missed-cleavages.

Carbamidomethyl cysteine was set as fixed modification, while phosphorylation of Ser/Thr/Tyr and methionine oxidation were set as variable modifications. Peptide and fragment tolerance were 10 ppm and 0.6 Da respectively. Percolator was used to calculate False Discovery Rate (FDR) based on the search against the corresponding randomized database. MS/MS spectra of phosphopeptides were manually inspected for confirmation and assignment of phosphorylation sites.

ATPase enzymatic assay

NSF ATPase activity was quantified using the Malachite Green Assay by measuring the release of inorganic phosphate (Pi) due to the ATP hydrolysis with spectrophotometer. The assay was adapted from the method of Lanzetta et al. [50]. The Malachite Green Stock solution used for the assay was a mixture of two different solutions (one with 34 mg Malachite Green oxalate salt (Sigma-Aldrich. St. Louis, MO, USA) into 40 ml HCl 1M and the other with 1 g $(NH_4)_2MoO_4$ (Sigma-Aldrich, St. Louis, MO, USA) into 14 ml HCl 4M to a final volume of 100 ml with distilled water and then filtered through 0,45 nm. The concentration of human NSF used for the ATPase assay was 216 nM (36 nM hexameric concentration) with different ATP concentration. Reaction was performed at 37°C and followed for 120 minutes. The time point aliquots collected (20 µl) were mixed with 150 µl of Malachite Green stock solution until the solution became homogenous and the absorbance measured at 640 nm using a corresponding Malachite Green solution as blank. The values of absorbance were then converted into µmol of free Pi in solution using a standard curve. To reported values for the kinetic constants (K_m, k_{cat} and V_{max}) were obtained by data fitting with the Michaelis-Menten kinetic model (Y = Vmax*S/(Km + [S])).

Reverse-phase HPLC ATPase assay

To determine the ATPase activity of NSF, 500 or 700 µM ATP was added to 0.2 µM 3xFlag-NSF wt. Proteins were purified as previously described and incubated at 37°C for 1 hour in the same kinase buffers and conditions of the Malachite Green Assay. At the reported time-points, aliquots (20 µl) were taken up to 120 minutes and heated for 3 minutes at 95°C with 0.1 M of EDTA to stop the reaction. Samples were stored at -80°C. Reverse Phase High-Performance Liquid Chromatography (RP-HPLC) was used to monitor the amount of ATP and ADP present in the sample. Nucleotides were separated on a Jupiter 5u C4 300A (Phenomenex) column using an Agilent HP 1100 HPLC, pre-equilibrated with 50 mM NaH_2PO_4 pH 6.5, 10 mM Tetra-n-butylammonium bromide and

4% ACN. The flow-rate used was 0.5 ml/min and the amount of the nucleotides was monitored measuring the increase in area of the peak corresponding to ADP measured at 256 nm with a total run time of 35 minutes. To convert this value to the Pi released by the reaction, a standard curve generated with different ADP concentration was used. ADP concentrations detected in the assay were plotted as a function of time and an equation was obtained through linear regression with GraphPad Prism 5.

Recombinant alpha SNAP and SNARE proteins production

Rat alpha-SNAP cloned in pET28 plasmid in fusion with a His-tag was a kind gift of Dr. Reinhard Jahn, Max-Planck-Institute, Göttingen). Alpha-SNAP was subsequently expressed in *E. Coli* in BL21(DE3) strain. Bacteria were grown at 37°C to an OD at 600nm of 0.4-0.6, then induced with 0.25 mM isopropyl β-D-1-thiogalactopyranoside (IPTG) for 4 hours. Cells were then harvested by centrifugation and the pellet of 250 ml of culture was resuspended in 5-10 ml of Tris-HCl pH 8.0. Phenylmethylsulfonyl fluoride (PMSF) 100μ M and a cocktail of protease inhibitors were added to the cells 1:100 (v/v) that were subsequently subjected to one French Press cycles (Constant Systems Ltd). The cell homogenate was centrifuged and the supernatant loaded onto a Co^{2+} affinity column and eluted with a 0-500 mM linear gradient of imidazole at 0.5 ml/min. Protein solution was dialyzed versus Tris-HCl 20 mM pH 7.5, NaCl 150 mM.

Soluble SNARE complex was obtained by co-expression of wild type SNAP-25A, of syntaxin-1A and of His-tagged VAMP2(1-96) using the Duet expression system (Novagen) in *E. Coli* in BL21(DE3) strain. VAMP2(1-96)-His6-TEV pACYC-Duet and syntaxin-1A/SNAP-25A pET-Duet were a kind gift of Prof. A. Brunger (Stanford University, California) [51]. Bacteria were grown at 37°C to an OD at 600nm of 0.6-0.8, then induced with 0.5 mM IPTG for 4 hours. Cell pellets of 250 ml of culture were suspended in 10 ml of 50 mM NaPi, pH 8.0, 300 mM NaCl, 20 mM imidazole and 0.5 mM Tris(2-carboxyethyl)phosphine (TCEP) (SNARE buffer), supplemented with PMSF 100 μM and protease inhibitors cocktail. Cell were lyses by two French Press cycles (Constant Systems Ltd) and the lysate was clarified by centrifugation for 1 hour at 15000g at 4°C. The supernatant was loaded onto a 1-ml Ni^{2+} affinity column, washed with 20 ml of SNARE buffer containing 7.5 M urea and then with 20 ml of SNARE buffer. The complex was then eluted with SNARE buffer containing 350 mM imidazole. After elution, SNARE complex was subjected to size exclusion chromatography using a Superdex 200 10/300

(GE Helthcare) that was equilibrated with 50 mM Tris-HCl, pH 7.5, 100 mM NaCl. The SNARE complex was checked and quantified by SDS-PAGE.

SNARE dissociation assay

As previously described [51] the SNARE dissociation assays were performed at 37°C in 240 µl in a 1.5 ml micro-tube. The assay buffer was composed of 25 mM Tris-HCl pH 7.5, 5 mM β–glycerophosphate, 2 mM dithiotreitol (DTT), 0.1 mM Na_3VO_4, 10 mM $MgCl_2$ and 0.007% polysorbate 20. Subsequently 1.5 µM αSNAP, 480 nM SNAREs, 24 nM NSF (hexameric concentration) phosphorylated or not by LRRK2 (ratio NSF:LRRK2 20:1) were added in the presence of 2 mM ATP to start the reaction. At defined time points, an aliquot (20 µl) was collected and loaded into an SDS-PAGE gel without boiling the samples: being the SNARE complex is SDS-resistant, it runs as a single band on SDS-PAGE gel. The intensity of each SNARE complex band was calculated and normalized to its time zero. The experiments were performed in triplicate up to 150 minutes of reaction.

Circular Dichroism (CD)

CD measurements were carried out on a JASCO J-810 spectropolarimeter interfaced with a personal computer. The CD spectra were acquired and processed using the J-700 software for Windows. All experiments were done at room temperature using an optical path length of 0.2 cm. The wavelength range of the measurements was 197–250 nm, using a bandwidth of 2 nm and a time constant of 8 s at a scan speed of 50 nm/min. The signal to noise ratio was improved by accumulating four scans. Spectra were acquired using purified proteins in the elution buffer (20 mM Tris-HCl pH 7.5, 150 mM NaCl and 0.007% polysorbate-20) using the same buffer with 3xFlag peptide as a control. All the spectra are reported in terms of mean residue molar ellipticity (deg cm^2 $dmol^{-1}$). Protein concentrations in the samples were determined by SDS-PAGE and all the spectra were normalized for the measured protein concentration.

Intrinsic fluorescence

Fluorescence emission spectra were recorded on a Cary Eclipse fluorescence spectrophotometer (Varian, Agilent Technologies, Santa Clara, CA) using the Cary Eclipse program. Sample measurements were carried out using optical path length of 10 mm. Fluorescence spectra were obtained using an excitation wavelength of 288 nm, with an excitation bandwidth of 5 nm and slit width of 10 nm. Emission spectra were recorded

between 300-400 nm at a scan rate of 30 nm/sec. Spectra were acquired using 80 nM proteins in 20 mM Tris/HCl buffer (pH 7.5), 150 mM NaCl and 0.02% Tween 20.

Statistical analysis

All quantitative data are expressed as mean ± SEM and represent at least three independent sets of experiments. Significance of differences between two groups was assessed by two-tailed unpaired t-test or one-way or two-way ANOVA with Bonferroni's post-test when more than two groups were compared. Significance was set at $p<0.05$.

Abbreviations

NSF: N-ethylmaleimide sensitive fusion

LRRK2: Leucine-rich repeat kinase 2

SNARE: soluble NSF-attachment protein receptor

PD: Parkinson's disease

ANOVA: Analysis of variance

TBS: Tris-buffered saline

SV: synaptic vesicles

sypHy: synaptophysin-pHluorin

CD: Circular Dichroism

MS: mass spectrometry

TEM: transmission electron microscopy

DIV: days *in vitro*

Competing interests

The author(s) declare that they have no competing interests

Authors' contributions

EB and AG performed and analyzed the kinase, ATPase and SNARE disassembling assays. MDC performed and analyzed the sypHy assay. AM performed the co-immunoprecipitation from synaptosomes. NP expressed and purified the SNARE complex. IR and LC helped with the *in vitro* experiments. SC cloned the NSF constructs. MPC measured LRRK2 steady state levels in primary neurons. CF and GA performed the LC-

MS/MS. MB, LB, FO, GP and EG conceived the study, designed the experiments and analyzed the data. EG wrote the paper with contribution from all authors.

Funding

We would like to thank Dr. Patrick Lewis for proofreading the manuscript. This study was supported by the Michael J Fox Foundation (to EG, FO and GP). We also thank the financial support of Telethon - Italy (Grant no. GGP12237 to EG, FO and GP) and the University of Padova (Progetto di Ateneo CPDA 124045/12 to MB) and Regione Lombardia (Projects MbMM-Convenzione No. 18099/RCC to GP). We gratefully thank Prof. Axel T. Brunger and Dr. Sandro Vivona for the kind gift of the soluble SNARE constructs. The authors wish to thank the “Cassa di Risparmio di Padova e Rovigo” (Cariparo) for funding the acquisition of the LTQ-Orbitrap XL mass spectrometer.

References

1. Gasper R, Meyer S, Gotthardt K, Sirajuddin M, Wittinghofer A (2009) It takes two to tango: regulation of G proteins by dimerization. Nat Rev Mol Cell Biol 10 (6):423-429. doi:nrm2689 [pii]
10.1038/nrm2689 [doi]
2. Taymans JM (2012) The GTPase function of LRRK2. Biochem Soc Trans 40 (5):1063-1069. doi:BST20120133 [pii]
10.1042/BST20120133 [doi]
3. Greggio E (2012) Role of LRRK2 kinase activity in the pathogenesis of Parkinson's disease. Biochem Soc Trans 40 (5):1058-1062. doi:BST20120054 [pii]
10.1042/BST20120054 [doi]
4. Paisan-Ruiz C, Jain S, Evans EW, Gilks WP, Simon J, van der Brug M, Lopez de Munain A, Aparicio S, Gil AM, Khan N, Johnson J, Martinez JR, Nicholl D, Carrera IM, Pena AS, de Silva R, Lees A, Marti-Masso JF, Perez-Tur J, Wood NW, Singleton AB (2004) Cloning of the gene containing mutations that cause PARK8-linked Parkinson's disease. Neuron 44 (4):595-600. doi:S0896627304006890 [pii]
10.1016/j.neuron.2004.10.023 [doi]
5. Zimprich A, Biskup S, Leitner P, Lichtner P, Farrer M, Lincoln S, Kachergus J, Hulihan M, Uitti RJ, Calne DB, Stoessl AJ, Pfeiffer RF, Patenge N, Carbajal IC, Vieregge P, Asmus F, Muller-Myhsok B, Dickson DW, Meitinger T, Strom TM, Wszolek ZK, Gasser T (2004) Mutations in LRRK2 cause autosomal-dominant parkinsonism with pleomorphic pathology. Neuron 44 (4):601-607. doi:S0896627304007202 [pii]
10.1016/j.neuron.2004.11.005 [doi]
6. Satake W, Nakabayashi Y, Mizuta I, Hirota Y, Ito C, Kubo M, Kawaguchi T, Tsunoda T, Watanabe M, Takeda A, Tomiyama H, Nakashima K, Hasegawa K, Obata F, Yoshikawa T, Kawakami H, Sakoda S, Yamamoto M, Hattori N, Murata M, Nakamura Y, Toda T (2009) Genome-wide association study identifies common variants at four loci as genetic risk factors for Parkinson's disease. Nat Genet 41 (12):1303-1307. doi:ng.485 [pii]
10.1038/ng.485 [doi]

7. Simon-Sanchez J, Schulte C, Bras JM, Sharma M, Gibbs JR, Berg D, Paisan-Ruiz C, Lichtner P, Scholz SW, Hernandez DG, Kruger R, Federoff M, Klein C, Goate A, Perlmutter J, Bonin M, Nalls MA, Illig T, Gieger C, Houlden H, Steffens M, Okun MS, Racette BA, Cookson MR, Foote KD, Fernandez HH, Traynor BJ, Schreiber S, Arepalli S, Zonozi R, Gwinn K, van der Brug M, Lopez G, Chanock SJ, Schatzkin A, Park Y, Hollenbeck A, Gao J, Huang X, Wood NW, Lorenz D, Deuschl G, Chen H, Riess O, Hardy JA, Singleton AB, Gasser T (2009) Genome-wide association study reveals genetic risk underlying Parkinson's disease. Nat Genet 41 (12):1308-1312. doi:ng.487 [pii] 10.1038/ng.487 [doi]
8. Rudenko IN, Cookson MR (2014) Heterogeneity of leucine-rich repeat kinase 2 mutations: genetics, mechanisms and therapeutic implications. Neurotherapeutics 11 (4):738-750. doi:10.1007/s13311-014-0284-z [doi]
9. Reynolds A, Doggett EA, Riddle SM, Lebakken CS, Nichols RJ (2014) LRRK2 kinase activity and biology are not uniformly predicted by its autophosphorylation and cellular phosphorylation site status. Front Mol Neurosci 7:54. doi:10.3389/fnmol.2014.00054 [doi]
10. Alegre-Abarrategui J, Christian H, Lufino MM, Mutihac R, Venda LL, Ansorge O, Wade-Martins R (2009) LRRK2 regulates autophagic activity and localizes to specific membrane microdomains in a novel human genomic reporter cellular model. Hum Mol Genet 18 (21):4022-4034. doi:ddp346 [pii] 10.1093/hmg/ddp346
11. Beilina A, Rudenko IN, Kaganovich A, Civiero L, Chau H, Kalia SK, Kalia LV, Lobbestael E, Chia R, Ndukwe K, Ding J, Nalls MA, Consortium IPsDG, Consortium NABE, Olszewski M, Hauser DN, Kumaran R, Lozano AM, Baekelandt V, Greene LE, Taymans J-M, Greggio E, Cookson MR (2014) Unbiased screen for interactors of leucine-rich repeat kinase 2 supports a common pathway for sporadic and familial Parkinson disease. Proceedings of the National Academy of Sciences 111 (7):2626-2631. doi:10.1073/pnas.1318306111
12. Berger Z, Smith KA, Lavoie MJ (2010) Membrane localization of LRRK2 is associated with increased formation of the highly active LRRK2 dimer and changes in its phosphorylation. Biochemistry 49 (26):5511-5523. doi:10.1021/bi100157u
13. Biskup S, Moore DJ, Celsi F, Higashi S, West AB, Andrabi SA, Kurkinen K, Yu SW, Savitt JM, Waldvogel HJ, Faull RL, Emson PC, Torp R, Ottersen OP, Dawson TM, Dawson VL (2006) Localization of LRRK2 to membranous and vesicular structures in mammalian brain. Ann Neurol 60 (5):557-569. doi:10.1002/ana.21019
14. Hatano T, Kubo S-i, Imai S, Maeda M, Ishikawa K, Mizuno Y, Hattori N (2007) Leucine-rich repeat kinase 2 associates with lipid rafts. Human Molecular Genetics 16 (6):678-690. doi:10.1093/hmg/ddm013
15. Shin N, Jeong H, Kwon J, Heo HY, Kwon JJ, Yun HJ, Kim CH, Han BS, Tong Y, Shen J, Hatano T, Hattori N, Kim KS, Chang S, Seol W (2008) LRRK2 regulates synaptic vesicle endocytosis. Exp Cell Res 314 (10):2055-2065. doi:S0014-4827(08)00108-0 [pii] 10.1016/j.yexcr.2008.02.015
16. Beccano-Kelly DA, Kuhlmann N, Tatarnikov I, Volta M, Munsie LN, Chou P, Cao LP, Han H, Tapia L, Farrer MJ, Milnerwood AJ (2014) Synaptic function is modulated by LRRK2 and glutamate release is increased in cortical neurons of G2019S LRRK2 knock-in mice. Front Cell Neurosci 8:301. doi:10.3389/fncel.2014.00301 [doi]
17. Li X, Patel JC, Wang J, Avshalumov MV, Nicholson C, Buxbaum JD, Elder GA, Rice ME, Yue Z (2010) Enhanced striatal dopamine transmission and motor performance with LRRK2 overexpression in mice is eliminated by familial Parkinson's disease mutation G2019S. The Journal of neuroscience : the official journal of the Society for Neuroscience 30 (5):1788-1797. doi:30/5/1788 [pii] 10.1523/JNEUROSCI.5604-09.2010

18. Li Y, Liu W, Oo TF, Wang L, Tang Y, Jackson-Lewis V, Zhou C, Geghman K, Bogdanov M, Przedborski S, Beal MF, Burke RE, Li C (2009) Mutant LRRK2(R1441G) BAC transgenic mice recapitulate cardinal features of Parkinson's disease. Nat Neurosci 12 (7):826-828. doi:nn.2349 [pii]
10.1038/nn.2349
19. Tong Y, Pisani A, Martella G, Karouani M, Yamaguchi H, Pothos EN, Shen J (2009) R1441C mutation in LRRK2 impairs dopaminergic neurotransmission in mice. Proc Natl Acad Sci U S A 106 (34):14622-14627. doi:0906334106 [pii]
10.1073/pnas.0906334106
20. Piccoli G, Condliffe SB, Bauer M, Giesert F, Boldt K, De Astis S, Meixner A, Sarioglu H, Vogt-Weisenhorn DM, Wurst W, Gloeckner CJ, Matteoli M, Sala C, Ueffing M (2011) LRRK2 controls synaptic vesicle storage and mobilization within the recycling pool. The Journal of neuroscience : the official journal of the Society for Neuroscience 31 (6):2225-2237. doi:31/6/2225 [pii]
10.1523/JNEUROSCI.3730-10.2011
21. Piccoli G, Onofri F, Cirnaru MD, Kaiser CJ, Jagtap P, Kastenmuller A, Pischedda F, Marte A, von Zweydorf F, Vogt A, Giesert F, Pan L, Antonucci F, Kiel C, Zhang M, Weinkauf S, Sattler M, Sala C, Matteoli M, Ueffing M, Gloeckner CJ (2014) LRRK2 binds to neuronal vesicles through protein interactions mediated by its C-terminal WD40 domain. Mol Cell Biol. doi:MCB.00914-13 [pii]
10.1128/MCB.00914-13
22. Cirnaru MD, Marte A, Belluzzi E, Russo I, Gabrielli M, Longo F, Arcuri L, Murru L, Bubacco L, Matteoli M, Fedele E, Sala C, Passafaro M, Morari M, Greggio E, Onofri F, Piccoli G (2014) LRRK2 kinase activity regulates synaptic vesicle trafficking and neurotransmitter release through modulation of LRRK2 macro-molecular complex. Front Mol Neurosci 7:49. doi:10.3389/fnmol.2014.00049 [doi]
23. Sudhof TC, Rizo J (2011) Synaptic vesicle exocytosis. Cold Spring Harb Perspect Biol 3 (12). doi:cshperspect.a005637 [pii]
10.1101/cshperspect.a005637 [doi]
24. Huynh H, Bottini N, Williams S, Cherepanov V, Musumeci L, Saito K, Bruckner S, Vachon E, Wang X, Kruger J, Chow CW, Pellecchia M, Monosov E, Greer PA, Trimble W, Downey GP, Mustelin T (2004) Control of vesicle fusion by a tyrosine phosphatase. Nat Cell Biol 6 (9):831-839. doi:10.1038/ncb1164 [doi]
ncb1164 [pii]
25. Liu Y, Cheng K, Gong K, Fu AK, Ip NY (2006) Pctaire1 phosphorylates N-ethylmaleimide-sensitive fusion protein: implications in the regulation of its hexamerization and exocytosis. The Journal of biological chemistry 281 (15):9852-9858. doi:M513496200 [pii]
10.1074/jbc.M513496200
26. Matveeva EA, Whiteheart SW, Vanaman TC, Slevin JT (2001) Phosphorylation of the N-ethylmaleimide-sensitive factor is associated with depolarization-dependent neurotransmitter release from synaptosomes. The Journal of biological chemistry 276 (15):12174-12181. doi:10.1074/jbc.M007394200
M007394200 [pii]
27. Reith AD, Bamborough P, Jandu K, Andreotti D, Mensah L, Dossang P, Choi HG, Deng X, Zhang J, Alessi DR, Gray NS (2012) GSK2578215A; a potent and highly selective 2-arylmethyloxy-5-substitutent-N-arylbenzamide LRRK2 kinase inhibitor. Bioorganic & medicinal chemistry letters 22 (17):5625-5629. doi:10.1016/j.bmcl.2012.06.104
28. Melrose HL, Dachsel JC, Behrouz B, Lincoln SJ, Yue M, Hinkle KM, Kent CB, Korvatska E, Taylor JP, Witten L, Liang YQ, Beevers JE, Boules M, Dugger BN, Serna VA, Gaukhman A, Yu X, Castanedes-Casey M, Braithwaite AT, Ogholikhan S, Yu N, Bass D,

Tyndall G, Schellenberg GD, Dickson DW, Janus C, Farrer MJ (2010) Impaired dopaminergic neurotransmission and microtubule-associated protein tau alterations in human LRRK2 transgenic mice. Neurobiology of disease 40 (3):503-517. doi:10.1016/j.nbd.2010.07.010
29. Granseth B, Odermatt B, Royle SJ, Lagnado L (2006) Clathrin-mediated endocytosis is the dominant mechanism of vesicle retrieval at hippocampal synapses. Neuron 51 (6):773-786. doi:S0896-6273(06)00675-1 [pii]
10.1016/j.neuron.2006.08.029 [doi]
30. Matteoli M, Takei K, Perin MS, Sudhof TC, De Camilli P (1992) Exo-endocytotic recycling of synaptic vesicles in developing processes of cultured hippocampal neurons. J Cell Biol 117 (4):849-861
31. Civiero L, Vancraenenbroeck R, Belluzzi E, Beilina A, Lobbestael E, Reyniers L, Gao F, Micetic I, De Maeyer M, Bubacco L, Baekelandt V, Cookson MR, Greggio E, Taymans JM (2012) Biochemical characterization of highly purified leucine-rich repeat kinases 1 and 2 demonstrates formation of homodimers. PloS one 7 (8):e43472. doi:10.1371/journal.pone.0043472
PONE-D-12-12614 [pii]
32. Webber PJ, Smith AD, Sen S, Renfrow MB, Mobley JA, West AB (2011) Autophosphorylation in the leucine-rich repeat kinase 2 (LRRK2) GTPase domain modifies kinase and GTP-binding activities. J Mol Biol 412 (1):94-110. doi:S0022-2836(11)00798-4 [pii]
10.1016/j.jmb.2011.07.033 [doi]
33. Zhao C, Slevin JT, Whiteheart SW (2007) Cellular functions of NSF: not just SNAPs and SNAREs. FEBS Lett 581 (11):2140-2149. doi:S0014-5793(07)00292-X [pii]
10.1016/j.febslet.2007.03.032
34. Cipriano DJ, Jung J, Vivona S, Fenn TD, Brunger AT, Bryant Z (2013) Processive ATP-driven Substrate Disassembly by the N-Ethylmaleimide-sensitive Factor (NSF) Molecular Machine. Journal of Biological Chemistry 288 (32):23436-23445. doi:10.1074/jbc.M113.476705
35. Vivona S, Cipriano DJ, O'Leary S, Li YH, Fenn TD, Brunger AT (2013) Disassembly of all SNARE complexes by N-ethylmaleimide-sensitive factor (NSF) is initiated by a conserved 1:1 interaction between alpha-soluble NSF attachment protein (SNAP) and SNARE complex. The Journal of biological chemistry 288 (34):24984-24991. doi:M113.489807 [pii]
10.1074/jbc.M113.489807 [doi]
36. Yun HJ, Park J, Ho DH, Kim H, Kim C-H, Oh H, Ga I, Seo H, Chang S, Son I, Seol W (2013) LRRK2 phosphorylates Snapin and inhibits interaction of Snapin with SNAP-25. Exp Mol Med 45:e36. doi:10.1038/emm.2013.68
37. Arranz AM, Delbroek L, Van Kolen K, Guimaraes MR, Mandemakers W, Daneels G, Matta S, Calafate S, Shaban H, Baatsen P, De Bock PJ, Gevaert K, Berghe PV, Verstreken P, De Strooper B, Moechars D (2015) LRRK2 functions in synaptic vesicle endocytosis through a kinase-dependent mechanism. J Cell Sci 128 (3):541-552. doi:jcs.158196 [pii]
10.1242/jcs.158196 [doi]
38. Matta S, Van Kolen K, da Cunha R, van den Bogaart G, Mandemakers W, Miskiewicz K, De Bock P-J, Morais Vanessa A, Vilain S, Haddad D, Delbroek L, Swerts J, Chávez-Gutiérrez L, Esposito G, Daneels G, Karran E, Holt M, Gevaert K, Moechars Diederik W, De Strooper B, Verstreken P (2012) LRRK2 Controls an EndoA Phosphorylation Cycle in Synaptic Endocytosis. Neuron 75 (6):1008-1021. doi:http://dx.doi.org/10.1016/j.neuron.2012.08.022

39. Martin I, Kim JW, Lee BD, Kang HC, Xu JC, Jia H, Stankowski J, Kim MS, Zhong J, Kumar M, Andrabi SA, Xiong Y, Dickson DW, Wszolek ZK, Pandey A, Dawson TM, Dawson VL (2014) Ribosomal protein s15 phosphorylation mediates LRRK2 neurodegeneration in Parkinson's disease. Cell 157 (2):472-485. doi:S0092-8674(14)00212-8 [pii]
10.1016/j.cell.2014.01.064 [doi]
40. Matveeva EA, He P, Whiteheart SW (1997) N-Ethylmaleimide-sensitive fusion protein contains high and low affinity ATP-binding sites that are functionally distinct. The Journal of biological chemistry 272 (42):26413-26418
41. Yu RC, Hanson PI, Jahn R, Brunger AT (1998) Structure of the ATP-dependent oligomerization domain of N-ethylmaleimide sensitive factor complexed with ATP. Nat Struct Biol 5 (9):803-811. doi:10.1038/1843 [doi]
42. Liu G, Sgobio C, Gu X, Sun L, Lin X, Yu J, Parisiadou L, Xie C, Sastry N, Ding J, Lohr KM, Miller GW, Mateo Y, Lovinger DM, Cai H (2015) Selective Expression of Parkinson's disease-related Leucine-rich Repeat Kinase 2 G2019S Missense Mutation in Midbrain Dopaminergic Neurons Impairs Dopamine Release and Dopaminergic Gene Expression. Hum Mol Genet. doi:ddv249 [pii]
10.1093/hmg/ddv249 [doi]
43. Fuji RN, Flagella M, Baca M, Baptista MA, Brodbeck J, Chan BK, Fiske BK, Honigberg L, Jubb AM, Katavolos P, Lee DW, Lewin-Koh SC, Lin T, Liu X, Liu S, Lyssikatos JP, O'Mahony J, Reichelt M, Roose-Girma M, Sheng Z, Sherer T, Smith A, Solon M, Sweeney ZK, Tarrant J, Urkowitz A, Warming S, Yaylaoglu M, Zhang S, Zhu H, Estrada AA, Watts RJ (2015) Effect of selective LRRK2 kinase inhibition on nonhuman primate lung. Science translational medicine 7 (273):273ra215. doi:10.1126/scitranslmed.aaa3634
44. Piccoli G, Verpelli C, Tonna N, Romorini S, Alessio M, Nairn AC, Bachi A, Sala C (2007) Proteomic analysis of activity-dependent synaptic plasticity in hippocampal neurons. Journal of proteome research 6 (8):3203-3215. doi:10.1021/pr0701308
45. Nakamura Y, Iga K, Shibata T, Shudo M, Kataoka K (1993) Glial plasmalemmal vesicles: a subcellular fraction from rat hippocampal homogenate distinct from synaptosomes. Glia 9 (1):48-56. doi:10.1002/glia.440090107
46. Sankaranarayanan S, Ryan TA (2000) Real-time measurements of vesicle-SNARE recycling in synapses of the central nervous system. Nat Cell Biol 2 (4):197-204. doi:10.1038/35008615 [doi]
47. Verderio C, Coco S, Bacci A, Rossetto O, De Camilli P, Montecucco C, Matteoli M (1999) Tetanus toxin blocks the exocytosis of synaptic vesicles clustered at synapses but not of synaptic vesicles in isolated axons. The Journal of neuroscience : the official journal of the Society for Neuroscience 19 (16):6723-6732
48. Salvi M, Trashi E, Cozza G, Franchin C, Arrigoni G, Pinna LA (2012) Investigation on PLK2 and PLK3 substrate recognition. Biochimica et biophysica acta 1824 (12):1366-1373. doi:10.1016/j.bbapap.2012.07.003
49. Venerando A, Franchin C, Cant N, Cozza G, Pagano MA, Tosoni K, Al-Zahrani A, Arrigoni G, Ford RC, Mehta A, Pinna LA (2013) Detection of phospho-sites generated by protein kinase CK2 in CFTR: mechanistic aspects of Thr1471 phosphorylation. PloS one 8 (9):e74232. doi:10.1371/journal.pone.0074232
50. Lanzetta PA, Alvarez LJ, Reinach PS, Candia OA (1979) An improved assay for nanomole amounts of inorganic phosphate. Analytical biochemistry 100 (1):95-97
51. Cipriano DJ, Jung J, Vivona S, Fenn TD, Brunger AT, Bryant Z (2013) Processive ATP-driven substrate disassembly by the N-ethylmaleimide-sensitive factor (NSF) molecular machine. The Journal of biological chemistry 288 (32):23436-23445. doi:10.1074/jbc.M113.476705

Figure legends

Figure 1. LRRK2 kinase activity modulates synaptic vesicle fusion.

(a) We recorded synaptophluorin fluorescence from DIV14 wild-type cortical neurons treated with DMSO (control) or treated with LRRK2 inhibitor GSK2578215A (GSK in, 0.2 μM, 2h) and from cortical neurons obtained from BAC hG2019S mice (hG2019S). Representative snapshots were taken at DIV16 from 1 Hz recordings at rest (0), after 40 action potential stimulation (40AP), after 300 action potential stimulation (300AP) and upon neutralization with 50 mM NH_4Cl to reveal total fluorescence (Fmax). Panels size is 113x113 μm. (b) The graph shows representative pattern of fluorescence. Y-axis reports ΔF/F0 at the given time point (second). (c) The graphs report the increase in fluorescence after 40AP (ΔF40/F0) and 300AP (ΔF300/F0) and the kinetic of signal after 300AP expressed as time constant describing the increase (tau upstroke) and decay (tau decay) of fluorescence. Data are expressed as mean ± SEM, n=4, at least 50 boutons from minimum 5 neurons were analyzed for experiment (* $p<0.05$; ** $p<0.01$ versus control, ANOVA). (d) The exo/endocytotic assay was performed at DIV14 on wild-type and BAC hG2019S cortical neurons infected at DIV4 with virus expressing GFP. Cycling SV appears as synaptotagmin (s-tagmin) positive clusters along neuron processes. Total SV pool was revealed by staining with anti-synaptophysin antibodies upon fixation and permeabilization. Images show signals acquired for synaptotagmin, synaptophysin and their superimposition plus GFP (merge). Panel size is 28 x 4 μm. (e) The percentage of s-tagmin and s-physin positive clusters within the totality of s-physin positive clusters reflects the pool of cycling vesicles. Data are expressed as mean ± SEM, n=4, at least 7 neurons were analyzed for experiment (** $p<0.01$ Student's t-test).

Figure 2. LRRK2 interacts with NSF

(a) Extracts of purified cortical synaptosomes were incubated with anti-LRRK2 antibodies or rabbit IgG. The immunocomplexes were sedimented with protein G-Sepharose and the samples were resolved by SDS-PAGE and analyzed by immunoblotting with anti NSF and anti LRRK2 antibodies. Immunoblotting against synaptotagmin 1 (S-tagmin1), synaptophysin (S-physin) and synaptobrevin (S-brevin) were performed to confirm purity of synaptosomal preparation. (b) Flag-NSF full-length or domains (N, D1, D2) purified from HEK293T and bound to M2 flag resin were incubated with a mouse brain lysate. Samples were subjected to immunoblotting using anti-LRRK2 (MJFF2) or stained with Coomassie

to show flag inputs. (c) Size exclusion chromatography fractions of HEK293T expressing ectopic flag-NSF alone or together with 2xMyc-LRRK2 spotted onto nitrocellulose membrane and probed with anti-flag antibody (n=3 independent experiments). (d) Immunofluorescence of primary cortical neurons stained for endogenous LRRK2 and endogenous NSF (scale bar is 10 µm).

Figure 3. LRRK2 phosphorylates NSF.

(a) *In vitro* radioactive kinase assays of 3x-Flag LRRK2 wild-type, K1906M (kinase dead) and G2019S (hyperactive) and flag-NSF purified from HEK293T cells at 1:10 ratio. Radioactivity incorporated was revealed by autoradiography (upper panel) and total proteins loaded by flag immunoblotting (lower panels). LRRK2 inhibitor IN-1 was used at 1 µM concentration to confirm LRRK2 specific phosphorylation on NSF. (b) *In vitro* kinase assays as in (a) with the hyperactive GST-LRRK2$^{970\text{-}2527}$ fragment. (c) Quantification of moles of ^{33}P incorporated by NSF using a calibration curve with known concentration of ^{33}P-ATP. (d) *In vitro* kinase assays as in (a) using NSF full-length or domains as substrates of LRRK2 GST-LRRK2$^{970\text{-}2527}$ kinase activity at 1:10 ratio LRRK2:NSFs. Radioactivity incorporated was revealed by autoradiography (upper panel) and total proteins loaded by coomassie brilliant blue (CBB) staining for NSF (middle panel) or LRRK2 immunoblotting (lower panel). (e) *In vitro* radioactive kinase assays of 3xFlag-LRRK1 or 3xFlag-LRRK2 and Flag-NSF as substrate at 1:10 ratio. Left panel is an example of autoradiography and right panel represents the corresponding immunoblot of total loading.

Figure 4. LRRK2 phosphorylates NSF at T645.

(a) *In vitro* kinase assays with 3xFlag-LRRK2 G2019S and NSF wild-type or non-phosphorylatable mutants T645A, T646A and S647A mutants at 1:10 ratio LRRK2:NSF. The G2019S hyperactive mutant was used to maximize ^{33}P incorporation. (b) Quantification of ^{33}P incorporated by NSF (autoradiography, upper panel) controlled for total NSF (NSF_{TOT}, coomassie staining, lower panel) from n=4 independent experiments (bars represent the mean ± SEM). One way-ANOVA with Bonferroni's post-test (**p<0.01).

Figure 5. Phosphorylated NSF exhibits enhanced ATPase activity.

(a) NSF ATPase activity was assessed with a Malachite green assays at 36nM NSF and increasing concentrations of ATP substrate (up to 1.4 mM) in the presence of NSF alone,

NSF pre-phosphorylated by LRRK2-G2019S$^{970\text{-}2527}$ (ΔG2019S) or LRRK2-G2019S$^{970\text{-}2527}$ (ΔG2019S) alone (NSF:LRRK2 20:1). Data were fitted with the Michaelis-Menten kinetic model to determine kinetic constants. (b) Phosphate generated by ATP hydrolysis in the presence of NSF wild-type, NSF^{T645A} NSF^{T646A} NSF^{S647A} pre-phosphorylated or not by ΔG2019S was measured with the Malachite Green Assay at 120 min with an initial concentration of ATP of 1.4 mM (NSF^{WT} vs NSF^{T645A} **p<0.01; NSF^{WT} vs P-NSF^{WT} ***p<0.001; NSF^{T645A} vs P-NSF^{T645A} p>0.05, non significant, n.s.; NSF^{T646A} vs P-NSF^{T646A} p>0.05, n.s.; NSF^{S647A} vs P-NSF^{S647A} **p<0.01; one-way ANOVA, Bonferroni's post-test, n≥3). UT=untrasfected cells subjected to Flag-affinity purification to monitor background activity (n=1; excluded from the statistical analysis).

Figure 6. Phosphorylated NSF exhibits increased rate of SNARE complex disassembling *in vitro*.

(a) Representative coomassie gels (CBB, coomassie brilliant blue) of SNARE complex incubated for increasing time with NSF phosphorylated or not by LRRK2-G2019S$^{970\text{-}2527}$ in the presence of the co-factor alpha-SNAP. (b) Quantification of n=3 independent experiments. Time points are relative to t=0 which was set at 100% (two-way ANOVA with Bonferroni's post-test, ***p<0.001).

Figure 1

Click here to download Figure Fig. 1R.png

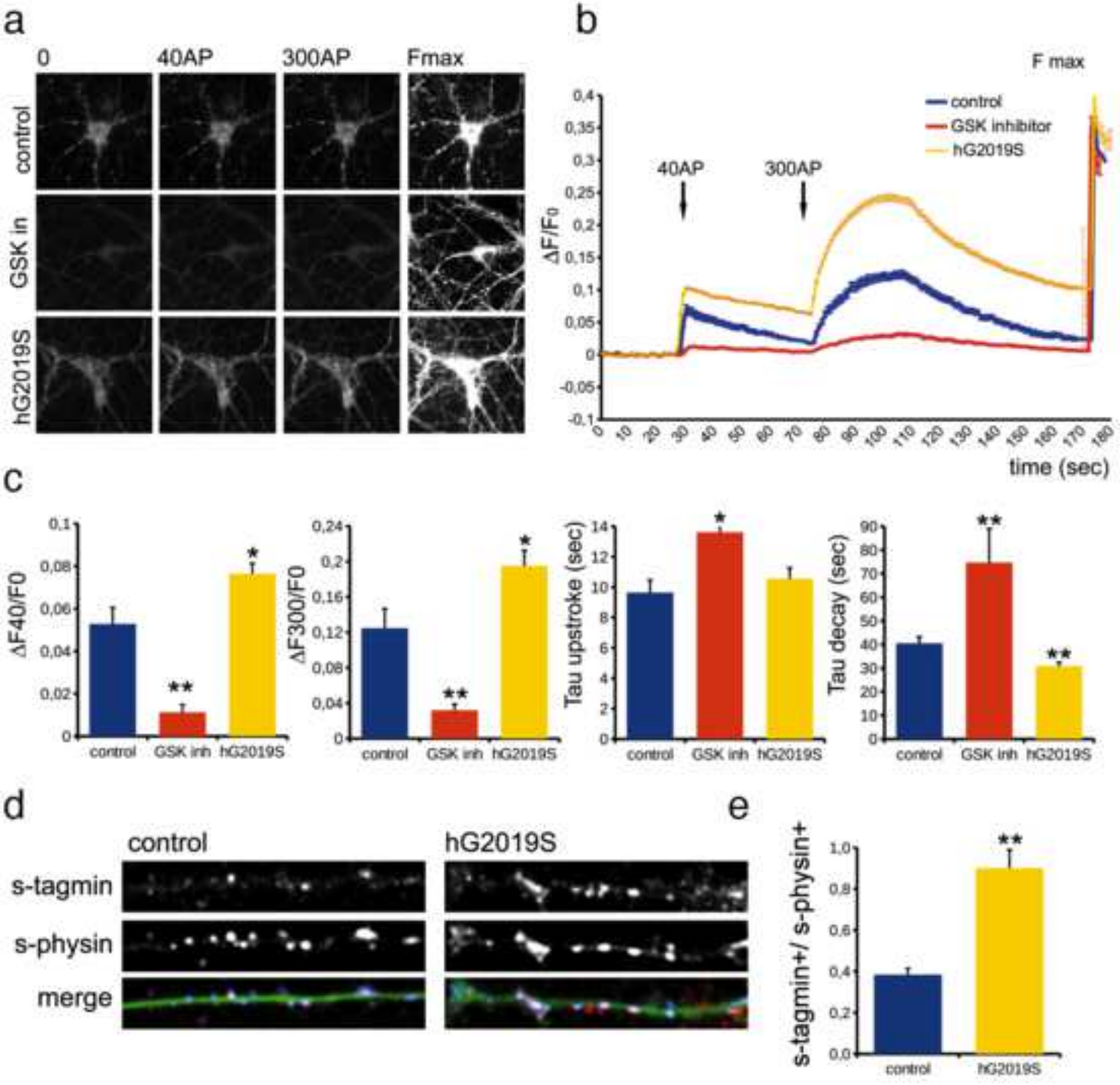

Figure 2

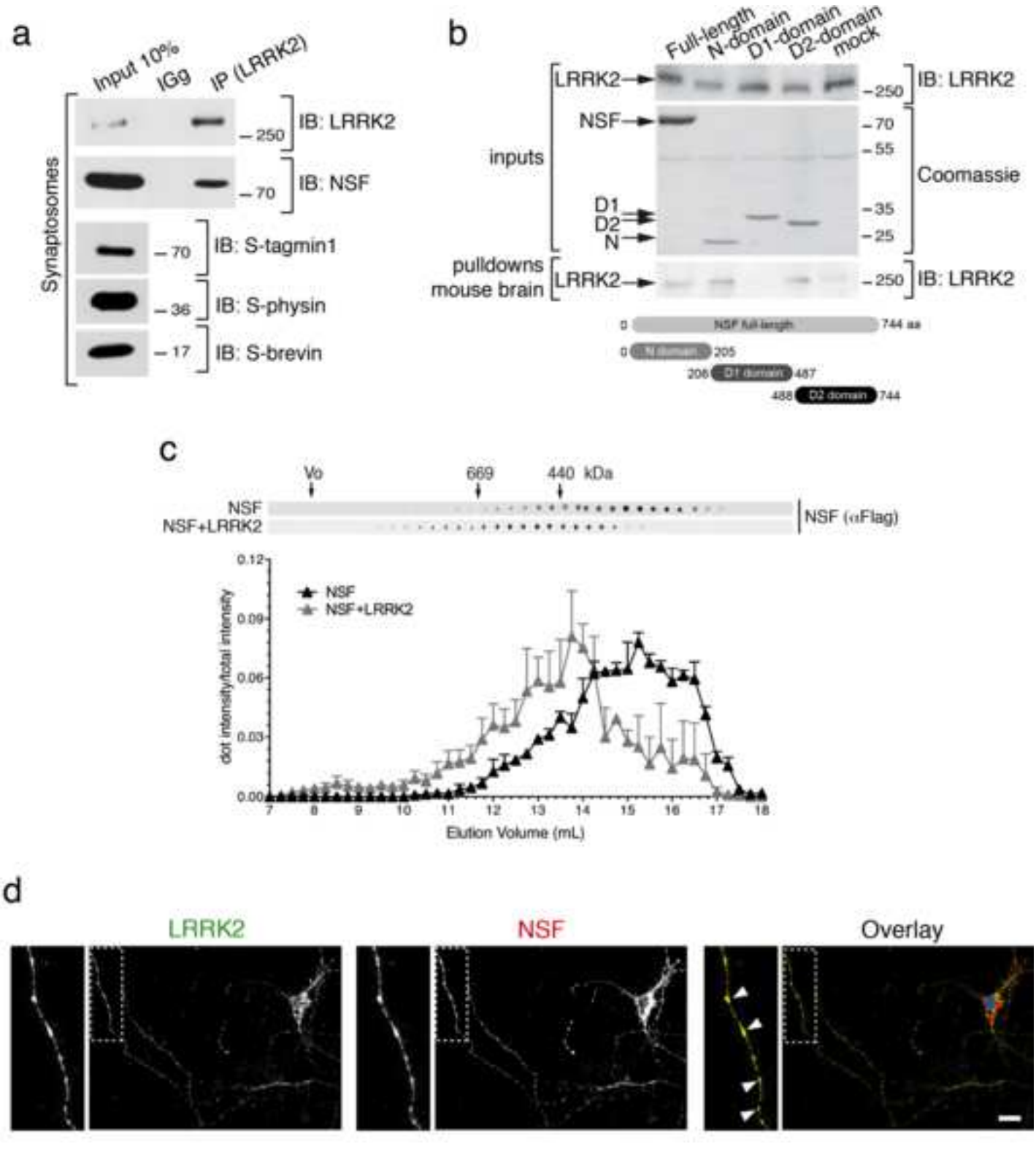

Figure 3

Click here to download Figure Fig. 3.png

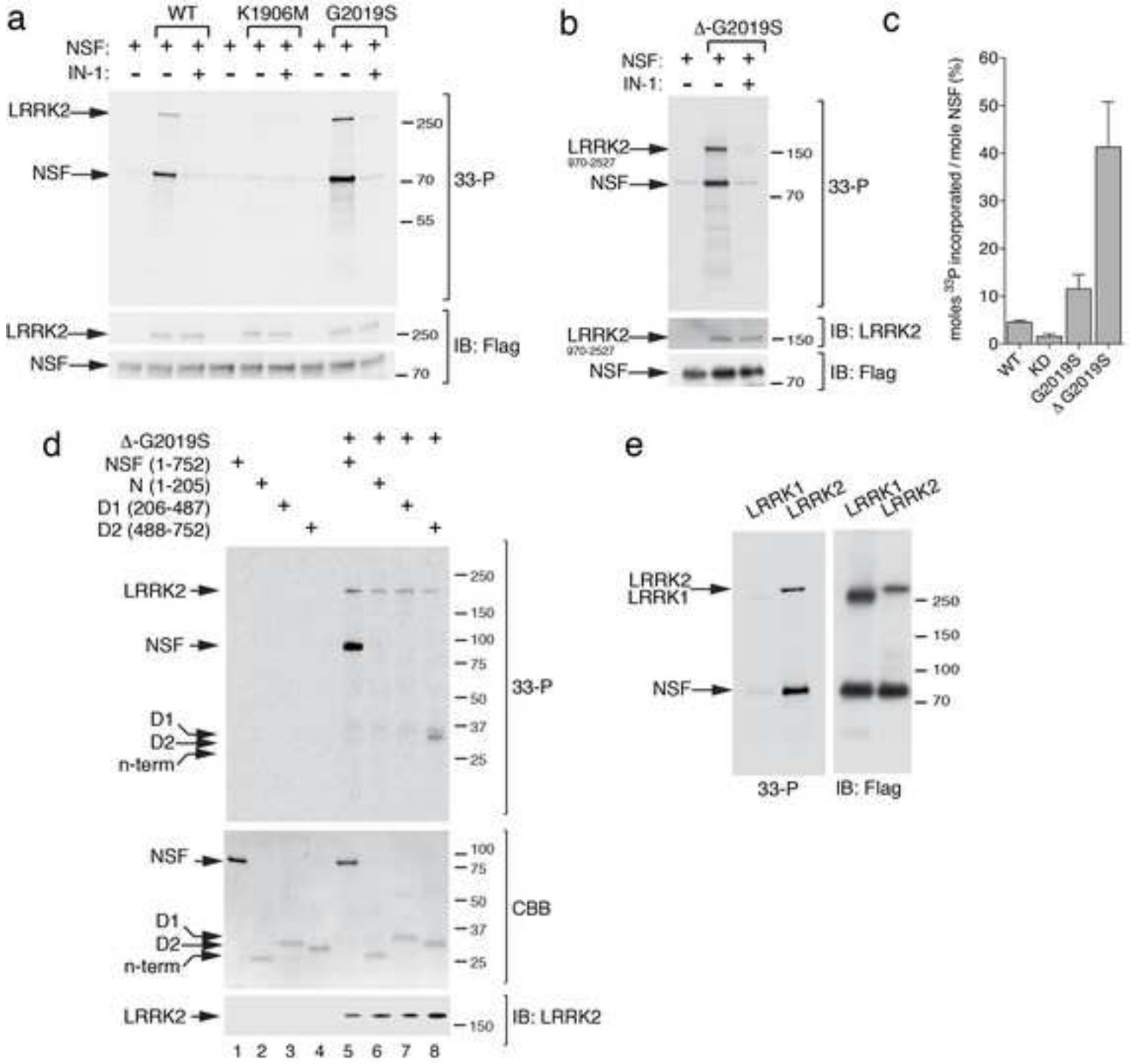

Figure 4

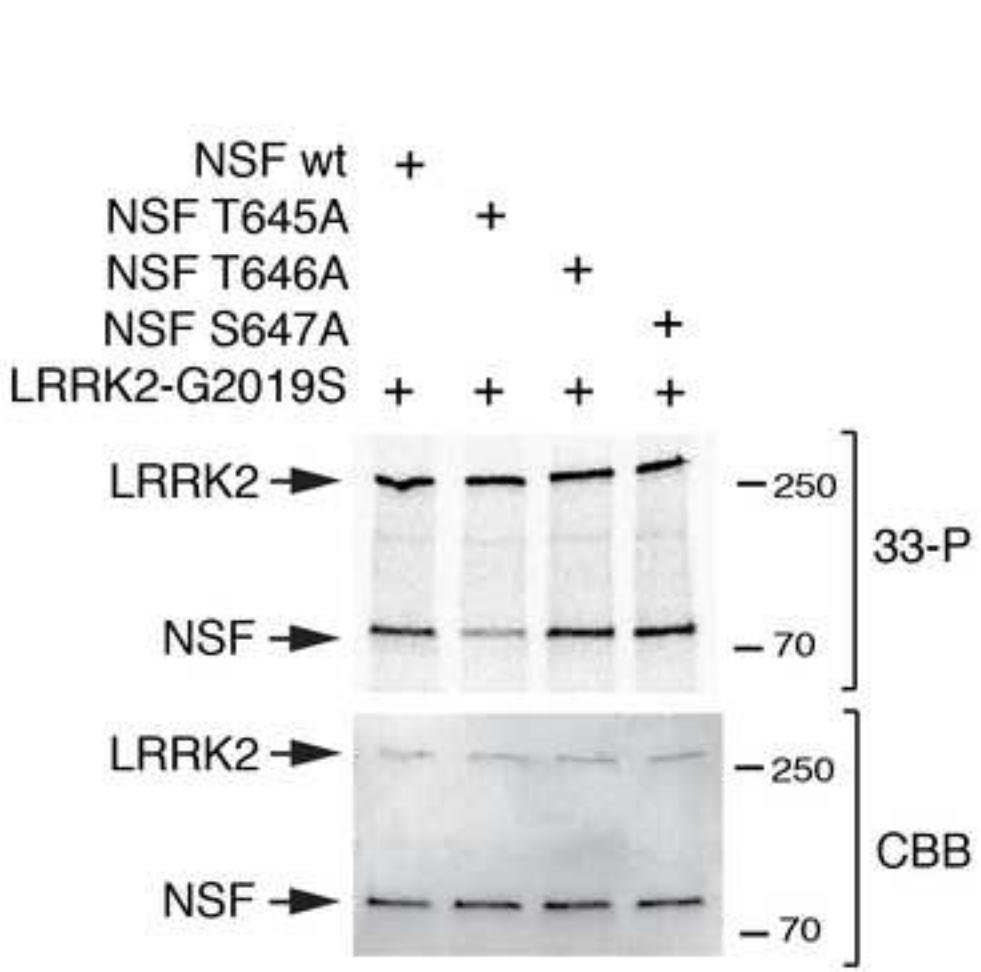

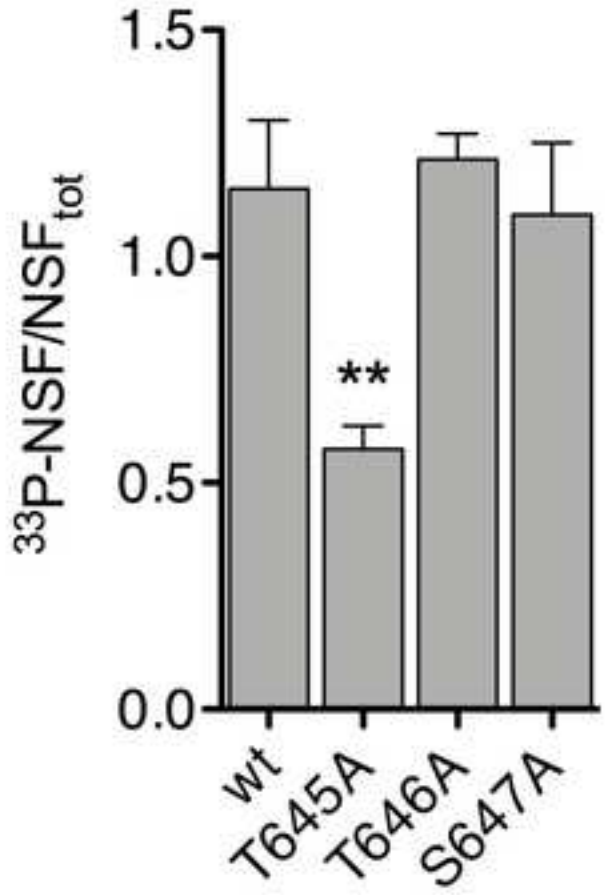

Figure 5

Click here to download Figure Figure 5.png

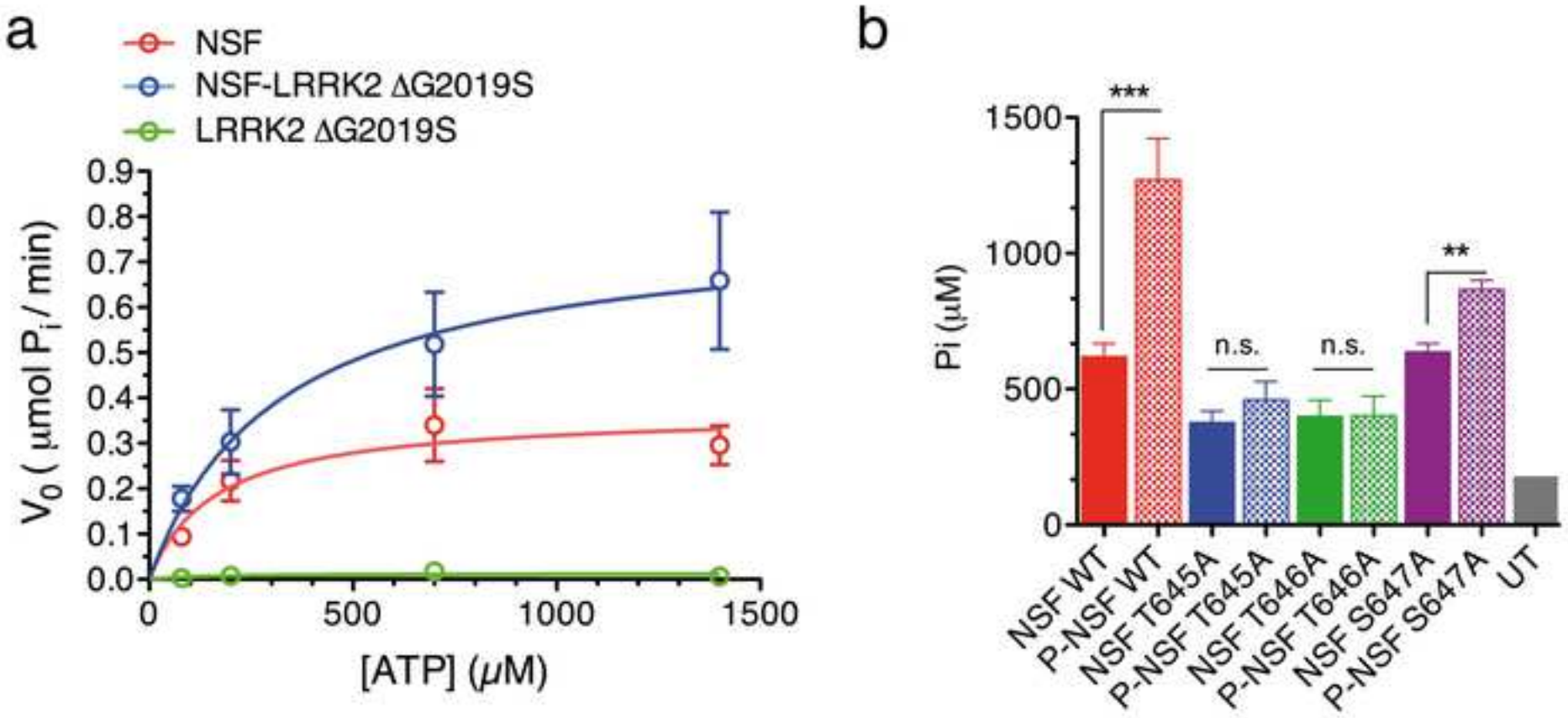

Figure 6